Degradation modeling for reliability analysis with time-dependent structure based on the inverse gaussian distribution

Lia Hanna Martins Morita

UNIVERSIDADE FEDERAL DE SÃO CARLOS
CENTRO DE CIÊNCIAS EXATAS E TECNOLOGIA
PROGRAMA INTERINSTITUCIONAL DE PÓS-GRADUAÇÃO EM ESTATÍSTICA UFSCar-USP

LIA HANNA MARTINS MORITA

DEGRADATION MODELING FOR RELIABILITY ANALYSIS WITH TIME-DEPENDENT STRUCTURE BASED ON THE INVERSE GAUSSIAN DISTRIBUTION

Thesis submitted to the Departamento de Estatística – Des/ UFSCar and to the Instituto de Ciências Matemáticas e de Computação – ICMC-USP, in partial fulfillment for the PhD degree in Statistics - Interinstitutional Program of Pos-Graduation in Statistics UFSCar-USP.

Advisor: Profa. Dra. Vera Lucia Damasceno Tomazella

São Carlos
January 2017

UNIVERSIDADE FEDERAL DE SÃO CARLOS

Centro de Ciências Exatas e de Tecnologia
Programa Interinstitucional de Pós-Graduação em Estatística

Folha de Aprovação

Assinaturas dos membros da comissão examinadora que avaliou e aprovou a Defesa de Tese de Doutorado da candidata Lia Hanna Martins Morita, realizada em 07/04/2017:

Profa. Dra. Vera Lucia Damasceno Tomazella
UFSCar

Prof. Dr. Francisco Louzada Neto
USP

Prof. Dr. Celso Rômulo Barbosa Cabral
UFAM

Prof. Dr. Enrico Antonio Colosimo
UFMG

Profa. Dra. Marta Afonso Freitas
UFMG

UNIVERSIDADE FEDERAL DE SÃO CARLOS
CENTRO DE CIÊNCIAS EXATAS E TECNOLOGIA
PROGRAMA INTERINSTITUCIONAL DE PÓS-GRADUAÇÃO EM ESTATÍSTICA UFSCar-USP

LIA HANNA MARTINS MORITA

MODELAGEM DE DEGRADAÇÃO PARA ANÁLISE DE CONFIABILIDADE COM ESTRUTURA DEPENDENTE DO TEMPO BASEADA NA DISTRIBUIÇÃO GAUSSIANA INVERSA

Tese apresentada ao Departamento de Estatística – Des/UFSCar e ao Instituto de Ciências Matemáticas e de Computação – ICMC-USP, como parte dos requisitos para obtenção do título de Doutor em Estatística - Programa Interinstitucional de Pós-Graduação em Estatística UFSCar-USP.

Orientadora: Profa. Dra. Vera Lucia Damasceno Tomazella

São Carlos
Maio de 2017

RESUMO

MORITA, L. H. M.. **Modelagem de degradação para análise de confiabilidade com estrutura dependente do tempo baseada na distribuição gaussiana inversa**. 2017. 131 p. Tese (Estatística - Programa Interinstitucional de Pós-Graduação em Estatística) - Departamento de Estatística - DEs-UFSCar e Instituto de Ciências Matemáticas e de Computação - ICMC-USP, São Carlos - SP.

As técnicas convencionais de análise de confiabilidade são voltadas para a ocorrência de falhas ao longo do tempo. Contudo, em determinadas situações nas quais a ocorrência de falhas é pequena ou quase nula, a estimação das quantidades que descrevem os tempos de falha fica comprometida. Neste contexto foram desenvolvidos os modelos de degradação, que possuem como dado experimental não a falha, mas sim alguma característica mensurável a ela atrelada. A análise de degradação pode fornecer informações sobre a distribuição de vida dos componentes sem realmente observar falhas. Assim, nesta tese nós propusemos diferentes metodologias para dados de degradação baseados na distribuição gaussiana inversa. Inicialmente, nós introduzimos o modelo de taxa de deterioração gaussiana inversa para dados de degradação e um estudo de suas propriedades assintóticas com dados simulados. Em seguida, nós apresentamos um modelo de processo gaussiano inverso com fragilidade considerando que a fragilidade é uma boa ferramenta para explorar a influência de covariáveis não observadas, e um estudo comparativo com o processo gaussiano inverso usual baseado em dados simulados foi realizado. Também mostramos um modelo de mistura de processos gaussianos inversos em testes de burn-in, onde o principal interesse é determinar o tempo de burn-in e o ponto de corte ótimo para separar os itens bons dos itens ruins em uma linha de produção, e foi realizado um estudo de má especificação com os processos de Wiener e gamma. Por fim, nós consideramos um modelo mais flexível com um conjunto de pontos de corte, em que as probabilidades de má classificação são estimadas através do método exato com distribuição gaussiana inversa bivariada ou em um método aproximado baseado na teoria de cópulas. A aplicação da metodologia foi realizada com três conjuntos de dados reais de degradação de componentes de LASER, rodas de locomotivas e trincas em metais.

Palavras-chave: Análise de degradação, Distribuição gaussiana inversa, Processo gaussiano inverso, Fragilidade, Testes de burn-in.

ABSTRACT

MORITA, L. H. M.. **Degradation modeling for reliability analysis with time-dependent structure based on the inverse gaussian distribution**. 2017. 131 p. Thesis (Statistics - Programa Interinstitucional de Pós-Graduação em Estatística) - Departamento de Estatística - DEs-UFSCar and Instituto de Ciências Matemáticas e de Computação - ICMC-USP, São Carlos - SP.

Conventional reliability analysis techniques are focused on the occurrence of failures over time. However, in certain situations where the occurrence of failures is tiny or almost null, the estimation of the quantities that describe the failure process is compromised. In this context the degradation models were developed, which have as experimental data not the failure, but some quality characteristic attached to it. Degradation analysis can provide information about the components lifetime distribution without actually observing failures. In this thesis we proposed different methodologies for degradation data based on the inverse Gaussian distribution. Initially, we introduced the inverse Gaussian deterioration rate model for degradation data and a study of its asymptotic properties with simulated data. We then proposed an inverse Gaussian process model with frailty as a feasible tool to explore the influence of unobserved covariates, and a comparative study with the traditional inverse Gaussian process based on simulated data was made. We also presented a mixture inverse Gaussian process model in burn-in tests, whose main interest is to determine the burn-in time and the optimal cutoff point that screen out the weak units from the normal ones in a production row, and a misspecification study was carried out with the Wiener and gamma processes. Finally, we considered a more flexible model with a set of cutoff points, wherein the misclassification probabilities are obtained by the exact method with the bivariate inverse Gaussian distribution or an approximate method based on copula theory. The application of the methodology was based on three real datasets in the literature: the degradation of LASER components, locomotive wheels and cracks in metals.

Keywords: Degradation analysis, Inverse gaussian distribution, Inverse gaussian process, Frailty, Burn-in tests.

LIST OF FIGURES

LIST OF ALGORITHMS

LIST OF TABLES

CONTENTS

CHAPTER

1

INTRODUCTION

1.1 Introduction and bibliographical review

Highly reliable products present a few or no failures, then it is difficult or impossible to access reliability with traditional life tests that record only time-to-failure. However, when failure can be related directly to a quality characteristic (QC) over time, we then have the possibility of measuring degradation over time and use it to estimate the product's reliability. It is possible to access the latent failure process characteristics and make inferences about the implied lifetime distribution. Some degradation studies consist in measuring physical degradation as a function of time (e.g., tire wear); in other applications it cannot be observed directly, but some measurements of product performance degradation (e.g., power output) may be available. Moreover, degradation analysis can have one or more variables in the underlying degradation process. Other applications of reliability prediction based on degradation modeling include reliability prediction of helicopter transmission systems, optimal degradation process control, reliability evaluation of distribution systems with aging equipment, reliability estimation of degraded structural components subject to corrosion, real-time conditional reliability prediction from online tool performance data (WANG; COIT, 2007) and degradation of nuclear power plant components (YUAN, 2007).

In reliability engineering there are two main classes of models, namely, the threshold models and the shock models; the striking difference between them is the way the failure is characterized. In the threshold models, a component reveals performance loss when its degradation level first reaches a certain threshold; this phenomenon is referred to as soft failure and the unit is usually switched off. In the shock models, a component is subject to external shocks, being able to survive or to fail; the eventual failures are referred to as hard failures or traumatic failures and the shocks usually occur according to a Poisson process whose intensity depends on degradation and environmental factors (LEHMANN, 2010). Within the class of threshold models, we can cite the general path model and the stochastic process models. The

general path model proposed by Meeker, Escobar and Lu (1998) fits the degradation observations by a regression model with random coefficients, while the stochastic process models consider the degradation over time as a stochastic process $\{D(t); t > 0\}$ to account for inherent randomness. Gorjian *et al.* (2010) presented a review of degradation models, with advantages and limitations.

In the literature of the general path model, we can cite Oliveira and Colosimo (2004) that used the classical approach in automobile tyre wear data, with analytical, numerical and approximate estimation methods to obtain the time-to-failure distribution and presented some comparisons; Peng and Tseng (2009) proposed a general linear degradation path in which the unit-to-unit variation of all test units can be considered simultaneously with the time-dependent structure in degradation paths. They derived an explicit expression of the product's lifetime distribution and its corresponding meantime to failure and analyzed the effects of model misspecification on these parameters. Freitas *et al.* (2010) presented a comprehensive study of various approaches for degradation data concerning the classical and Bayesian ones. Chen and Zheng (2005) proposed an alternative method which consists in making inference directly on the lifetime distribution itself. Zuo, Jiang and Yam (1999) introduced three approaches for reliability modeling of continuous state devices based on the random process model, the general path model and the multiple linear regression model, respectively. They also proposed a mixture model which can be used to model both catastrophic failures and degradation failures. Meeker, Escobar and Lu (1998) reviewed the literature concerning accelerated degradation analysis and extended the approach of Lu and Meeker (1993) to allow for acceleration. Crk (2000) developed a methodology based on a multiple multivariate regression model for the component performance degradation function whose parameters may be random, correlated and stress dependent. Chinnam (1999) used neural networks for modeling degradation signals and Eghbali and Elsayed (2001) developed a concept of degradation rate in which the degradation hazard function is written in terms of time and degradation measure.

The random deterioration rate model is a specific stochastic model usually applied to model corrosion and wear phenomena; see Fenyvesi, Lu and Jack (2004), EPRI (2006) and Huyse and Roodselaar (2010). The motivation in the random variable model is to capture the randomness in the individual differences across population. This model incorporates only sample uncertainty of the degradation and no temporal variability is involved. The measurement error models appear to work around this issue. Pandey and Lu (2013) developed a methodology for the estimation of the growth rate parameters in noisy degradation measurement data, whose random sizing error occurs due to inspection tools. They assigned the exponential and gamma distributions to the deterioration rate, and normal distribution to the measurement errors.

The degradation models based on stochastic processes are very intuitive since degradation is a continuous process of wear over time. Based on the assumption of additive accumulation of degradation, two classes of degradation models have been well studied, namely, the Wiener and the gamma processes. Several papers in the literature assume the degradation paths to follow the

Wiener process, for example, Doksum (1991) used a Wiener process with accelerating factors to analyze degradation data, Wang (2010) presented a Wiener process with random effects for degradation data. In the Wiener process the sample paths are not necessarily monotone, which might not be meaningful in many applications.

As an alternative, the gamma process is often adopted when monotonicity is required. The gamma process is the limit of a compound Poisson process with the jump size conforming to a certain distribution (LAWLESS; CROWDER, 2004). This interpretation underpins the gamma process as an appropriate degradation model because many reliability engineers believe that degradation is often caused by a series of external shocks, each with random and tiny damage (ESARY; MARSHALL, 1973). The gamma process has therefore been discussed by several authors, for example, Noortwijk (2009) made a comparative study between gamma process and random variable models in which the first one provided advantages for taking into account the time-dependent structure inherent in degradation data. Park and Padgett (2005) presented new degradation models incorporating accelerating variables in stochastic processes including gamma process and Wang (2008) proposed an estimation method grounded on the semiparametric pseudo-likelihood for modeling degradation data through gamma process with random effects model.

Another degradation model with monotone paths is the inverse Gaussian process introduced by Wasan (1968) with some recent papers in the literature, for example, Wang and Xu (2010) proposed an inverse Gaussian process with random effects and covariates to account for heterogeneity. Ye and Chen (2014) regarded the inverse Gaussian process as the limit of a compound Poisson process whose arrival rate goes to infinity while the jump size goes to zero in a certain way; they included a random drift in the mean function of the inverse Gaussian process, leading to individual degradation paths with different slopes. Peng (2015) proposed a degradation model based on an inverse normalgamma mixture of an inverse Gaussian process. Qin, Zhang and Zhou (2013) introduced an inverse Gaussian process-based model with Bayesian approach to characterize the growth of metal loss corrosion defects on energy pipelines, wherein the measurement errors in the paths are considered. Liu *et al.* (2014) developed a reliability model for systems with s-dependent degradation processes using copulas, wherein the degradation processes are s-dependent among each other and the marginal degradation process is modeled by an inverse Gaussian process with time scale transformation and random drift to account for possible heterogeneity.

The frailty model is a specific approach to include randomness which allows us to incorporate the variability of the observed times coming from two distinct fonts. The first is the natural variability, which is explained by the hazard function, and the second is the common variability of the individuals from the same group or the broach variability of the several events of the same individual, which is explained by the frailty variable. Vaupel, Manton and Stallard (1979) coined the phrase “frailty” in connection with a particular version of such a stochastic

model, in which the individual i was assumed to have death intensity $z_i h_0(t)$ at age t where the random variable z_i (the "frailty") is assumed to follow gamma distribution. The assumptions that the frailty term is time independent and acts multiplicatively on an underling intensity $h_0(t)$ are in principle arbitrary, but have been taken as the basis for much subsequent work on random heterogeneity in survival analysis. The frailty models are likely to be particularly useful for modeling multivariate survival times, whether "serial" or "parallel" (OAKES, 1989). Hougaard (1986) pointed out the double role of the frailty distribution with finite mean in describing both nonproportionality and interclass correlation. Unkel and Farrington (2012) provided a useful representation of bivariate current status data to facilitate the choice of a frailty model. In the context of degradation analysis, we can cite interesting papers, for example, Lin, Pulido and Asplund (2014) reported an accelerated failure time (AFT) model with frailty for the analysis of locomotive wheel's degradation under piecewise constant hazard rate and gamma frailty; and Lin and Asplund (2014) presented a similar approach under Weibull baseline hazard rate. In these works, the lifetime information are based on the pseudo lifetimes, which are obtained when we assume some standard form for the degradation rate such as, for example, linear, exponential or power law.

Burn-in test is a technique applied to increase the quality of components and systems by testing the units before fielding them in the market. The traditional burn-in tests consist in putting the units to operate under certain conditions wherein failures are expected to occur. These tests are inefficient for highly reliable products among which even the weak units take a long time to fail. The condition-based burn-in tests arise to work around this issue, where a QC related to failure is chosen and the units with deterioration levels below a specified cutoff value are considered normal units and released to field service, whereas the ones with deterioration levels exceeding this cutoff point are considered weak ones and discarded. In the last decades, the manufacturing industry has been dedicating much effort in designing burn-in policies that eliminate latent failures before fielding them in the market. Such failures that generally occur in a small proportion among the manufactured products are caused by manufacturing defects and lead to high warranty and replacement costs. Many burn-in policies have been extensively studied in the degradation literature; see for example Jensen (1982), Kuo (1984) and Leemis and Beneke (1990).

The use of mixture distributions is an important feature in burn-in policies because the components lifetime distribution is commonly bimodal from a mixture of two distributions, in which the weak units tend to fail earlier than the normal ones and the degradation values may present bimodal behavior as well. This heterogeneity is often caused either by the manufacturing process with variation of material flaws or by the fact that the components come from different suppliers. Burn-in policies are liable to misclassification errors, which are of much importance in burn-in studies. Tseng, Tang and Ku (2003) designed an economic model based on misclassification errors, and set up an optimal burn-in policy based on termination time and a set of cutoff points, whose degradation paths are modeled by a mixture of two Wiener processes. Tseng

and Peng (2004) studied an efficient burn-in procedure based on an integrated Wiener process for the cumulative degradation and Wu and Xie (2007) suggested the use of receiver operating characteristic (ROC) for the removal of the weak group from the production row; Tsai, Tseng and Balakrishnan (2011) proposed a mixed gamma process for modeling degradation paths and presented an optimal burn-in policy for classifying LASER components based on a cost model. Zhang, Ye and Xie (2015) presented a mixed inverse Gaussian process for degradation data, wherein the optimal burn-in policy to screen out the components are based on burn-time and a single cutoff point in the decision rule. Xiang, Coit and Feng (2013) developed a burn-in policy for preventive replacement of devices consisting of n subpopulations from various stochastic processes with different degradation rates. They used mixtures of Wiener and gamma processes models and presented some comparisons.

1.2 Objectives of the thesis

The purpose of this study is to show the different methodologies for modeling degradation data. Some specific objectives are specified below:

- ✔ To introduce an inverse Gaussian distribution in the random deterioration rate model with measurement errors in order to take into account the variability among different components,
- ✔ To introduce a frailty term in the degradation modeling in order to take into account the unobserved heterogeneity or the dependence between the measurements of the same experimental unit, even as the presence of unobserved variables in practice,
- ✔ To present a decision rule for classifying a unit as normal or weak, based on burn-in time and a set of cutoff points.

1.3 Organization of the chapters

This thesis is organized as follows.

In the second chapter we introduce the concept of degradation data and the main continuous processes for degradation data known in the literature, the frailty model and the selection models criteria with a brief description.

In the third chapter we propose a random deterioration rate model based on the inverse Gaussian distribution to account for both sampling and temporal variability associated with a deterioration process.

In the fourth chapter we propose an inverse Gaussian process frailty model in order to capture the variability among different units and within the same unit.

In the fifth chapter we introduce the concepts of mixture inverse Gaussian process, burn-in test and burn-in policy, where the main objective is to screen out the weak units from the normal ones in a production row. An economic model is set for determining the optimal termination time and the other parameters of a burn-in test.

In the sixth chapter we present a general and more flexible burn-in policy under the mixture inverse Gaussian process, in which the decision rule to separate the weak units from the normal ones is based on burn-in time and a set of cutoff points.

Finally, in the seventh chapter we present the conclusion of this thesis and the ideas for future research, followed by the bibliographic references.

CHAPTER

2

BACKGROUND

2.1 Introduction

In this chapter, we present some features of degradation data and degradation processes in reliability analysis, followed by a brief description of frailty models and model selection criteria.

2.2 Degradation data

In a degradation test, we can observe n experimental units during a fixed period of time. Commonly, we collect the measurements in equidistant time intervals. For each unit i, we have the observed degradation measurements at the inspection times $0 = t_{i0} < t_{i1} < \ldots < t_{in_i}$, with observations $D_i(t_{ij}), j = 0,1,\ldots,n_i$. The vector of measurements for each unit i is called degradation path and represented by $\mathbf{D}_i \equiv [D_i(t_{i1}), D_i(t_{i2}), \ldots, D_i(t_{in_i})]$. Table 1 shows the general representation of degradation data.

Table 1 – General representation of degradation data.

unit	Inspection times	degradation measures
1	$t_{10} = 0, t_{11}, \ldots, t_{1n_1}$	$\mathbf{D}_1 \equiv [D_1(t_{10}) = 0, D_1(t_{11}), \ldots, D_1(t_{1n_1})]$
2	$t_{20} = 0, t_{21}, \ldots, t_{2n_2}$	$\mathbf{D}_2 \equiv [D_2(t_{20}) = 0, D_2(t_{21}), \ldots, D_2(t_{2n_2})]$
$\ldots$	$\ldots$	$\ldots$
n	$t_{n0} = 0, t_{n1}, \ldots, t_{nn_n}$	$\mathbf{D}_n \equiv [D_n(t_{n0}) = 0, D_n(t_{n1}), \ldots, D_n(t_{nn_n})]$

In several problems the inspections $0 = t_{i0} < t_{i1} < \ldots < t_{in_i}$ are in time scale, but other problems exhibit the degradation in function of a variable other than the time.

The examples 2.2.1, 2.2.2 and 2.2.3 exhibit some datasets in the literature. The motivation for these examples is that the degradation paths present increasing behavior, which is a striking feature of the degradation models based on IG distribution.

Example 2.2.1 (**LASER data**). Some devices for light amplification by stimulated emission, called LASER (Light Amplification by Stimulated Emission of Radiation), present degradation over time, which results in a reduction in the emitted light. This luminosity can be maintained substantially constant with an increase in operating current. When this current reaches a very high value, it is considered that the unit has failed. Meeker and Escobar (1998) presented a study with degradation data of 15 LASER units from GaAs type (compound with Gallium and Arsenic elements), with observations made up to $4,000$ hours of operation, with 16 equidistant time intervals. The degradation measure for each unit is the percent increase in current over time related to the nominal current, and a unit is considered to have failed when its degradation measure reaches 10%. Table 38 in Appendix B displays these data and Figure 1 (a) shows the corresponding degradation paths, indicating the critical value related to failure. An interesting feature of this dataset is the presence of soft failures because some components exceed the boundary but remain until the end of the experiment. Soft failures cause a performance loss but do not prevent the devices from continuing to run.

Example 2.2.2 (**locomotive wheels data**). Wheel failures account for much of the railroad vehicle accidents, which lead to high costs for private companies and government. The railway maintenance services are responsible for mechanical repairs of the locomotives and hold some detailed information about preventive or corrective interventions. This dataset is part of a study led by a Brazilian railroad company presented by Freitas *et al.* (2009) and containing the diameter (in mm) of 14 locomotive wheels obtained from 13 inspections done up to $600,000$ km travelled in equidistant intervals. The degradation measure for each wheel is the wear (in mm) on the wheel diameter over the travelled distance, more specifically, the difference between the actual wheel diameter and the diameter of a new wheel (966 mm) over km travelled. A wheel is considered not be working when its degradation measure reaches 77 mm, that is, when the wheel diameter is far 77 mm from a new wheel. Table 39 in Appendix B displays these data and Figure 1 (b) shows the corresponding degradation paths, indicating the boundary related to failure. The wheels that reach the critical value remain until the subsequent inspection, when they are replaced due to preventive measures.

Example 2.2.3 (**fatigue crack size data**). The fatigue crack size data presented by Hudak *et al.* (1978) was collected to obtain the fatigue cracks as a function of the number of cycles of applied stress for 21 test specimens. The data are explored by Lu and Meeker (1993) as a motivational example in the context of nonlinear mixed effects models for degradation data. There are 21 sample paths, one for each of the 21 test units, the test stops after 0.12 million cycles and a threshold value of 1.6 inches is set to define soft failures. Table 40 in Appendix B displays these data and Figure 1 (c) shows the corresponding degradation paths, indicating the critical value related to failure. Likewise the locomotive wheels example, a specimen does not continue in the study whether it is noticed that its crack length has already exceeded the boundary.

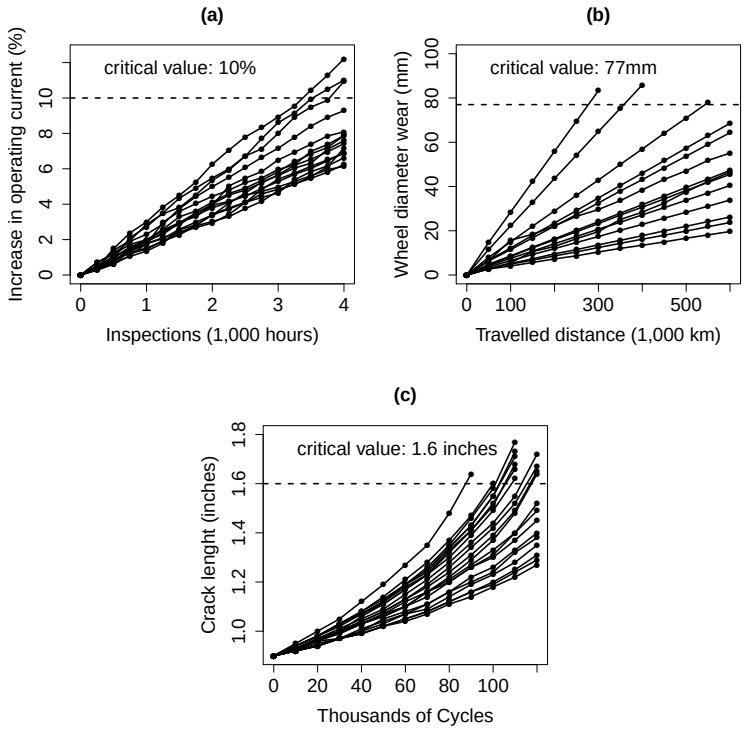

Figure 1 – (a) Degradation paths for example 2.2.1, (b) Degradation paths for example 2.2.2, (c) Degradation paths for example 2.2.3.

2.3 The degradation model

In this work, the degradation path of a specific QC of a product is denoted by $D(t)$, and it is a continuous-time stochastic process $\{D(t), t \geq 0\}$, that is, $D(t)$ is a random quantity for all $t \geq 0$.

Usually, degradation has increasing behavior over time, then the product's lifetime T is suitably defined as the first passage time when $D(t)$ exceeds a threshold ρ, which must be fixed in general

$$T = inf\{t \geq 0 | D(t) \geq \rho\}. \tag{2.1}$$

The formula (2.1) is referred to as the first passage time distribution, which plays an important role in predicting the remaining useful life as well as in determining optimal maintenance strategies (NOORTWIJK, 2009).

The aleatory uncertainties of a degradation process can be characterized using various types of probabilistic models. In the context of stochastic processes, we can cite the random deterioration rate model, the Wiener process, the gamma process and the inverse Gaussian process. The following section presents a description of these stochastic processes with special attention to the inverse Gaussian process and the inverse Gaussian distribution.

2.4 Stochastic processes for degradation data

2.4.1 The random deterioration rate model

The most simple stochastic process is defined as a time-dependent function for which the average rate of deterioration per unit time is a random quantity (NOORTWIJK, 2009). The random deterioration rate model (or random rate model) describes the deterioration growth in a group of components using a linear function and a random parameter. Many other more complicated nonlinear models can be transformed into a linear random deterioration rate model using a time-transformation. Here we consider a simple random deterioration rate model as

$$D(t) = Rt \geq 0, \text{ with } R > 0, \tag{2.2}$$

where R is randomly distributed and reflects the uncertain nature of deterioration in a population of similar components.

The random rate model presents advantages when the experiment is based on a few inspections with no measurement errors due to its easy interpretation. However, when the number of inspections is large, the individual deterioration rate surely varies with time and the inferences for the parameters are inappropriate.

2.4.2 The Wiener process with drift

The Wiener process, also known as Brownian motion, is one of the most important stochastic processes known in the literature. Originally introduced by Brown (1828) in the study of microscopic particles movement suspended in liquid, it has its mathematical properties explored lately by Wiener (1923). The Wiener process is a continuous stochastic process $\{D(t), t > 0\}$, whose degradation path is given by

$$D(t) = D(0) + vt + \sigma B(t), \tag{2.3}$$

where $D(0)$ is the starting point, v is the drift parameter, σ is the diffusion parameter and $B(t) \sim N(0,t)$ is referred to as standard Brownian motion.

It has the following properties

- Each increment $Y = \Delta D(t)$ in the time interval $\Delta t > 0$ is normally distributed:

$$Y \sim N\left(v\Delta t, \sigma^2 \Delta t\right);$$

- The increments are independent and stationary.

From Chhikara and Folks (1989), the first passage time (2.1) of a Wiener process with positive drift $(v > 0)$ is inverse Gaussian distributed:

$$T \sim \text{IG}\left(\frac{\rho - D(0)}{v}, \frac{(\rho - D(0))^2}{\sigma^2}\right).$$

In this thesis, we consider the special case when $D(0) = 0$, which means that the degradation paths have increasing behavior starting at the origin of the coordinate system.

2.4.3 The gamma process

The gamma process is a continuous stochastic process $\{D(t); t \geq 0\}$ with shape function $\varphi_{\boldsymbol{\psi}}(t)$ and scale parameter υ (NOORTWIJK, 2009) given by

$$D(t) \sim \text{ Gamma } \left[\varphi_{\boldsymbol{\psi}}(t), \upsilon\right], \tag{2.4}$$

where $\varphi_{\boldsymbol{\psi}}(.)$ is a monotone increasing function of time t indexed by the parameter vector $\boldsymbol{\psi}$, with $\varphi_{\boldsymbol{\psi}}(0) = 0$.

It holds the following properties:

- $D(0) = 0$;
- Each increment $Y = \Delta D(t)$ in the time interval $\Delta t > 0$ is gamma distributed:

$$Y \sim \text{ Gamma } \left(\Delta\varphi_{\boldsymbol{\psi}}(t), \upsilon\right),$$

  where $\Delta\varphi_{\boldsymbol{\psi}}(t)$ is the increment of $\varphi_{\boldsymbol{\psi}}(.)$ in the time interval Δt;
- The increments are independent.

The increments are always positive with probability density function (PDF) given by

$$f(y) = \frac{y^{\Delta\varphi_{\boldsymbol{\psi}}(t)-1}}{\Gamma[\Delta\varphi_{\boldsymbol{\psi}}(t)]\upsilon^{\Delta\varphi_{\boldsymbol{\psi}}(t)}} \exp\left(-\frac{y}{\upsilon}\right).$$

Therefore, the mean and variance of the degradation increments are given by

$$\mathrm{E}(y) = \Delta\varphi_{\boldsymbol{\psi}}(t)\upsilon \text{ and } \mathrm{VAR}(y) = \Delta\varphi_{\boldsymbol{\psi}}(t)\upsilon^2.$$

2.4.4 The inverse Gaussian process

First we present a brief review of the inverse Gaussian distribution.

2.4.4.1 The inverse Gaussian distribution

The inverse Gaussian (IG) distribution has its PDF given by

$$f_{IG}(y|\mu,\lambda) = \sqrt{\frac{\lambda}{2\pi y^3}} \times \exp\left[-\frac{\lambda(y-\mu)^2}{2\mu^2 y}\right], \tag{2.5}$$

where $y > 0$, $\mu > 0$ is the mean and $\lambda > 0$ is the shape parameter.

Then we can write $Y \sim \text{IG}(\mu, \lambda)$ to indicate that the random variable Y is inverse Gaussian distributed with mean μ and shape parameter λ.

The cumulative distribution function (CDF) of the IG distribution is given by

$$F_{IG}(y|\mu,\lambda) = \Phi\left[\sqrt{\frac{\lambda}{y}}\left(\frac{y}{\mu}-1\right)\right] + \exp\left(\frac{2\lambda}{\mu}\right)\Phi\left[-\sqrt{\frac{\lambda}{y}}\left(\frac{y}{\mu}+1\right)\right], \tag{2.6}$$

where $\Phi(.)$ is the standard normal CDF.

More references on theoretical results concerning the IG distribution can be found in Seshadri (2012).

Figure 2 presents several scenarios for PDF and CDF of IG distribution.

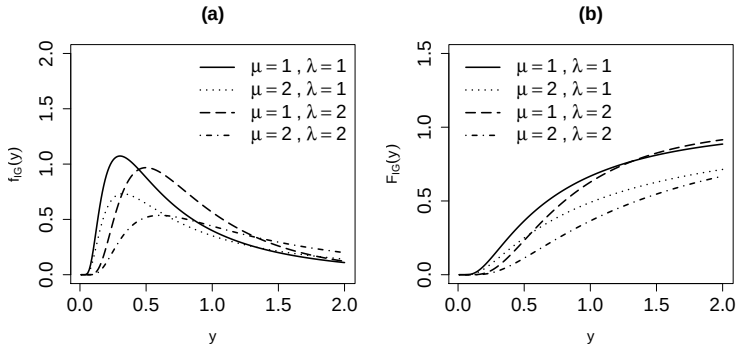

Figure 2 – (a) PDF of IG distribution under different scenarios, (b) CDF of IG distribution under different scenarios.

2.4.4.2 The inverse Gaussian process

An inverse Gaussian process (IGP) $\{D(t); t \geq 0\}$ with mean function $g_{\boldsymbol{\theta}}(t)$ and shape parameter η is a continuous-time stochastic process given by

$$D(t) \sim \text{IG}\left(g_{\boldsymbol{\theta}}(t), \eta g_{\boldsymbol{\theta}}^2(t)\right), \tag{2.7}$$

where $g_{\boldsymbol{\theta}}(.)$ is a monotone increasing function of time t indexed by the parameter vector $\boldsymbol{\theta}$, with $g_{\boldsymbol{\theta}}(0) = 0$ and $\eta > 0$.

It possesses the following properties:

- $D(0) = 0$;
- The distribution of each increment $Y = \Delta D(t)$ in the time interval Δt is given by

$$Y \sim \text{IG}\left(\Delta g_{\boldsymbol{\theta}}(t), \eta(\Delta g_{\boldsymbol{\theta}}(t))^2\right), \forall \Delta t \geq 0,$$

  where $\Delta g_{\boldsymbol{\theta}}(t)$ of $g_{\boldsymbol{\theta}}(t)$ in the time interval Δt.
- The increments are independent.

The function $g_{\boldsymbol{\theta}}(t)$ has a meaningful interpretation being the mean function of IGP and η is inversely proportional to the variance of IGP:

$$\mathrm{E}(D(t)) = g_{\boldsymbol{\theta}}(t) \text{ and } \mathrm{VAR}(D(t)) = \frac{g_{\boldsymbol{\theta}}(t)}{\eta}.$$

2.4.4.2.1 Distribution of the degradation increments

The CDF of the degradation increment Y in the time interval Δt is the probability of Y to be lower than y, and come directly from CDF of IG distribution:

$$\begin{aligned} F_{IGP}(y|\Delta g_{\boldsymbol{\theta}}(t),\eta) &= F_{IG}(y|\mu = \Delta g_{\boldsymbol{\theta}}(t), \lambda = \eta(\Delta g_{\boldsymbol{\theta}}(t))^2) \\ &= \Phi\left[\sqrt{\frac{\eta}{y}}(y - \Delta g_{\boldsymbol{\theta}}(t))\right] + \exp(2\eta\Delta g_{\boldsymbol{\theta}}(t))\Phi\left[-\sqrt{\frac{\eta}{y}}(y + \Delta g_{\boldsymbol{\theta}}(t))\right], \end{aligned} \tag{2.8}$$

where $F_{IG}(.)$ is as given in (2.6).

From (2.8) we can build up an algorithm to generate degradation paths from IGP model, which can be modified to a simpler form when dealing with softwares like R (R Core Team, 2016) and Ox (DOORNIK, 2009) which possess specific packages for generating random values from IG distribution.

Algorithm 1 : Generating degradation paths from IGP

1 Fix values for n, $g_{\boldsymbol{\theta}}(.)$ and η;
2 For each unit i, $(1 \leq i \leq n)$:

- Set $t_{i0} = 0$ and fix values for n_i and $t_{i1}, \ldots, t_{in_i}$;
- For each index j, $(1 \leq j \leq n_i)$:
  - Compute $\Delta t_{ij} = t_{i,j} - t_{i,j-1}$ and $\Delta g_{\boldsymbol{\theta}}(t_{ij}) = g_{\boldsymbol{\theta}}(t_{i,j}) - g_{\boldsymbol{\theta}}(t_{i,j-1})$;
  - Generate a random number u_{ij} from $U(0,1)$;
  - Solve the nonlinear equation for y_{ij}: $F_{IGP}(y_{ij}|\Delta g_{\boldsymbol{\theta}}(t_{ij}),\eta) = u_{ij}$;
- Compute the cumulative degradation values $d_{i1} = y_{i1}, d_{i2} = y_{i1} + y_{i2} \ldots, d_{in_i} = y_{i1} + \ldots + y_{in_i}$.

Therefore, the reliability function of the degradation increment Y is interpreted as the probability of Y to be higher than y and is given by

$$R_{IGP}(y) = 1 - F_{IGP}(y|\Delta g_{\boldsymbol{\theta}}(t),\eta). \tag{2.9}$$

This function has an inverse relationship with the component reliability because the components with high degradation increments are prone to be less reliable and present early failures.

The PDF is given by

$$\begin{aligned} f_{IGP}(y|\Delta g_{\boldsymbol{\theta}}(t),\eta) &= f_{IG}(y|\mu=\Delta g_{\boldsymbol{\theta}}(t),\lambda=\eta(\Delta g_{\boldsymbol{\theta}}(t))^2) \\ &= \sqrt{\frac{\eta}{2\pi y^3}}\Delta g_{\boldsymbol{\theta}}(t)\exp\left[-\frac{\eta(y-\Delta g_{\boldsymbol{\theta}}(t))^2}{2y}\right], \end{aligned}$$

where f_{IG} is as given in (2.5).

Another important function in reliability analysis is the intensity function

$$h_{IGP}(y|\Delta g_{\boldsymbol{\theta}}(t),\eta) = \frac{f_{IGP}(y|\Delta g_{\boldsymbol{\theta}}(t),\eta)}{R_{IGP}(y|\Delta g_{\boldsymbol{\theta}}(t),\eta)}. \tag{2.10}$$

Additionally, the cumulative intensity function is given by the integral $H_{IGP}(y|\Delta g_{\boldsymbol{\theta}}(t),\eta) = \int_0^y h_{IGP}(u|\Delta g_{\boldsymbol{\theta}}(t),\eta)du$, or equivalently

$$H_{IGP}(y|\Delta g_{\boldsymbol{\theta}}(t),\eta) = -\log(R_{IGP}(y|\Delta g_{\boldsymbol{\theta}}(t),\eta)). \tag{2.11}$$

These functions will be explored in the chapter 4 in the context of frailty models.

2.4.4.2.2 Lifetime distribution

Considering (2.1), the lifetime CDF is obtained directly from using the fact that the cumulative degradation $D(t)$ is the degradation increment in the time interval $[0,t]$ and $g_{\boldsymbol{\theta}}(t)$ is the increment of the mean function of IGP in this time interval

$$\begin{aligned} F_{T_{IGP}}(t) &= 1 - F_{IGP}(y=\rho|g_{\boldsymbol{\theta}}(t),\eta), \text{where } F_{IGP}(.) \text{ is as given in (2.8)} \\ &= \Phi\left[-\sqrt{\frac{\eta}{\rho}}(\rho - g_{\boldsymbol{\theta}}(t))\right] - \exp(2\eta g_{\boldsymbol{\theta}}(t))\Phi\left[-\sqrt{\frac{\eta}{\rho}}(\rho + g_{\boldsymbol{\theta}}(t))\right]. \end{aligned} \tag{2.12}$$

An interesting property from (2.12) turns up when $\eta g_{\boldsymbol{\theta}}(t)$ is large, which happens for large t values, then $D(t)$ is approximately normal with mean $g_{\boldsymbol{\theta}}(t)$ and variance $\frac{g_{\boldsymbol{\theta}}(t)}{\eta}$ (CHHIKARA; FOLKS, 1989). From Tang and Chang (1995), the CDF of T has Birnbaum-Saunders distribution, which is a failure time model largely used in fatigue data problems (DESMOND, 1985). Furthermore, the quantiles t_p from the lifetime distribution are obtained through the equation $F_{T_{IGP}}(t) = p$ in (2.12).

Therefore, the lifetime PDF is given by

$$\begin{aligned} f_{T_{IGP}}(t) &= \frac{\partial F_{T_{IGP}}(t)}{\partial t} \\ &= \phi\left[-\sqrt{\frac{\eta}{\rho}}(\rho - g_{\boldsymbol{\theta}}(t))\right]\frac{\partial g_{\boldsymbol{\theta}}(t)}{\partial t}\sqrt{\frac{\eta}{\rho}} \\ &\quad -\exp(2\eta g_{\boldsymbol{\theta}}(t))\Phi\left[-\sqrt{\frac{\eta}{\rho}}(\rho + g_{\boldsymbol{\theta}}(t))\right]\frac{2\eta\partial g_{\boldsymbol{\theta}}(t)}{\partial t} \\ &\quad +\exp(2\eta g_{\boldsymbol{\theta}}(t))\phi\left[-\sqrt{\frac{\eta}{\rho}}(\rho + g_{\boldsymbol{\theta}}(t))\right]\frac{\partial g_{\boldsymbol{\theta}}(t)}{\partial t}\sqrt{\frac{\eta}{\rho}}, \end{aligned} \tag{2.13}$$

where $\phi(.)$ is the standard normal PDF.

Note that (2.13) has closed form, unlike gamma process model, in which case the lifetime PDF needs to be obtained through numerical methods; see Pandey and Noortwijk (2004).

Peng (2015) obtained the meantime to failure (MTTF) from (2.13), for special case when $g_{\boldsymbol{\theta}}(t) = \theta t$, as

$$\text{MTTF} = \frac{1}{\theta}\sqrt{\frac{\rho}{\eta}}\phi(\sqrt{\eta\rho}) + \left(\frac{1}{\theta\eta} + \frac{\rho}{\theta}\right)\Phi(\sqrt{\eta\rho}) - \frac{1}{2\theta\eta}. \tag{2.14}$$

2.4.4.2.3 Inference for unknown parameters in IGP model

The likelihood function for n units being observed at the inspection times $t_{ij}, j = 0,\ldots,n_i$ is given by

$$L(g_{\boldsymbol{\theta}}(t),\eta) = \prod_{i=1}^{n}\prod_{j=1}^{n_i}\sqrt{\frac{\eta}{2\pi y_{ij}^3}}\Delta g_{\boldsymbol{\theta}}(t_{ij})\exp\left[-\frac{\eta(y_{ij} - \Delta g_{\boldsymbol{\theta}}(t_{ij}))^2}{2y_{ij}}\right],$$

where $\Delta g_{\boldsymbol{\theta}}(t_{ij}) = g_{\boldsymbol{\theta}}(t_{ij}) - g_{\boldsymbol{\theta}}(t_{i,j-1})$ is the observed increment of the mean function in the time interval $[t_{j-1}, t_j]$.

The corresponding log-likelihood function for n units up for a constant is given by

$$\begin{aligned} l(g_{\boldsymbol{\theta}}(t),\eta) &= \frac{m}{2}\log(\eta) + \sum_{i=1}^{n}\sum_{j=1}^{n_i}\log(\Delta g_{\boldsymbol{\theta}}(t_{ij})) - \frac{\eta}{2}\sum_{i=1}^{n}\sum_{j=1}^{n_i} y_{ij} \\ &\quad +\eta\sum_{i=1}^{n}\sum_{j=1}^{n_i}\Delta g_{\boldsymbol{\theta}}(t_{ij}) - \frac{\eta}{2}\sum_{i=1}^{n}\sum_{j=1}^{n_i}\frac{\left(\Delta g_{\boldsymbol{\theta}}(t_{ij})\right)^2}{y_{ij}}, \end{aligned} \tag{2.15}$$

where $m = \sum_{i=1}^{n} n_i$.

The maximum likelihood estimates (MLEs) of the parameters can be obtained by the maximization of (2.15). The interval estimates for the parameters can be based on the asymptotic normal distribution of the MLEs.

Figure 3 shows some simulated degradation paths from the random rate model, Wiener, gamma and IG processes models. Each chart consists of eight degradation paths, in which the

time scale is set from 0 up to 4 with 16 equidistant intervals. The shape function for the gamma process was specified as $\varphi_{\boldsymbol{\psi}}(t) = \psi t$, $\psi > 0$ and the mean function for the IGP was specified as $g_{\boldsymbol{\theta}}(t) = \theta t$, $\theta > 0$. All the parameter values are exhibited in the charts.

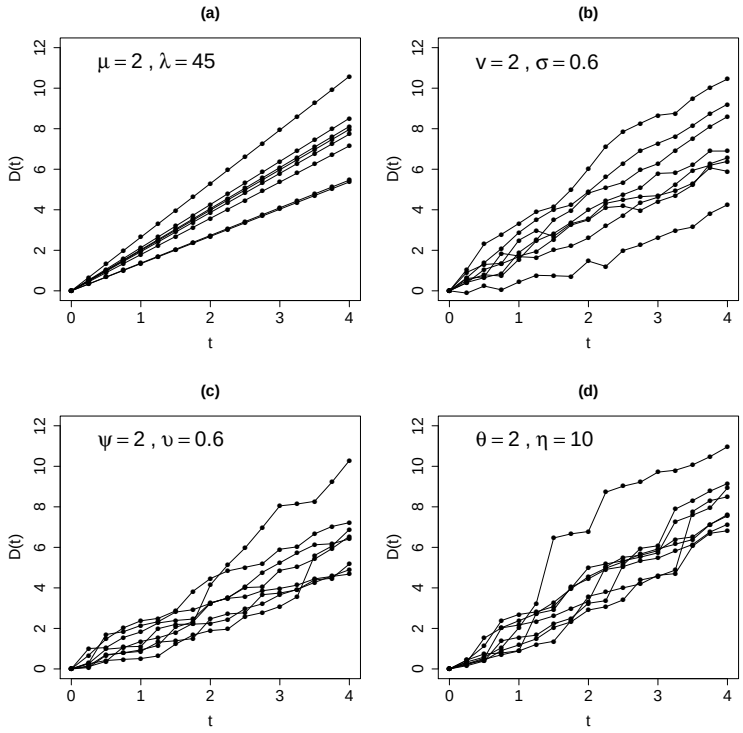

Figure 3 – Simulated degradation paths (a) random rate model (2.2), (b) Wiener process model (2.3), (c) gamma process model (2.4), (d) IGP model (2.7).

From Figure 3 we can observe that the random rate model enables different degradation slopes but does not account for temporal variability. The Wiener, gamma and IG processes show no clear difference between the degradation slopes but account for temporal variability within the paths. Moreover, the degradation paths from Wiener process can increase or decrease over time, while the paths from gamma and IG processes always grow over time.

2.5 Frailty models

In reliability analysis, incorporating the unobserved heterogeneity among experimental units is called frailty. In this thesis, the frailty term will act in the reliability of the equipments as an unobserved covariate, helping in this way to estimate the population reliability function.

Clayton (1978) introduced a frailty term in the Cox model (COX, 1972) in a multiplicative way, that is, the random variable representing the frailty, z, acts multiplicatively in the baseline hazard function $h_0(t)$ then

$$h(t|z) = zh_0(t). \tag{2.16}$$

In the multiplicative frailty model (2.16), z is a positive unobservable random variable called frailty that increases the individual hazard if $z > 1$ or decreases if $z < 1$. Intuitively,

the greater the individual frailty, the greater the probability of failure (VAUPEL; MANTON; STALLARD, 1979).

The individual hazard function $h(t|z)$ is interpreted as the conditional hazard function given z. Thus, the reliability function conditional to the frailty z is given by

$$R(t|z) = \exp\left[-\int_0^t h(s|z)ds\right] = \exp\left[-z\int_0^t h_0(s)ds\right] = \exp\left[-zH_0(t)\right], \tag{2.17}$$

where $H_0(t)$ is the cumulative baseline hazard function in time t.

The unconditional reliability function $R(t)$ is obtained by integrating (2.17) out the frailty component by means of the frailty PDF $f_{\boldsymbol{\alpha}}(z)$, indexed by the parameter vector $\boldsymbol{\alpha}$

$$R(t) = \int_0^\infty R(t|z) f_{\boldsymbol{\alpha}}(z)dz = \int_0^\infty \exp\left[-zH_0(t)\right] f_{\boldsymbol{\alpha}}(z)dz, \tag{2.18}$$

which can be obtained by Laplace transform (ABRAMOWITZ; STEGUN, 1972), stated below

Definition 2.5.1. Given a function $f(x)$, the Laplace transform of $f(x)$ with real argument s is defined as

$$\mathscr{L}[f(x)](s) = \int_0^\infty \exp(-sx) f(x)dx.$$

Therefore, the unconditional reliability function (2.18) can be rewritten as a Laplace transform:

$$R(t) = \mathscr{L}[f_{\boldsymbol{\alpha}}(z)](H_0(t)). \tag{2.19}$$

The Laplace transform plays an important role in the context of frailty models as it facilitates the achievement of unconditional reliability functions (WIENKE, 2010). In this thesis, the Laplace transforms are obtained through Wolfram Mathematica software (RESEARCH, 2016).

A remarkable feature in frailty models is related to its identifiability. According to Elbers and Ridder (1982), it is necessary that the distribution of the frailty term has finite expectation and the variance of the frailty term is interpreted as a measure of population heterogeneity. Because the frailty z is a positive random variable, we can consider different distributions such as gamma, lognormal, IG, among others positive-valued distributions. General characteristics of the distributions for the frailty term were studied by Hougaard (1995).

2.6 Model selection criteria

In order to make some comparisons between different models in the chapters along the thesis, we introduce some known criteria in the literature with a brief description.

The Akaike information criterion (AIC) (SAKAMOTO; ISHIGURO; KITAGAWA, 1986) and the Bayesian information criterion (BIC)(SCHWARZ, 1978) are measures of relative quality of a statistical model for a given dataset. The calculus of AIC and BIC are given by

$$\mathrm{AIC} = -2\log(L) + 2p,$$

where L is the maximized value of likelihood function and p is the number of parameters in the model.

$$\mathrm{BIC} = -2\log(L) + p\log(n),$$

where n is the sample size of the study.

Given a set of candidate models for the data, the preferred model is the one with the minimum AIC and BIC values. These criteria not only reward goodness of fit, but also include a penalty (they become bigger when we include more parameters in the model).

CHAPTER

3

THE RANDOM DETERIORATION RATE MODEL BASED ON INVERSE GAUSSIAN DISTRIBUTION

3.1 Introduction

In this chapter, we present the random deterioration rate model with measurement errors in order to incorporate the variability among different components. The random rate analysis is based on repeated measurements of flaw sizes created by a degradation process over time in a components population. Some features of the random rate model based on IG distribution are investigated. We conduct a simulation study to evaluate the behavior of the parameter estimators and illustrate the potentiality of the proposed model with two real-world datasets.

3.2 The random deterioration rate model with measurement errors

In engineering problems, usually data can neither be collected nor recorded precisely due to various uncertainties such as human errors, machine errors or incomplete information (XIAO *et al.*, 2012). Thereby, a source of variability may be added due to measurement errors. The random deterioration rate model is explored according to the proposal from Pandey and Lu (2013), in which a measurement error is added to the deterministic model (2.2) in order to explain the source of variability between the measurements from the same individual path. This model is an extension of (2.2), in which the degradation path of the i-th unit at time t is given by

$$D_i(t) = r_i t + \varepsilon, \tag{3.1}$$

where r_i is the random deterioration rate and ε is the measurement error.

The model (3.1) has the same formulation as the general path model (MEEKER; ESCOBAR; LU, 1998), in which the main characteristic is the randomness between units. Lu and Meeker (1993) presented an approach to analyze noisy degradation data based on the nonlinear mixed effects regression model considering normal distribution with zero mean and positive variance for the measurement errors. In this work, ε belongs to normal distribution with real mean and positive variance: $\varepsilon \sim N(\mu_\varepsilon, \sigma_\varepsilon^2)$.

From (3.1) we can build up an algorithm to generate degradation paths from random deterioration rate model given as

Algorithm 2 : Generating degradation paths from random deterioration rate model.

1 Fix values for n, μ_ε and σ_ε^2;
2 For each unit i, $(1 \leq i \leq n)$:

- Set $t_{i0} = 0$ and fix values for n_i and $t_{i1}, \ldots, t_{in_i}$;
- Generate a random number r_i from the random rate distribution (e.g. IG or gamma);
- For each index j, $(1 \leq j \leq n_i)$, generate a random value ε_{ij} from $N(\mu_\varepsilon, \sigma_\varepsilon^2)$;
- Compute the degradation values: $d_{i1} = r_i t_{i1} + \varepsilon_{i1}, d_{i2} = r_i t_{i2} + \varepsilon_{i1} \ldots, d_{in_i} = r_i t_{in_i} + \varepsilon_{in_i}$.

3.2.1 Inference for unknown parameters in random deterioration rate model

Let $d_i = d_{i1}, d_{i2}, \ldots, d_{in_i}$ be the vector of degradation measurements for the i-th unit, and the data consist of $i = 1, 2, \ldots, n$ units, then (3.1) can be rewritten:

$$D_{ij} = D_i(t_{ij}) = r_i t_{ij} + \varepsilon_{ij}, \tag{3.2}$$

where $\varepsilon_{ij} \sim N(\mu_\varepsilon, \sigma_\varepsilon^2)$.

The analysis is based on hierarchical modeling used in Bayesian literature (KASS; STEFFEY, 1989) consisting of two stages. In the first stage, the deterioration rate r_i is regarded as a latent parameter whose distribution is modeled in the second stage with a hyperparameter vector $\boldsymbol{\beta}$. These stages are reported below

- ✔ Stage 1: The vector $\mathbf{d}_i$ is conditioned on given r_i and $\boldsymbol{\beta}$, which is seen as a latent parameter for unit i, with distribution $f(\mathbf{d}_i | r_i, \boldsymbol{\beta})$,
- ✔ Stage 2: Conditionally on $\boldsymbol{\beta}$, r_i constitutes an independent and identically distributed (i.i.d.) sample from $f(r_i|\boldsymbol{\beta})$, and r_i and $\boldsymbol{\beta}$ are referred to as "random" and "fixed" effects, respectively.

Therefore, from conditional independence, the joint density of the data from all units, $\mathbf{d} = \mathbf{d}_1, \ldots, \mathbf{d}_n$ is a product of specified densities:

$$f(\mathbf{d}|\boldsymbol{\beta}) = \prod_{i=1}^{n} f(\mathbf{d}_i|\boldsymbol{\beta}),$$

where the unit specific density is a marginal distribution as follows

$$f(\mathbf{d}_i|\boldsymbol{\beta}) = \int_{R_i} f(\mathbf{d}_i|\boldsymbol{\beta}) f(r_i|\boldsymbol{\beta}) dr_i.$$

The hierarchical approach is coherent for analyzing noisy data and is not limited to linear degradation law.

Considering (3.2) and r_i fixed, the degradation measure $D_{ij} \sim N(\mu_\varepsilon + r_i t_{ij}, \sigma_\varepsilon^2)$. Thus the PDF of a measured degradation is given as

$$f(d_{ij}|r_i) = \frac{1}{\sqrt{2\pi}\sigma_\varepsilon} \exp\left[-\frac{\left(d_{ij} - \mu_\varepsilon - r_i t_{ij}\right)^2}{2\sigma_\varepsilon^2}\right].$$

From the concept of the hierarchical modeling, the degradation measures $\mathbf{d}_i$, are normally distributed with the deterioration rate r_i as a parameter, while r_i itself has the PDF $f_{\boldsymbol{\beta}}(r_i)$.

Using the theorem of total probability, the marginal likelihood function for measurements of an i-th unit can be written as

$$\begin{aligned} L_i(\mu_\varepsilon, \sigma_\varepsilon^2, \boldsymbol{\beta}) &= \int_0^\infty \prod_{j=1}^{n_i} \frac{1}{\sqrt{2\pi}\sigma_\varepsilon} \exp\left[-\frac{(d_{ij} - \mu_\varepsilon - r_i t_{ij})^2}{2\sigma_\varepsilon^2}\right] f_{\boldsymbol{\beta}}(r_i) dr_i \\ &= \int_0^\infty \left(\frac{1}{\sqrt{2\pi}\sigma_\varepsilon}\right)^{n_i} \exp\left[-\frac{1}{2\sigma_\varepsilon^2} \sum_{j=1}^{n_i} (d_{ij} - \mu_\varepsilon - r_i t_{ij})^2\right] f_{\boldsymbol{\beta}}(r_i) dr_i \\ &= L_{1i} \times L_{2i}, \end{aligned} \tag{3.3}$$

where the first term in L_{1i} does not depend on $\boldsymbol{\beta}$ and the second term L_{2i} depends on $\boldsymbol{\beta}$ through the integral over r_i.

The likelihood function for a sample of n independent units is the product of the terms $L_1, \ldots, L_n$:

$$L(\mu_\varepsilon, \sigma_\varepsilon^2, \boldsymbol{\beta}) = \prod_{i=1}^{n} L_{1i} \times L_{2i}.$$

Therefore, the corresponding log-likelihood is

$$l(\mu_\varepsilon, \sigma_\varepsilon^2, \boldsymbol{\beta}) = \sum_{i=1}^{n} \log(L_{1i}) + \sum_{i=1}^{n} \log(L_{2i}). \tag{3.4}$$

3.2.2 Lifetime distribution

Considering (2.1), the lifetime CDF is given by

$$F_T(t) = P[D(t) \geq \rho] = P[rt \geq \rho] = 1 - F_R\left(\frac{\rho}{t}\right), \tag{3.5}$$

where $F_R(.)$ is the deterioration rate CDF.

The quantiles t_p are obtained through the equation $F_T(t) = p$.

Therefore, the lifetime PDF is obtained

$$f_T(t) = \frac{\partial F_T(t)}{\partial t}. \tag{3.6}$$

Considering the nature of degradation data, one may assume a positive-valued distribution for the deterioration rate r. In this work we assume IG distribution for r.

3.2.3 IG distribution for the random deterioration rate

We shall assume that r_i's are an i.i.d. sample from IG distribution, then we have

$$D_i(t_{ij}) = r_{ij}t + \varepsilon_{ij}, \text{ where } r_i \sim \text{IG}(\mu,\lambda), \mu > 0 \text{ and } \lambda > 0, \tag{3.7}$$

and the PDF for IG distribution is as given in (2.5).

Figure 4 displays some degradation paths from IG random rate model (3.7) as a result of Algorithm 2. Each chart consists of 10 units being evaluated from 0 up to 4 time units with 8 equidistant intervals. The parameter values are exhibited in the charts. We can observe that a decrease in λ leads to an increase in the variability between the paths, while an increase in σ_ε^2 leads to an increase in the variability within the paths. Even though the paths possess increasing behavior, the model formulation allows ups and downs due to measurement errors.

3.2.3.1 Inference

The second term in (3.3) can be rewritten as

$$L_{2i} = \int_0^\infty \exp\left[-\frac{1}{2\sigma_\varepsilon^2}\sum_{j=1}^{n_i}(d_{ij} - \mu_\varepsilon - r_i t_{ij})^2\right]\sqrt{\frac{\lambda}{2\pi r_i^3}}\exp\left[-\frac{\lambda(r_i-\mu)^2}{2\mu^2 r_i}\right]dr_i, \tag{3.8}$$

which is intractable analytically due to the fact that the integral does not have closed expression.

The Gaussian quadrature method arises to solve this problem. This method aims to approximate an integral of a continuous function with respect to a quantity x on X as a weighted sum of this function evaluated at a set of nodes (also called quadrature points):

$$\int_X f(x)dx \approx \sum_{q=1}^{Q} w_j f(x_j),$$

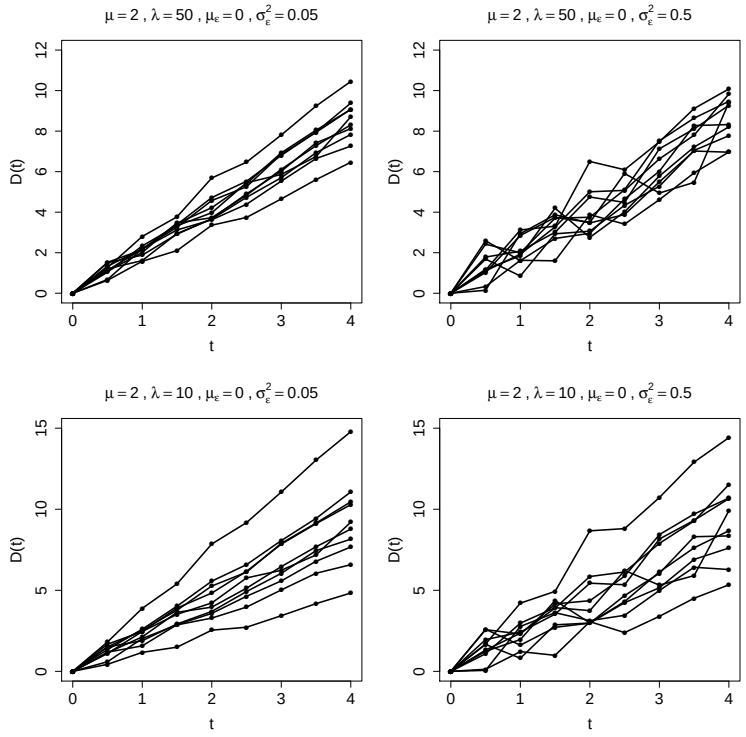

Figure 4 – Degradation paths from IG random rate model under different scenarios.

where the coefficients $w_1, \ldots, w_Q$ are the weights and $x_1, \ldots, x_N \in X$ are the nodes.

Some papers concerning Gaussian quadrature in regression modeling with random effects include Pinheiro and Bates (1995), Lesaffre and Spiessens (2001), Carrasco, Ferrari and Arellano-Valle (2014) and Crowther *et al.* (2016).

The Monte Carlo integration technique is another alternative to solve integrals though one may rewrite (3.8) so that the integral becomes over another distribution with known parameters. Therefore, one can use the Probability Integral Transform (NELSON *et al.*, 2006) or the reformulation likelihood method (LIU; YU, 2008).

The Gaussian quadrature is faster than the Monte Carlo method in obtaining numeric integrals. In this work we obtained the approximation of the integral in (3.8) by the one-dimensional globally adaptive integrator 15-points Gauss-Kronrod with extrapolation over infinite intervals, which is an extension of Gaussian quadrature.

Once we have obtained the numerical result for the mentioned integral, the MLEs can be obtained by direct maximization of (3.4) with respect to the parameters. Intervals estimates and hypothesis tests are obtained asymptotically.

3.2.3.2 Lifetime distribution

Considering IG distribution for the random rate, the lifetime CDF (3.5) becomes

$$F_T(t) = \Phi\left[-\sqrt{\frac{\lambda t}{\rho}}\left(\frac{\rho}{t\mu} - 1\right)\right] - \exp\left(\frac{2\lambda}{\mu}\right) \times \Phi\left[-\sqrt{\frac{\lambda t}{\rho}}\left(\frac{\rho}{t\mu} + 1\right)\right]. \tag{3.9}$$

The quantiles of (3.9) have no analytical form, so they are obtained numerically.

Therefore the lifetime PDF in (3.5) becomes

$$f_T(t) = \exp\left[-\frac{\lambda(-\mu t+\rho)^2}{2\mu^2 t\rho}\right]\sqrt{\frac{\lambda}{2\pi\rho t}}.$$

Hence, the MTTF is given by

$$\text{MTTF} = \frac{\rho(\mu+\lambda)}{\mu\lambda}.$$

Peng and Tseng (2009) gave special attention to MTTF estimation, which may be greatly influenced by model misspecification in degradation analysis.

3.3 Simulation study

A simulation study was carried out based on the generation of 1,000 artificial datasets from IG random rate model (3.7) with five different sample sizes (n): 10, 20, 30, 50 and 100. The components are evaluated from 0 up to 4 time units with 10 equidistant intervals. The scale parameters are kept fixed: $\mu = 2$ and $\mu_\varepsilon = 0$, while the shape parameters assume different values: $\lambda = 10$ or 50, and $\sigma_\varepsilon^2 = 0.05$ or 0.5. These parameter values provide degradation paths with similar characteristics to the LASER data (example 2.2.1), in which the variation of λ and σ_ε^2 characterizes a source of variation among and within the paths, respectively.

The MLEs of the model parameters, the coverage probabilities at level 95% (95% CPs) and the mean square errors of the MLEs (MSEs) under different λ and σ_ε^2 values are discussed.

Table 2 shows the MLEs, 95% CPs and MSEs under $\sigma_\varepsilon^2 = 0.05$ and $\sigma_\varepsilon^2 = 0.5$, in which we conclude that in general the MLEs are close to the corresponding true values.

Figure 5 shows the 95% CPs and Figure 6 shows the MSEs. In order to analyze the 95% CPs, we report two scenarios:

- ✔ When $\sigma_\varepsilon^2 = 0.05$ and n increases, the 95% CPs for μ and λ are closer to 95% and the 95% CPs for μ_ε and σ_ε^2 are closer to 90% which is acceptable,
- ✔ When $\sigma_\varepsilon^2 = 0.5$ and n increases, all 95% CPs are closer to the nominal value (95%).

Additionally, the MSEs are lower as n increases for different σ_ε^2 values.

Regarding the 95% CP values close to 90% for $\sigma_\varepsilon^2 = 0.05$ we can observe that the lower the σ_ε^2, the smaller the variability within the paths. Meanwhile, the larger the sample size, the higher the variability among the paths. Thereby, the MLEs of μ_ε and σ_ε^2 carry a tiny bias even for large sample sizes.

Table 2 – MLEs, 95% CPs and MSEs under different σ_ε^2 values.

		$\sigma_\varepsilon^2 = 0.05$			$\sigma_\varepsilon^2 = 0.5$		
n	Parameter	MLE	95% CP	MSE	MLE	95% CP	MSE
10	$\mu(2)$	1.9988	0.9130	0.0153	1.9997	0.9230	0.0184
	$\lambda(50)$	73.830	0.9620	2946.0	78.7930	0.9550	5627.0
	$\mu_\varepsilon(0)$	0.0001	0.9370	0.0024	0.0008	0.9380	0.0234
	σ_ε^2	0.0495	0.9300	0.0001	0.4951	0.9300	0.0055
20	$\mu(2)$	2.0022	0.9300	0.0080	1.9992	0.9230	0.0101
	$\lambda(50)$	59.8800	0.9670	630.86	61.4230	0.9700	802.81
	$\mu_\varepsilon(0)$	0.0006	0.9520	0.0012	0.0002	0.9500	0.0113
	σ_ε^2	0.0499	0.9530	0.00002	0.4981	0.9400	0.0028
30	$\mu(2)$	1.9992	0.9450	0.0052	2.0013	0.9380	0.0067
	$\lambda(50)$	56.0010	0.9650	269.31	55.8910	0.9700	292.90
	$\mu_\varepsilon(0)$	0.00004	0.9570	0.0007	-0.0012	0.9480	0.0078
	σ_ε^2	0.0500	0.9490	0.00002	0.4995	0.9490	0.0019
50	$\mu(2)$	1.9997	0.9530	0.0030	2.0008	0.9600	0.0036
	$\lambda(50)$	53.2550	0.9560	124.8400	53.3090	0.9670	148.6100
	$\mu_\varepsilon(0)$	-0.0031	0.9300	0.0007	-0.0012	0.9590	0.0046
	σ_ε^2	0.0506	0.9130	0.00003	0.4993	0.9440	0.0012
100	$\mu(2)$	1.9989	0.9470	0.0016	1.9989	0.9590	0.0019
	$\lambda(50)$	52.0270	0.9600	57.7280	51.7530	0.9520	69.1820
	$\mu_\varepsilon(0)$	-0.0023	0.9160	0.0003	0.0013	0.9490	0.0023
	σ_ε^2	0.0509	0.8920	0.00002	0.5008	0.9500	0.0005

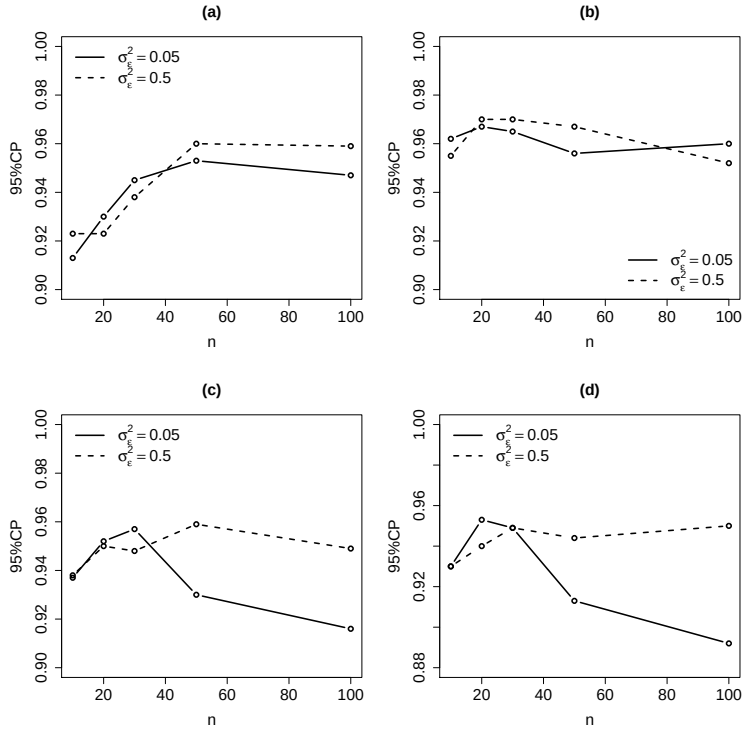

Figure 5 – 95% CPs under different σ_ε^2 values: (a) 95% CPs for μ, (b) 95% CPs for λ, (c) 95% CPs for μ_ε, (d) 95% CPs for σ_ε^2.

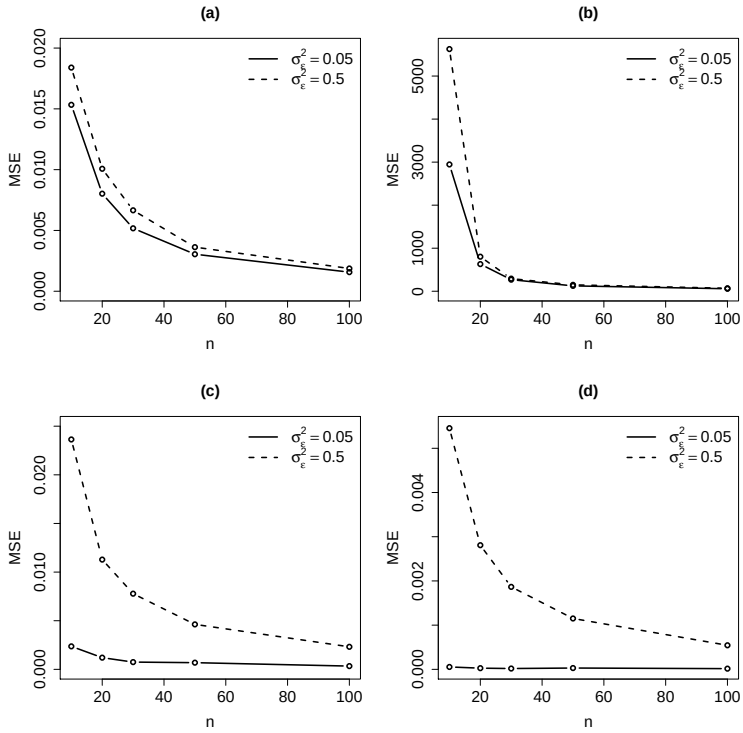

Figure 6 – MSEs under different σ_ε^2 values: (a) MSEs for μ, (b) MSEs for λ, (c) MSEs for μ_ε, (d) MSEs for σ_ε^2.

Table 3 shows the MLEs, 95% CPs and MSEs under $\lambda = 20$ and $\lambda = 50$. Figure 7 shows the 95% CPs and Figure 8 shows the MSEs of the MLEs. We conclude that the MLEs are close to the corresponding true values for different λ values. Moreover, as n increases, the 95% CPs are closer to the nominal value and the MSEs are lower.

Table 3 – MLEs, 95% CPs and MSEs under different λ values.

		$\lambda = 20$			$\lambda = 50$		
n	Parameter	MLE	95% CP	MSE	MLE	95% CP	MSE
10	$\mu(2)$	2.0016	0.9240	0.0396	1.9997	0.9230	0.0184
	λ	29.8610	0.9610	567.21	78.7930	0.9550	5627.0
	$\mu_\varepsilon(0)$	0.0011	0.9400	0.0236	0.0008	0.9380	0.0234
	$\sigma^2_\varepsilon(0.5)$	0.4951	0.9290	0.0055	0.4951	0.9300	0.0055
20	$\mu(2)$	1.9977	0.9160	0.0222	1.9992	0.9230	0.0101
	λ	24.3220	0.9690	114.42	61.4230	0.9700	802.81
	$\mu_\varepsilon(0)$	0.0003	0.9510	0.0113	0.0002	0.9500	0.0113
	$\sigma^2_\varepsilon(0.5)$	0.4981	0.9400	0.0028	0.4981	0.9400	0.0028
30	$\mu(2)$	2.0021	0.9400	0.0145	2.0013	0.9380	0.0067
	λ	22.2440	0.9660	44.076	55.8910	0.9700	292.90
	$\mu_\varepsilon(0)$	-0.0011	0.9480	0.0078	-0.0012	0.9480	0.0078
	$\sigma^2_\varepsilon(0.5)$	0.4995	0.9510	0.0017	0.4995	0.9490	0.0019
50	$\mu(2)$	2.0008	0.9500	0.0081	2.0008	0.9600	0.0036
	λ	21.2260	0.9650	21.5060	53.3090	0.9670	148.6100
	$\mu_\varepsilon(0)$	-0.0011	0.9570	0.0046	-0.0012	0.9590	0.0046
	$\sigma^2_\varepsilon(0.5)$	0.4993	0.9440	0.0012	0.4993	0.9440	0.0012
100	$\mu(2)$	1.9981	0.9640	0.0041	1.9989	0.9590	0.0019
	λ	20.6555	0.9530	10.4000	51.7530	0.9520	69.1820
	$\mu_\varepsilon(0)$	0.0013	0.9470	0.0023	0.0013	0.9490	0.0023
	$\sigma^2_\varepsilon(0.5)$	0.5008	0.9510	0.0005	0.5008	0.9500	0.0005

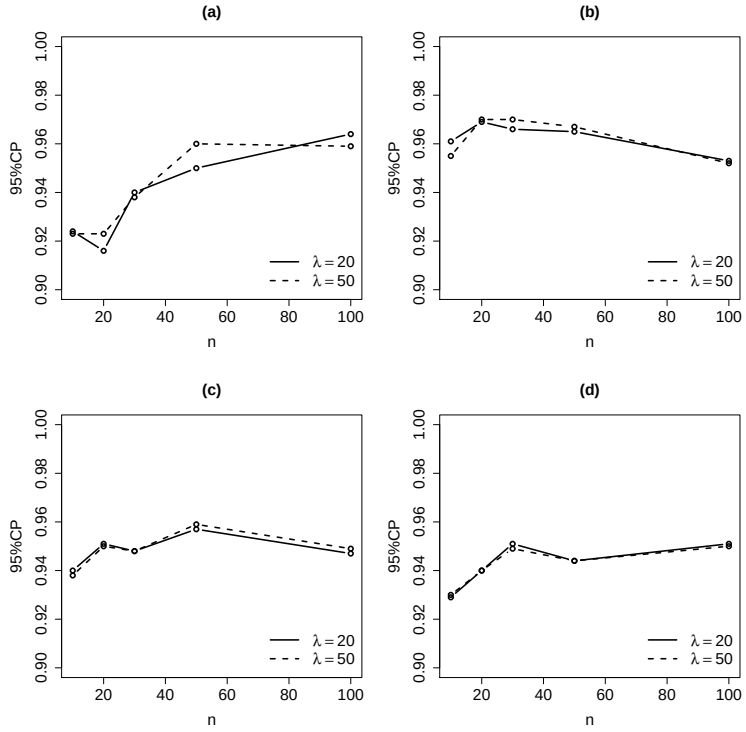

Figure 7 – 95% CPs under different λ values: (a) 95% CPs for μ, (b) 95% CPs for λ, (c) 95% CPs for μ_ε, (d) 95% CPs for σ^2_ε.

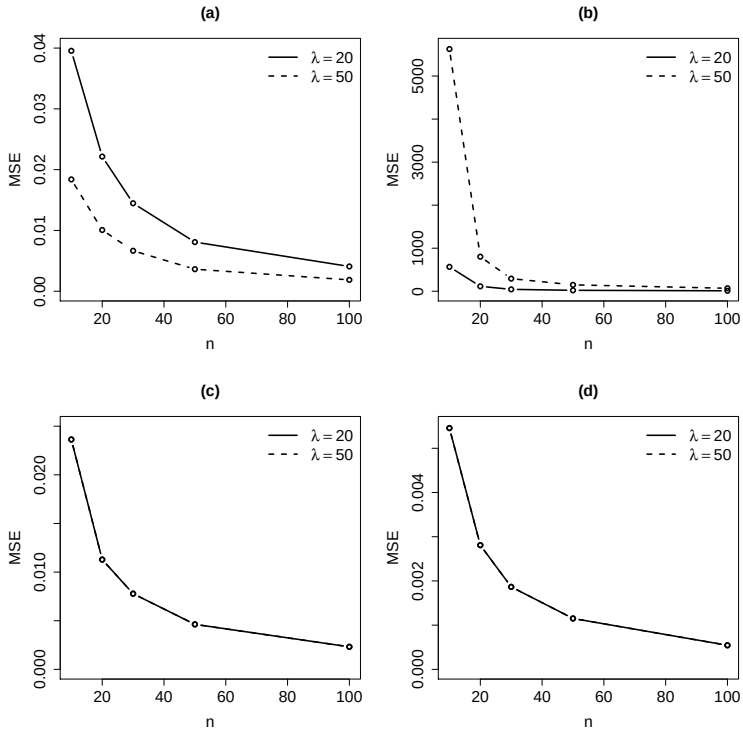

Figure 8 – MSEs under different λ values: (a) MSEs for μ, (b) MSEs for λ, (c) MSEs for μ_ε, (d) MSEs for σ^2_ε.

3.4 Application

For the sake of analysis, we bring forward the random deterioration rate with gamma distribution (PANDEY; LU, 2013), referred to as Gamma random rate model along the section.

$$D_i(t_{ij}) = r_i t_{ij} + \varepsilon_{ij}, \text{ where } r_i \sim \text{Gamma}(\varphi, \upsilon), \varphi > 0 \text{ and } \upsilon > 0, \tag{3.10}$$

whose PDF is $f(r_i) = \frac{\upsilon^\varphi}{\Gamma(\varphi)} r_i^{\varphi-1} \exp\left(-\frac{r_i}{\upsilon}\right)$.

In the application with the LASER and locomotive wheels data, the parameter estimation was achieved by the Quasi-Newton optimization method through BFGS algorithm. The values used to initialize this algorithm in IG random rate model were obtained by the following steps:

1. Let $\mu^{(0)}$, $\lambda^{(0)}$, $\mu_\varepsilon^{(0)}$ and $\sigma_\varepsilon^{2(0)}$ be the starting values of μ, λ, μ_ε and σ^2_ε, respectively;
2. For each degradation path, fit the model (3.7) by the least square method, obtaining the observed degradation rates $\widehat{r_1}, \widehat{r_2}, \ldots, \widehat{r_n}$ of $r_1, r_2, \ldots, r_n$, respectively;
3. Suppose that $\widehat{r_1}, \widehat{r_2}, \ldots, \widehat{r_n} \sim IG(\mu, \lambda)$ then $\mu^{(0)}$ and $\lambda^{(0)}$ are taken as the MLEs of μ and λ, respectively;
4. Obtain the residuals $\widehat{e_{ij}} = D_i(t_{ij}) - \widehat{r_i} t_{ij}$ ($i = 1, \ldots, n$ and $j = 1, \ldots, n_i$), then $\mu_\varepsilon^{(0)}$ and $\sigma_\varepsilon^{2(0)}$ are taken as the sample mean and the sample variance of the residuals, respectively.

The starting values for gamma random rate model are obtained similarly.

3.4.1 The LASER data (example 2.2.1)

It is worth mentioning that these LASER data were firstly analyzed by Meeker and Escobar (1998) under the approximate degradation analysis. They first fitted straight lines through the origin for each degradation path, then obtained the pseudo times to failure. Therefore, they proceeded with likelihood analysis under Weibull distribution for the failure times and made inferences about the time to failure distribution.

Table 4 shows the MLEs, the standard errors of the MLEs (SEs) and the 95% confidence intervals (95% CIs) of the parameters under IG random rate model (3.7) and Gamma random rate model (3.10) based on the LASER data, from which we conclude that the MLEs of μ_ε and σ_ε^2 are identical in both models as well as the corresponding SEs and 95% CIs. Furthermore, the measurement errors are slightly offset to the right, assuming more positive values than negative values. For illustrative purposes, each unit time stands for $1,000$ hours of operation, then the MLE of μ and λ in model (3.7) as well as the MLE of υ in model (3.10) must be divided by $1,000$ for practical interpretation.

Table 4 – MLEs, SEs and 95% CIs of the model parameters based on the LASER data.

Model	Parameter	MLE	SE	95% CI
IG random rate model (3.7)	μ	2.0418	0.1094	[1.8275; 2.2562]
	λ	47.976	17.5780	[13.524; 82.4290]
	μ_ε	0.0131	0.0279	[−0.0416; 0.0677]
	σ_ε^2	0.0424	0.0040	[0.0346; 0.0502]
Gamma random rate model (3.10)	φ	23.0620	8.3833	[6.6309; 39.4930]
	υ	0.0885	0.0325	[0.0248; 0.15228]
	μ_ε	0.0130	0.0279	[−0.0416; 0.0677]
	σ_ε^2	0.0424	0.0040	[0.0346; 0.0502]

Table 5 exhibits the model selection criteria AIC and BIC (for more detail one may refer to section 2.6), in which we conclude that the IG random rate model best fitted this dataset given that the BIC and AIC values are the smallest.

Table 5 – AIC and BIC based on the LASER data.

Model	AIC	BIC
IG random rate model 3.7	19.1214	21.9536
Gamma random rate model 3.10	19.9464	22.7786

In addition, we resort to P-P plot and Anderson-Darling (AD) test of the observed degradation rates to assess the goodness-of-fit of IG and gamma random rate models. The observed degradation rates are computed through a simple linear regression model without intercept fitted to each degradation path. The test is explored according to the proposal of Villaseñor and Gonzalez-Estrada (2015), which consists in transforming IG variables into

gamma variables and using the AD test for the gamma distribution. According to the authors, this method presents satisfactory performance even for small sample sizes. Figure 9 shows the IG and gamma P-P plots along with the AD test for the observed degradation rates, from which we conclude that both IG and Gamma random rate models are suitable for describing the LASER degradation data (the p-values are greater than 0.05 in both cases).

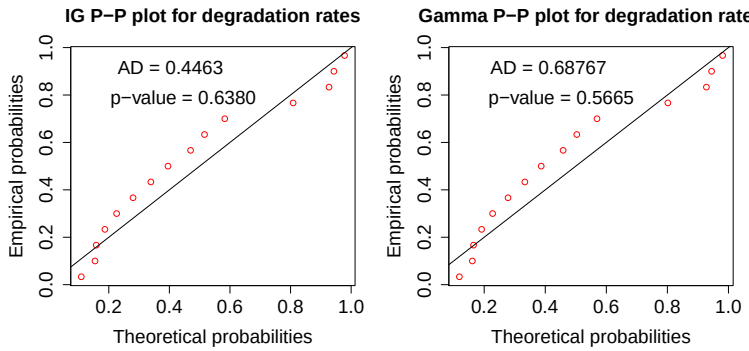

Figure 9 – IG P-P plot and gamma P-P plot of the observed degradation rates based on the LASER data.

Finally, Table 6 shows the lifetime percentiles and MTTF for the LASER components. From Table 6 we observe that the estimated lifetime percentiles and MTTF are similar to each other and approximately 80% of the LASER components are supposed to have failed up to 6,000 hours of operation. These results are similar to the analysis from Meeker and Escobar (1998), in which the 80-th percentile of the pseudo lifetimes under Weibull distribution is equal to 5932.2250 hours, whereas the MTTF is equal to 5127.8600 hours. Indeed, they pointed out that the results by the approximate method are satisfactory when the degradation paths are relatively simple.

Figure 10 displays the charts of the estimated CDF and PDF under IG and Gamma random rate models, from which we conclude that the PDF and CDF curves are similar to each other.

Table 6 – MLEs and 95% CIs of the lifetime quantiles and MTTF based on the LASER data.

	IG random rate model (3.7)		Gamma random rate model (3.7)	
Quantity	MLE	95% CI	MLE	95% CI
$t_{0.1}$	3.8468	[3.3088; 4.3849]	3.8429	[3.3373; 4.3486]
$t_{0.5}$	5.0014	[4.4815; 5.5213]	4.9691	[4.4399; 5.4984]
$t_{0.8}$	5.9424	[5.2234; 6.6614]	5.9589	[5.1742; 6.7435]
MTTF	5.1060	[4.5698; 5.6422]	5.1195	[4.5519; 5.6871]

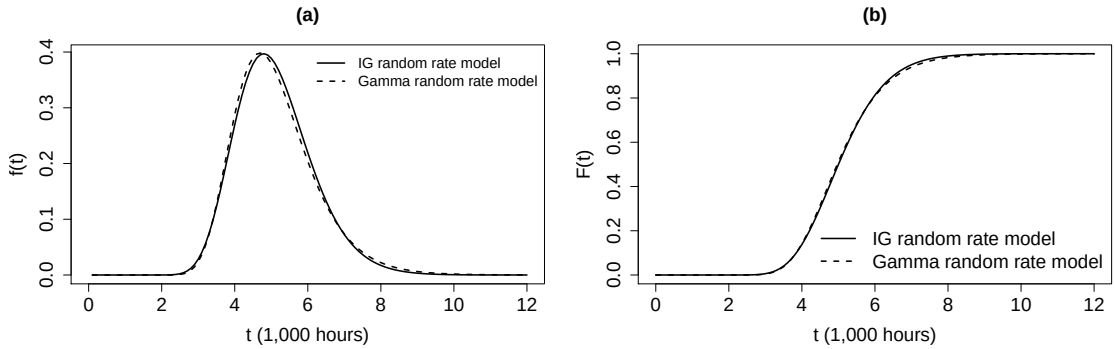

Figure 10 – Lifetime distribution based on LASER data: (a) Lifetime PDF, (b) Lifetime CDF.

3.4.2 The locomotive wheels data (example 2.2.2)

Table 7 shows the MLEs, SEs and 95% CIs of the parameters under IG random rate model (3.7) and Gamma random rate model (3.10) based on the locomotive wheels data, from which we conclude that the MLEs of μ_ε and σ_ε^2 are identical in both models and the corresponding SEs and 95% CIs are similar to each other. It is worth mentioning that the measurement errors distribution is shifted to the right of zero, which means that the errors tend to assume more positive values than negative ones. For easy viewing, the distance scale is expressed in $1,000$ km traveled, then the MLE of μ and λ in (3.7), as well as the MLE of υ in (3.10) must be divided by $1,000$ in practical situations.

Table 7 – MLEs, SEs and 95% CIs of model parameters based on the locomotive wheels data.

Model	Parameter	MLE	SE	95% CI
IG random rate model (3.7)	μ	0.0994	0.0174	[0.0653; 0.1334]
	λ	0.2324	0.0879	[0.0600; 0.4048]
	μ_ε	1.0331	0.1445	[0.7499; 1.3164]
	σ_ε^2	0.7151	0.0846	[0.5493; 0.8808]
Gamma random rate model (3.10)	φ	2.7985	1.0016	[0.83534; 4.7617]
	υ	0.0355	0.0139	[0.0082; 0.0628]
	μ_ε	1.0331	0.1445	[0.7505; 1.3171]
	σ_ε^2	0.7151	0.0846	[0.5493; 0.8808]

Table 8 exhibits the model selection criteria AIC and BIC, in which we conclude that the IG random rate model best fitted this dataset.

Table 8 – AIC and BIC based on the locomotive wheels data.

Model	AIC	BIC
IG random rate model (3.7)	517.940	520.497
Gamma random rate model (3.10)	519.727	522.283

Additionally, Figure 11 shows the IG and gamma P-P plots along with the AD test of the observed degradation rates, from which we conclude that both IG and Gamma random rate models are suitable for describing the locomotive wheels data (the p-values are greater than 0.05 in both cases).

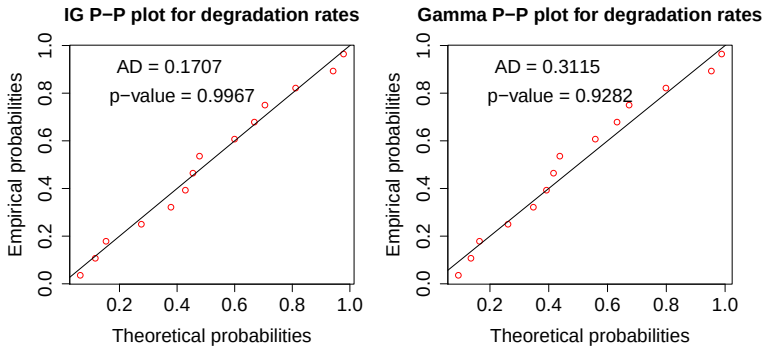

Figure 11 – IG P-P plot and gamma P-P plot of the observed degradation rates based on the locomotive wheels data.

Finally, Table 9 shows the lifetime percentiles and MTTF for the locomotive wheels and Figure 10 displays the charts of the estimated CDF and PDF under IG and Gamma random rate models. From Table 6 we observe that the estimated lifetime percentiles and MTTF are similar to each other and approximately 80% of the wheels need to be switched off up to $1,560,000$ km travelled. From Figure 12 we observe that PDF and CDF curves are similar to each other.

Table 9 – MLEs and 95% CIs of the lifetime quantiles and MTTF based on the locomotive wheels data.

	IG random rate model (3.7)		Gamma random rate model (3.7)	
Quantity	MLE	95% CI	MLE	95% CI
$t_{0.1}$	430.19	[279.91;580.48]	423.45	[240.15;606.74]
$t_{0.5}$	876.86	[591.09;1162.6]	936.55	[645.08;1228.0]
$t_{0.8}$	1563.8	[848.92;2278.7]	1559.80	[1005.0;2114.6]
MTTF	1205.78	[602.44;1809.1]	1106.24	[744.27;1468.2]

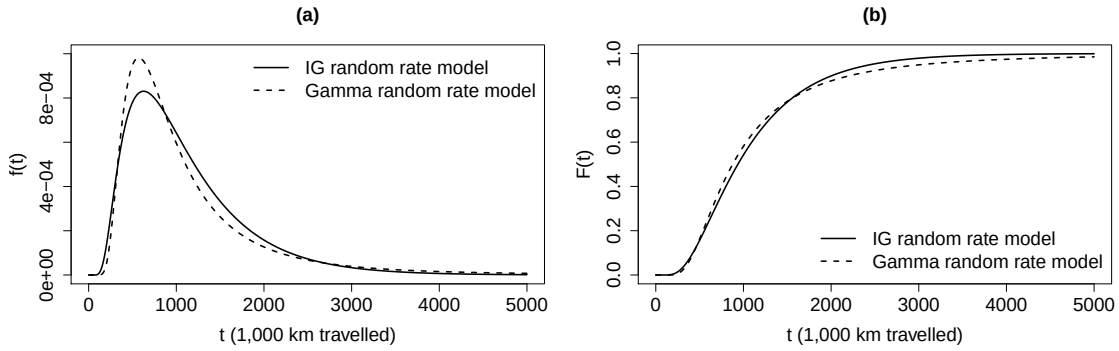

Figure 12 – Lifetime distribution based on the locomotive wheels data: (a) Lifetime PDF, (b) Lifetime CDF.

3.5 Concluding remarks

We have proposed a random deterioration rate model with measurement errors, in which the individual random rates belong to IG distribution. The IG random rate model takes into account the variability in the degradation data coming from distinct fonts: the unit-varying uncertainty among different units, the temporal variability and the variability due to measurement errors. Due to intractable integrals in the likelihood function and its derivatives, we proposed to approximate it by a quadrature method and then determine the MLEs of the model parameters. The methodology was implemented by the QUADPACK routine (PIESSENS *et al.*, 2012) along with the Quasi-Newton optimization method through BFGS algorithm available in Ox software (DOORNIK, 2009). The methods presented convergence in the simulation study and in the application with the real datasets. The simulation study showed that in general the MLEs tend to be unbiased and consistent even when the data are disturbed by the variability of the measurement errors, which means that the asymptotic intervals are propitious to use in practical situations. The application with the LASER data and the locomotive wheels data showed that the IG and Gamma random rate models provided similar results, however the first one best fitted both datasets.

CHAPTER

4

INVERSE GAUSSIAN PROCESS WITH FRAILTY TERM IN RELIABILITY ANALYSIS

4.1 Introduction

This chapter aims to include a frailty term in the stochastic process that expresses the variability between individuals and the variability in the measurements of the same individual. Also, it can take into account important variables that can neither be observed nor measured. We introduce the IGP with frailty term, referred to as IGP frailty model along the sections. Ye and Chen (2014) considered an IGP model with random drift varying between units, similar to Crowder and Lawless (2007) and Peng and Tseng (2009) that incorporated random effects in Wiener process. We consider an alternative to the IGP with random effects, in which the random effect called frailty is incorporated in the intensity function of the IGP model. We conduct a simulation study to evaluate the behavior of the parameter estimators and illustrate the potentiality of the proposed model with two real-world datasets.

4.2 The IGP frailty model based on degradation increments

The construction of a frailty IGP grounded on the multiplicative frailty model (2.16) may possess some peculiarities. Firstly, the intensity function describes the intensity over the degradation increments, which is different from the hazard rate in lifetime analysis. Secondly, the frailty must have an inversely proportional relationship with intensity, that is, the higher the frailty value, the greater the probability of large degradation increments related to failure. Then for each unit i, the degradation increment Y in the time interval Δt has its intensity function defined as,

$$h_i(y|\Delta g_{\boldsymbol{\theta}}(t),\eta,z_i) = \frac{1}{z_i} \times h_{IGP}(y|\Delta g_{\boldsymbol{\theta}}(t),\eta), \tag{4.1}$$

where $h_{IGP}(y|\Delta g_{\boldsymbol{\theta}}(t),\eta)$ is referred to as the baseline intensity function with expression as given in (2.10), $\Delta g_{\boldsymbol{\theta}}(t)$ and η are as given in section 2.4.4.2.

The equation (4.1) can be easily understood as follows

- ✔ The lower the z_i, the greater the intensity function for small degradation increments, which means that the less fragile components will probably take a long time to reach the threshold related to failure,
- ✔ Inversely, the higher the z_i, the lower the intensity function for small degradation increments, which means that the most fragile components are likely to reach the threshold early.

From (2.11) and (2.17), the conditional reliability function for IGP frailty model (4.1) is given by

$$R_i(y|\Delta g_{\boldsymbol{\theta}}(t),\eta,z_i) = [R_{IGP}(y|\Delta g_{\boldsymbol{\theta}}(t),\eta)]^{\frac{1}{z_i}},$$

where $R_{IGP}(.)$ is as given in (2.9).

Therefore, the conditional CDF for IGP frailty model (4.1) is given by

$$F_i(y|\Delta g_{\boldsymbol{\theta}}(t),\eta,z_i) = 1 - R_i(y|\Delta g_{\boldsymbol{\theta}}(t),\eta,z_i). \tag{4.2}$$

From (4.2), we can build up the following algorithm to generate degradation paths from IGP frailty model

Algorithm 3 : Generating degradation paths from IGP frailty model.

1 Fix values for n, $g_{\boldsymbol{\theta}}(.)$ and η,
2 For each unit i, $(1 \leq i \leq n)$,

- Set $t_{i0} = 0$ and fix values for n_i and $t_{i1},\ldots,t_{in_i}$;
- Generate a random number z_i from the frailty distribution (e.g. gamma, lognormal or IG);
- For each index j, $(1 \leq j \leq n_i)$:
  - Compute $\Delta t_{ij} = t_{i,j} - t_{i,j-1}$ and $\Delta g_{\boldsymbol{\theta}}(t_{ij}) = g_{\boldsymbol{\theta}}(t_{i,j}) - g_{\boldsymbol{\theta}}(t_{i,j-1})$;
  - Generate a random number u_{ij} from $U(0,1)$;
  - Solve the nonlinear equation for y_{ij}: $F_i(y_{ij}|\Delta g_{\boldsymbol{\theta}}(t_{ij}),\eta,z_i) = u_{ij}$;
- Compute the cumulative degradation values $d_{i1} = y_{i1}, d_{i2} = y_{i1} + y_{i2} \ldots, d_{in_i} = y_{i1} + \ldots + y_{in_i}$.

Figure 13 shows three degradation paths for three different z_i values, as a result of Algorithm 3. The chart consists of 3 units being evaluated from 0 up to 4 time units with 10 equidistant intervals. The mean function for IGP was specified as $g_{\boldsymbol{\theta}}(t) = \theta t$, $\theta > 0$ and the parameter values are exhibited in the chart. For the sake of analysis, the z_i values are fixed instead of random, and we note that large degradation values are related to high frailty values.

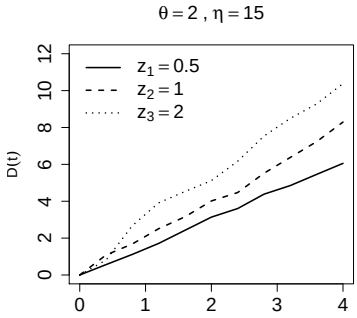

Figure 13 – Degradation paths for different frailty values.

4.2.1 Unconditional reliability function, CDF and PDF of the degradation increments

The unconditional reliability function for the increment Y in time interval Δt is similar to (2.18) with some modification, that is, the lifetime values give way to the degradation increments and the contribution of the frailty term in the exponent is $\frac{1}{z_i}$ rather than z_i

$$R(y|\Delta g_{\boldsymbol{\theta}}(t),\eta,\boldsymbol{\alpha}) = \int_0^\infty R_i(y|\Delta g_{\boldsymbol{\theta}}(t),\eta,z_i) f_{\boldsymbol{\alpha}}(z_i) dz_i = \int_0^\infty \exp\left[-\frac{1}{z_i} H_{IGP}(y|\Delta g_{\boldsymbol{\theta}}(t),\eta)\right] f_{\boldsymbol{\alpha}}(z_i) dz_i. \tag{4.3}$$

Note that (4.3) depends on $\boldsymbol{\alpha}$, which means that marginalization incorporates the frailty information in the reliability function through the parameter vector $\boldsymbol{\alpha}$.

From (4.3) and the relation $H_{IGP}(y|\Delta g_{\boldsymbol{\theta}}(t),\eta) = -\log[R_{IGP}(y|\Delta g_{\boldsymbol{\theta}}(t),\eta)]$ described in (2.11) we can observe the following cases:

- ✔ Case 1: For too large y values $R_{IGP}(y|\Delta g_{\boldsymbol{\theta}}(t),\eta) \approx 0$ then $H_{IGP}(y|\Delta g_{\boldsymbol{\theta}}(t),\eta) \approx \infty$,
- ✔ Case 2: For too small y values $R_{IGP}(y|\Delta g_{\boldsymbol{\theta}}(t),\eta) \approx 1$ then $H_{IGP}(y|\Delta g_{\boldsymbol{\theta}}(t),\eta) \approx 0$.

Based on these situations, we rewrite (4.3):

$$R(y|\Delta g_{\boldsymbol{\theta}}(t),\eta,\boldsymbol{\alpha}) = \begin{cases} 0, \text{ if } R_{IGP}(y|\Delta g_{\boldsymbol{\theta}}(t),\eta) = 0, \\ \int_0^\infty \exp\left[-\frac{1}{z_i} H_{IGP}(y|\Delta g_{\boldsymbol{\theta}}(t),\eta)\right] f_{\boldsymbol{\alpha}}(z_i) dz_i, \text{ if } 0 < R_{IGP}(y|\Delta g_{\boldsymbol{\theta}}(t),\eta) < 1, \\ 1, \text{ if } R_{IGP}(y|\Delta g_{\boldsymbol{\theta}}(t),\eta) = 1. \end{cases} \tag{4.4}$$

The formula (4.4) based on three situations intends to avoid indeterminate values occurring in simulated studies. Additionally, the integral in (4.4) can be solved analytically or numerically, depending on frailty distribution.

Therefore, the unconditional CDF is given by

$$F(y|\Delta g_{\boldsymbol{\theta}}(t),\eta,\boldsymbol{\alpha}) = \begin{cases} 0, \text{ if } F_{IGP}(y|\Delta g_{\boldsymbol{\theta}}(t),\eta) = 0, \\ R(y|\Delta g_{\boldsymbol{\theta}}(t),\eta,\boldsymbol{\alpha}), \text{ if } 0 < F_{IGP}(y|\Delta g_{\boldsymbol{\theta}}(t),\eta) < 1, \\ 1, \text{ if } F_{IGP}(y|\Delta g_{\boldsymbol{\theta}}(t),\eta) = 1. \end{cases} \tag{4.5}$$

From (4.5) we conclude that IGP frailty model has monotone behavior as well, because $F_{IGP}(y|\Delta g_{\boldsymbol{\theta}}(t),\eta)$ is positive merely for positive y values, otherwise it is null. Additionally, an alternative algorithm is derived to generate degradation paths from IGP frailty model and it is necessary to set up the PDF for frailty $f_{\boldsymbol{\alpha}}(z)$ and solve the integral in (4.4) previously (unless this integral has no analytical form).

Algorithm 4 : Generating degradation paths from IGP frailty model - alternative method.

1 Fix values for n, $g_{\boldsymbol{\theta}}(.)$, η and α;
2 For each unit i, $(1 \leq i \leq n)$;

- Set $t_{i0} = 0$ and fix values for n_i and $t_{i1},\ldots,t_{in_i}$;
- For each index j, $(1 \leq j \leq n_i)$:
  - Compute $\Delta t_{ij} = t_{i,j} - t_{i,j-1}$ and $\Delta g_{\boldsymbol{\theta}}(t_{ij}) = g_{\boldsymbol{\theta}}(t_{i,j}) - g_{\boldsymbol{\theta}}(t_{i,j-1})$;
  - Generate a random number u_{ij} from $U(0,1)$;
  - Solve the nonlinear equation for y_{ij}: $F(y_{ij}|\Delta g_{\boldsymbol{\theta}}(t_{ij}),\eta,\boldsymbol{\alpha}) = u_{ij}$;
- Compute the cumulative degradation values $d_{i1} = y_{i1}, d_{i2} = y_{i1} + y_{i2} \ldots, d_{in_i} = y_{i1} + \ldots + y_{in_i}$.

Figure 14 shows the simulated degradation paths from IGP model and IGP frailty model as a result of algorithms 1 and 4, respectively, where gamma distribution with unitary mean and α variance is assigned for the frailty term. Each chart consists of 20 units being evaluated from 0 up to 4 time units with 16 equidistant intervals. Likewise in Figure 13, $g_{\boldsymbol{\theta}}(t) = \theta t$, $\theta > 0$ and the parameter values are $\theta = 2$ and $\eta = 15$. We conclude that when α variance increases, the degradation paths become more disperse.

The unconditional PDF is the derivative of (4.5) with respect to y:

$$f(y|\Delta g_{\boldsymbol{\theta}}(t),\eta,\boldsymbol{\alpha}) = \begin{cases} 0, \text{ if } f_{IGP}(y|\Delta g_{\boldsymbol{\theta}}(t),\eta) = 0, \\ \frac{\partial F(y|\Delta g_{\boldsymbol{\theta}}(t),\eta,\boldsymbol{\alpha})}{\partial y}, \text{ if } f_{IGP}(y|\Delta g_{\boldsymbol{\theta}}(t),\eta) > 0. \end{cases} \tag{4.6}$$

4.2.2 Lifetime distribution

Considering (2.1), the lifetime CDF for IGP frailty model is obtained directly from the unconditional CDF in (4.5), considering that the cumulative degradation $D(t)$ is equal to the degradation increment in the time interval from 0 up to t: $\Delta t \equiv [0,t]$, then we have

$$F_T(t) = P[D(t) \geq \rho] = 1 - F(y = \rho|g_{\boldsymbol{\theta}}(t),\eta,\boldsymbol{\alpha}). \tag{4.7}$$

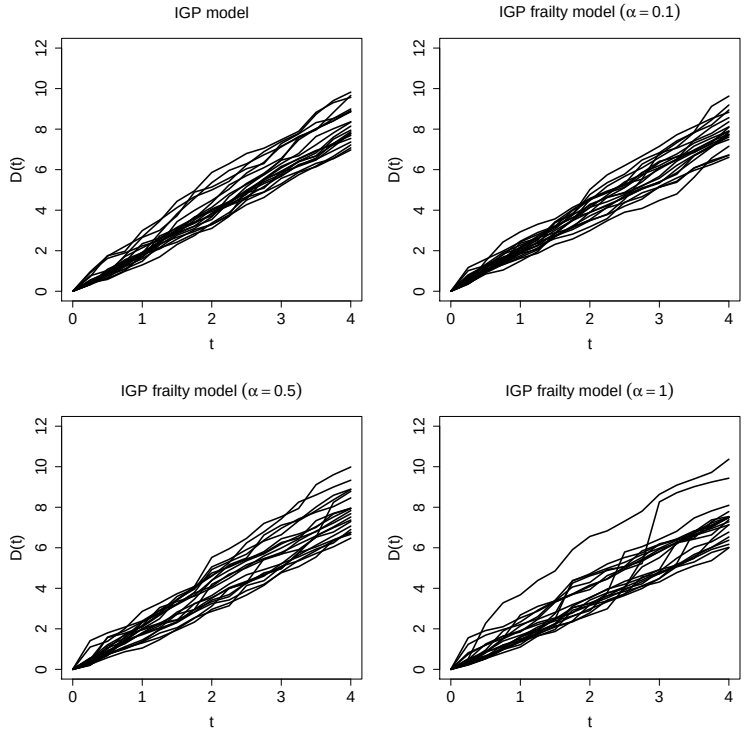

Figure 14 – Degradation paths from IGP and IGP frailty model under different α values.

The lifetime PDF is obtained from the derivative of (4.7) with respect to t:

$$f_T(t) = \frac{\partial F_T(t)}{\partial t}. \tag{4.8}$$

4.2.3 Inference for unknown parameters in IGP frailty model

Considering z_i frailty variable i.i.d with PDF $f_{\boldsymbol{\alpha}}(z_i)$, the likelihood function for n units is given by

$$L(g_{\boldsymbol{\theta}}(t), \eta, \mathbf{z}) = \prod_{i=1}^{n} \prod_{j=1}^{n_i} h_i(y_{ij}|\Delta g_{\boldsymbol{\theta}}(t_{ij}), \eta, z_i) R_i(y_{ij}|\Delta g_{\boldsymbol{\theta}}(t_{ij}), \eta, z_i) f_{\boldsymbol{\alpha}}(z_i). \tag{4.9}$$

Therefore, the unconditional likelihood is obtained by integrating out the variable z_i

$$L(g_{\boldsymbol{\theta}}(t), \eta, \boldsymbol{\alpha}) = \int_0^{\infty} L(g_{\boldsymbol{\theta}}(t), \eta, \mathbf{z}) f_{\boldsymbol{\alpha}}(z_i) dz_i. \tag{4.10}$$

For the sake of clarity, we first obtain the contribution of each unit i in the likelihood function, with n_i observed degradation data at the inspection times $t_{ij} (j = 1, \ldots, n_i)$

$$\begin{aligned} L_i &= \int_0^{\infty} \prod_{j=1}^{n_i} h_i(y_{ij}|\Delta g_{\boldsymbol{\theta}}(t_{ij}), \eta, z_i) R_i(y_{ij}|\Delta g_{\boldsymbol{\theta}}(t_{ij}), \eta, z_i) f_{\boldsymbol{\alpha}}(z_i) dz_i \\ &= \prod_{j=1}^{n_i} h_{IGP}(y_{ij}|\Delta g_{\boldsymbol{\theta}}(t_{ij}), \eta) \times \int_0^{\infty} \left(\frac{1}{z_i}\right)^{n_i} \exp\left[-\sum_{j=1}^{n_i} H_{IGP}(y_{ij}|\Delta g_{\boldsymbol{\theta}}(t_{ij}), \eta) \frac{1}{z_i}\right] f_{\boldsymbol{\alpha}}(z_i) dz_i \\ &= L_{1i} \times L_{2i}, \end{aligned} \tag{4.11}$$

where L_{1i} does not depend on frailty distribution and the second term L_{2i} depends on the assigned frailty distribution.

Then, the likelihood function in (4.10) for n units is rewritten as

$$L(g_{\boldsymbol{\theta}}(t), \eta, \boldsymbol{\alpha}) = \prod_{i=1}^{n} L_{1i} \times L_{2i}.$$

Therefore, the corresponding log-likelihood is given by

$$l(g_{\boldsymbol{\theta}}(t), \eta, \boldsymbol{\alpha}) = \sum_{i=1}^{n} \log(L_{1i}) + \sum_{i=1}^{n} \log(L_{2i}). \tag{4.12}$$

The MLEs of the parameters can be obtained by maximization of (4.12) and the confidence intervals are constructed from asymptotic properties of the MLEs.

4.2.4 Inference for individual frailties

The individual frailties can be obtained through the Bayesian inference approach (GELMAN *et al.*, 2014), where the frailty PDF for each unit i given the observed data is given by

$$f(z_i|\mathbf{Y}) \propto L(g_{\boldsymbol{\theta}}(t), \eta, \mathbf{z}), \tag{4.13}$$

where $L(g_{\boldsymbol{\theta}}(t), \eta, \mathbf{z})$ is as given in (4.9) and the terms that do not depend on z_i are taken out from the formula.

There are many choices for the frailty distribution such as, for example, gamma distribution (CLAYTON, 1978), positive stable distribution (HOUGAARD, 1986), compound Poisson distribution (AALEN, 1992) and lognormal distribution (MCGILCHRIST; AISBETT, 1991).

4.2.5 Gamma distribution for frailty

In this section we assume that z_i's are an i.i.d sample from gamma distribution, which is one of the most popular distributions for modeling the frailty term (NIELSEN *et al.*, 1992). In order to keep the identifiability of our model (ELBERS; RIDDER, 1982) we shall assume a gamma distribution with unitary mean and α variance for z_i, then we have

$$h_i(y|\Delta g_{\boldsymbol{\theta}}(t), \eta, z_i) = \frac{1}{z_i} \times h_{IGP}(y|\Delta g_{\boldsymbol{\theta}}(t), \eta), \text{ where } z_i \sim \text{ Gamma } \left(\frac{1}{\alpha}, \alpha\right), \tag{4.14}$$

and $f_{\boldsymbol{\alpha}}(z_i) = \frac{z_i^{\frac{1}{\alpha}-1} \alpha^{-\frac{1}{\alpha}} \exp\left(-\frac{z_i}{\alpha}\right)}{\Gamma\left(\frac{1}{\alpha}\right)}$.

The model (4.14) is referred to as IGP-Gamma frailty model along the chapter.

The unconditional reliability function of the degradation increments in IGP-Gamma frailty model is based on following proposition

Proposition 4.2.1.

$$R(y|\Delta g_{\boldsymbol{\theta}}(t),\eta,\boldsymbol{\alpha}) = \begin{cases} 0, \text{ if } R_{IGP}(y|\Delta g_{\boldsymbol{\theta}}(t),\eta) = 0, \\ \frac{2\alpha^{-\frac{1}{\alpha}}(\alpha H_{IGP}(y|\Delta g_{\boldsymbol{\theta}}(t),\eta))^{\frac{1}{2\alpha}}A}{\Gamma(\frac{1}{\alpha})}, \text{ if } 0 < R_{IGP}(y|\Delta g_{\boldsymbol{\theta}}(t),\eta) < 1, \\ 1, \text{ if } R_{IGP}(y|\Delta g_{\boldsymbol{\theta}}(t),\eta) = 1, \end{cases} \tag{4.15}$$

where $A = \text{Besselk}\left[\frac{1}{\alpha}, \frac{2\sqrt{H_{IGP}(y|\Delta g_{\boldsymbol{\theta}}(t),\eta)}}{\sqrt{\alpha}}\right]$ and Besselk$[n,z]$ is the modified Bessel function of the second kind $K_n(z)$.

Proof. The proof is exhibited in Appendix A. □

The CDF is easily obtained from (4.5). Therefore, the PDF of the degradation increments in IGP-Gamma frailty model is based on following proposition

Proposition 4.2.2.

$$f(y|\Delta g_{\boldsymbol{\theta}}(t),\eta,\boldsymbol{\alpha}) = \begin{cases} 0, \text{ if } f_{IGP}(y|\Delta g_{\boldsymbol{\theta}}(t),\eta) = 0, \\ \frac{h_{IGP}(y|\Delta g_{\boldsymbol{\theta}}(t),\eta)(H_{IGP}(y|\Delta g_{\boldsymbol{\theta}}(t),\eta))^{\frac{1}{2\alpha}}}{\alpha^{\frac{1}{2\alpha}+\frac{1}{2}}\Gamma(\frac{1}{\alpha})}\left[\frac{(A_1+A_2)}{\sqrt{H_{IGP}(y|\Delta g_{\boldsymbol{\theta}}(t),\eta)}} - \frac{A}{\sqrt{\alpha}H}\right], \\ \text{if } f_{IGP}(y|\Delta g_{\boldsymbol{\theta}}(t),\eta) > 0, \end{cases} \tag{4.16}$$

where $A_1 = \text{Besselk}\left[-1+\frac{1}{\alpha}, 2\frac{\sqrt{H_{IGP}(y|\Delta g_{\boldsymbol{\theta}}(t),\eta)}}{\sqrt{\alpha}}\right]$ and $A_2 = \text{Besselk}\left[1+\frac{1}{\alpha}, 2\frac{\sqrt{H_{IGP}(y|\Delta g_{\boldsymbol{\theta}}(t),\eta)}}{\sqrt{\alpha}}\right]$.

Proof. The proof is shown in Appendix A. □

Figure 15 shows the charts of the unconditional CDF and PDF for IGP model (2.7) and IGP-Gamma frailty model (4.14), considering $g_{\boldsymbol{\theta}}(t) = 2t$, $\Delta t = 5$, $\eta = 5$ and different α values, from which we observe that the curves are similar to each other, and the lower α, the closer the curves.

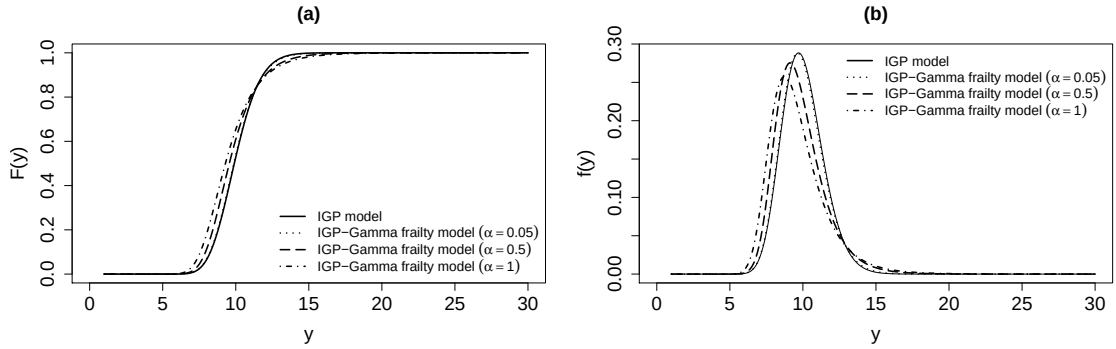

Figure 15 – CDF and PDF of the degradation increments in IGP and IGP-Gamma frailty models: (a) CDF, (b) PDF.

The lifetime PDF of the degradation increments in IGP-Gamma frailty model is based on following proposition

Proposition 4.2.3.

$$f_T(t) = f_{T_{IGP}} \frac{H_{IGP}(y=\rho|g_{\boldsymbol{\theta}}(t),\eta)[\sqrt{\alpha H_{IGP}(y=\rho|g_{\boldsymbol{\theta}}(t),\eta)}(A_1+A_2)-A]}{\alpha^{\frac{1}{2\alpha}+1}\Gamma\left(\frac{1}{\alpha}\right) R_{IGP}(y=\rho|g_{\boldsymbol{\theta}}(t),\eta)}, \tag{4.17}$$

where $f_{T_{IGP}}(.)$ is as given in (2.13), A_1 and A_2 are as given in proposition 4.2.2 and A is as given in proposition 4.2.1.

Proof. The proof is presented in Appendix A. □

The inference for unknown parameters in IGP-Gamma frailty model is based on following proposition

Proposition 4.2.4. The second term in (4.11) is given by

$$L_{2i} = \frac{2\alpha^{-\frac{1}{\alpha}}\left(\alpha\sum_{j=1}^{n_i} H_{IGP}(y_{ij}|\Delta g_{\boldsymbol{\theta}}(t_{ij}),\eta)\right)^{\frac{1}{2\alpha}-\frac{n_i}{2}} A_{1i}}{\Gamma\left(\frac{1}{\alpha}\right)}, \tag{4.18}$$

where $A_{1i} = \text{Besselk}\left[\frac{1}{\alpha}-n_i, 2\sqrt{\frac{\sum_{j=1}^{n_i} H_{IGP}(y_{ij}|\Delta g_{\boldsymbol{\theta}}(t_{ij}),\eta)}{\alpha}}\right]$.

Proof. The proof is exhibited in Appendix A. □

Considering the proposition 4.2.4 the likelihood function for n units is rewritten as

$$L(g_{\boldsymbol{\theta}}(t),\eta,\boldsymbol{\alpha}) = \prod_{i=1}^{n}\left[\prod_{j=1}^{n_i} h_{IGP}(y_{ij}|\Delta g_{\boldsymbol{\theta}}(t_{ij}),\eta)\right] \frac{2\alpha^{-\frac{1}{\alpha}}\left(\alpha\sum_{j=1}^{n_i} H_{IGP}(y_{ij}|\Delta g_{\boldsymbol{\theta}}(t_{ij}),\eta)\right)^{\frac{1}{2\alpha}-\frac{n_i}{2}} A_{1i}}{\Gamma\left(\frac{1}{\alpha}\right)}.$$

Therefore, the corresponding log-likelihood function is given by

$$\begin{aligned} l(g_{\boldsymbol{\theta}}(t),\eta,\boldsymbol{\alpha}) &= \sum_{i=1}^{n}\sum_{j=1}^{n_i}\log\left[h_{IGP}(y_{ij}|\Delta g_{\boldsymbol{\theta}}(t_{ij}),\eta)\right] + n\log(2) - \frac{n}{\alpha}\log(\alpha) \\ &\quad + \sum_{i=1}^{n}\left(\frac{1}{2\alpha}-\frac{n_i}{2}\right)\log\left[\alpha\sum_{j=1}^{n_i} H_{IGP}(y_{ij}|\Delta g_{\boldsymbol{\theta}}(t_{ij}),\eta)\right] \\ &\quad + \sum_{i=1}^{n}\log(A_{1i}) - n\log\left[\Gamma\left(\frac{1}{\alpha}\right)\right]. \end{aligned}$$

The inference for individual frailties in IGP-Gamma frailty model is based on following proposition

Proposition 4.2.5. The frailty for each unit i given the observed data belongs to Generalized IG distribution

$$z_i|\mathbf{Y} \sim \text{GIG}\left(\frac{2}{\alpha}, 2\sum_{j=1}^{n_i} H_{IGP}(y_{ij}|\Delta g_{\boldsymbol{\theta}}(t_{ij}), \eta), \frac{1}{\alpha} - n_i\right), \tag{4.19}$$

whose mean and variance are given by

$$\begin{aligned} \text{E}(z_i|\mathbf{Y}) &= A_{2i}\sqrt{\alpha\sum_{j=1}^{n_i} H_{IGP}(y_{ij}|\Delta g_{\boldsymbol{\theta}}(t_{ij}), \eta)} \text{ and} \\ \text{VAR}(z_i|\mathbf{Y}) &= (A_{3i} - A_{2i}^2)\alpha\sum_{j=1}^{n_i} H_{IGP}(y_{ij}|\Delta g_{\boldsymbol{\theta}}(t_{ij}), \eta), \end{aligned}$$

where $A_{2i} = \dfrac{\text{Besselk}\left[\frac{1}{\alpha} - n_i + 1, 2\sqrt{\frac{\sum_{j=1}^{n_i} H_{IGP}(y_{ij}|\Delta g_{\boldsymbol{\theta}}(t_{ij}), \eta)}{\alpha}}\right]}{\text{Besselk}\left[\frac{1}{\alpha} - n_i, 2\sqrt{\frac{\sum_{j=1}^{n_i} H_{IGP}(y_{ij}|\Delta g_{\boldsymbol{\theta}}(t_{ij}), \eta)}{\alpha}}\right]}$ and $A_{3i} = \dfrac{\text{Besselk}\left[\frac{1}{\alpha} - n_i + 2, 2\sqrt{\frac{\sum_{j=1}^{n_i} H_{IGP}(y_{ij}|\Delta g_{\boldsymbol{\theta}}(t_{ij}), \eta)}{\alpha}}\right]}{\text{Besselk}\left[\frac{1}{\alpha} - n_i, 2\sqrt{\frac{\sum_{j=1}^{n_i} H_{IGP}(y_{ij}|\Delta g_{\boldsymbol{\theta}}(t_{ij}), \eta)}{\alpha}}\right]}$.

Proof. The proof is shown in Appendix A. □

4.2.6 IG distribution for frailty

We assume that z_i's are an i.i.d sample from IG distribution with unitary mean and α variance, then we have

$$h_i(y|\Delta g_{\boldsymbol{\theta}}(t), \eta, z_i) = \frac{1}{z_i} \times h_{IGP}(y|\Delta g_{\boldsymbol{\theta}}(t), \eta), \text{ where } z_i \sim \text{IG}\left(1, \frac{1}{\alpha}\right), \tag{4.20}$$

and $f_{\boldsymbol{\alpha}}(z_i) = \left(\frac{1}{2\pi\alpha z_i^3}\right)^{\frac{1}{2}} \times \exp\left[-\frac{(z_i-1)^2}{2\alpha z_i}\right]$.

The model (4.20) is referred to as IGP-IG frailty model along the chapter.

The unconditional reliability function of the degradation increments in IGP-IG frailty model is based on following proposition

Proposition 4.2.6.

$$R(y|\Delta g_{\boldsymbol{\theta}}(t), \eta, \boldsymbol{\alpha}) = \begin{cases} 0, \text{if } R_{IGP}(y|\Delta g_{\boldsymbol{\theta}}(t), \eta) = 0, \\ \frac{e^{-\frac{1}{\alpha}\left(\sqrt{1+2\alpha H_{IGP}(y|\Delta g_{\boldsymbol{\theta}}(t), \eta)} - 1\right)}}{\sqrt{1+2\alpha H_{IGP}(y|\Delta g_{\boldsymbol{\theta}}(t), \eta)}}, \text{if } 0 < R_{IGP}(y|\Delta g_{\boldsymbol{\theta}}(t), \eta) < 1, \\ 1, \text{if } R_{IGP}(y|\Delta g_{\boldsymbol{\theta}}(t), \eta) = 1. \end{cases} \tag{4.21}$$

Proof. The proof is displayed in Appendix A. □

Therefore, the corresponding CDF is obtained from the relation (4.5).

The unconditional PDF of the degradation increments in IGP-IG frailty model is based on following proposition

Proposition 4.2.7.

$$f(y|\Delta g_{\boldsymbol{\theta}}(t),\eta,\boldsymbol{\alpha}) = \begin{cases} 0, \text{if } f_{IGP}(y|\Delta g_{\boldsymbol{\theta}}(t),\eta) = 0, \\ \frac{e^{-\frac{1}{\alpha}(\sqrt{1+2\alpha H_{IGP}(y|\Delta g_{\boldsymbol{\theta}}(t),\eta)}-1)} h_{IGP}(y|\Delta g_{\boldsymbol{\theta}}(t),\eta)}{1+2\alpha H_{IGP}(y|\Delta g_{\boldsymbol{\theta}}(t),\eta)} \left(1+\frac{\alpha}{\sqrt{1+2\alpha H_{IGP}(y|\Delta g_{\boldsymbol{\theta}}(t),\eta)}}\right), \\ \text{if } f_{IGP}(y|\Delta g_{\boldsymbol{\theta}}(t),\eta) > 0. \end{cases} \tag{4.22}$$

Proof. The equation (4.22) is obtained from (4.6) and the relation $\frac{\partial H_{IGP}(y|\Delta g_{\boldsymbol{\theta}}(t),\eta)}{\partial y} = h_{IGP}(y|\Delta g_{\boldsymbol{\theta}}(t),\eta)$. □

Figure 16 shows the charts for the unconditional CDF and PDF for IGP model and IGP-IG frailty model, considering $g_{\boldsymbol{\theta}}(t) = 2t$, $\Delta t = 5$, $\eta = 5$ and different α values. Similarly to Figure 15, the curves of IGP model and IGP-IG frailty model are close to each other for small α values.

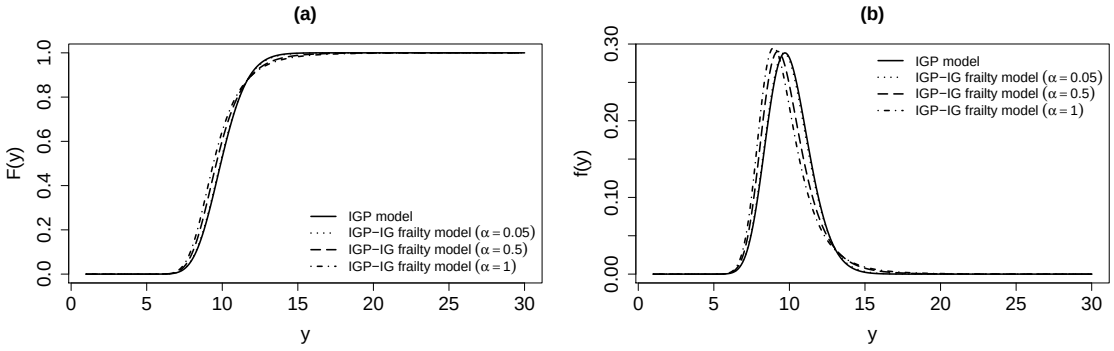

Figure 16 – (a) CDF of IGP and IGP-IG frailty models, (b) PDF of IGP and IGP-IG frailty models.

The lifetime PDF in IGP-IG frailty model is based on following proposition

Proposition 4.2.8.

$$f_T(t) = \frac{f_{t_{IGP}}(t) e^{-\frac{1}{\alpha}(\sqrt{1+2\alpha H_{IGP}(y=\rho|g_{\boldsymbol{\theta}}(t),\eta)}-1)}}{R_{IGP}(y=\rho|g_{\boldsymbol{\theta}}(t),\eta)[1+2\alpha H_{IGP}(y=\rho|g_{\boldsymbol{\theta}}(t),\eta)]} \times \left[1+\frac{\alpha}{\sqrt{1+2\alpha H_{IGP}(y=\rho|g_{\boldsymbol{\theta}}(t),\eta)}}\right], \tag{4.23}$$

where $f_{T_{IGP}}(t)$ is as given in (2.13).

Proof. The equation (4.24) is obtained from the relation $\frac{\partial H_{IGP}(y|\Delta g_{\boldsymbol{\theta}}(t),\eta)}{\partial t} = -\frac{f_{T_{IGP}}(t)}{R_{IGP}(y|\Delta g_{\boldsymbol{\theta}}(t),\eta)}$. □

The inference for unknown parameters in IGP-IG frailty model is based on following proposition

Proposition 4.2.9. The second term in (4.11) is given by

$$L_{2i} = \sqrt{\frac{2}{\pi\alpha}}\exp\left(\frac{1}{\alpha}\right)\left(\frac{1}{1+2\alpha\sum_{j=1}^{n_i}H_{IGP}(y_{ij}|\Delta g_{\boldsymbol{\theta}}(t_{ij}),\eta)}\right)^{\frac{1}{4}+\frac{n_i}{2}} B_{1i}, \tag{4.24}$$

where $B_{1i} = \text{Besselk}\left[\frac{1}{2}+n_i, B\right]$ and $B = \frac{\sqrt{1+2\alpha\sum_{j=1}^{n_i}H_{IGP}(y_{ij}|\Delta g_{\boldsymbol{\theta}}(t_{ij}),\eta)}}{\alpha}$.

Proof. The proof is presented in Appendix A. □

Considering the proposition (4.2.9), the likelihood function for n units is

$$\begin{aligned} L(g_{\boldsymbol{\theta}}(t),\eta,\boldsymbol{\alpha}) &= \prod_{i=1}^{n}\left[\prod_{j=1}^{n_i}h_{IGP}(y_{ij}|\Delta g_{\boldsymbol{\theta}}(t_{ij}),\eta)\right]\sqrt{\frac{2}{\pi\alpha}}\exp\left(\frac{1}{\alpha}\right) \\ &\quad\times\left(\frac{1}{1+2\alpha\sum_{j=1}^{n_i}H_{IGP}(y_{ij}|\Delta g_{\boldsymbol{\theta}}(t_{ij}),\eta)}\right)^{\frac{1}{4}+\frac{n_i}{2}} B_{1i}. \end{aligned}$$

Therefore, the corresponding log-likelihood function is

$$\begin{aligned} l(g_{\boldsymbol{\theta}}(t),\eta,\boldsymbol{\alpha}) &= \sum_{i=1}^{n}\sum_{j=1}^{n_i}\log\left[h_{IGP}(y_{ij}|\Delta g_{\boldsymbol{\theta}}(t_{ij}),\eta)\right]+\frac{n}{\alpha} \\ &\quad-\sum_{i=1}^{n}\left(\frac{1}{4}+\frac{n_i}{2}\right)\log\left(1+2\alpha\sum_{j=1}^{n_i}H_{IGP}(y_{ij}|\Delta g_{\boldsymbol{\theta}}(t_{ij}),\eta)\right) \\ &\quad+\frac{n}{2}\log(2)-\frac{n}{2}\log(\pi)+\sum_{i=1}^{n}\log(B_{1i})-\frac{n}{2}\log(\alpha). \end{aligned}$$

The inference for individual frailties in IGP-IG frailty model is based on following proposition

Proposition 4.2.10. The frailty for each unit i given the observed data belongs to Generalized IG distribution

$$z_i|\mathbf{Y} \sim \text{GIG}\left(\frac{1}{\alpha}, 2\sum_{j=1}^{n_i}H_{IGP}(y_{ij}|\Delta g_{\boldsymbol{\theta}}(t_{ij}),\eta)+\frac{1}{\alpha}, -\frac{3}{2}-n_i+1\right), \tag{4.25}$$

whose mean and variance are given by $\text{E}(z_i|\mathbf{Y}) = B_{2i}\sqrt{1+2\alpha\sum_{j=1}^{n_i}H_{IGP}(y_{ij}|\Delta g_{\boldsymbol{\theta}}(t_{ij}),\eta)}$ and

$\text{VAR}(z_i|\mathbf{Y}) = (B_{3i}-B_{2i}^2)\left(1+2\alpha\sum_{j=1}^{n_i}H_{IGP}(y_{ij}|\Delta g_{\boldsymbol{\theta}}(t_{ij}),\eta)\right)$,

where $B_{2i} = \frac{\text{Besselk}\left[-\frac{3}{2}-n_i+2,B\right]}{\text{Besselk}\left[-\frac{3}{2}-n_i+1,B\right]}$ and $B_{3i} = \frac{\text{Besselk}\left[-\frac{3}{2}-n_i+3,B\right]}{\text{Besselk}\left[-\frac{3}{2}-n_i+1,B\right]}$.

Proof. The proof is shown in Appendix A. □

4.3 Simulation study

A simulation study was carried out based on the generation of 5,000 artificial datasets from IGP frailty model (4.1) with five different sample sizes (n): 20, 50, 100, 200 and 500. The values assigned to the parameters are motivated by the LASER data (example 2.2.1), in which the degradation paths possess linear behavior. The components are evaluated from 0 up to 4 time units with 10 equidistant intervals. The parameter values are specified as $g_{\boldsymbol{\theta}}(t) = \theta t$ with $\theta = 2$, $\eta = 15$ and two scenarios for α:

- ✔ $\alpha = 0.05$ characterizes small unobserved heterogeneity,
- ✔ $\alpha = 0.5$ characterizes moderate unobserved heterogeneity.

Then, we made inferences for the model parameters in IGP model (2.7) and IGP frailty model (4.1). In other words, we generated data with frailty and made inferences ignoring or not ignoring frailty. The MLEs of the model parameters, the 95% CPs and the MSEs of the MLEs under different models, different frailty distributions and different α values are discussed.

4.3.1 Gamma distribution for frailty

Tables 10 and 11 show the MLEs, 95% CPs and MSEs under $\alpha = 0.05$ and $\alpha = 0.5$, respectively. We observe that in IGP frailty model (4.1), the MLEs are closer to the corresponding true values as n increases. For IGP model (2.7), the MLEs of θ remain close to its true value as n increases, but the MLEs of η are further from its true value as n increases.

Figures 17 and 18 show the 95% CPs considering $\alpha = 0.05$ and $\alpha = 0.5$, respectively, and Figures 19 and 20 show MSEs of the MLEs considering $\alpha = 0.05$ and $\alpha = 0.5$, respectively. We conclude that as n grows, the MSEs are lower even when frailty is ignored. However the 95% CPs are further from the nominal value (95%) as n grows and frailty is ignored. Furthermore, the MLEs of η in IGP model (2.7) are further from its true value as α increases because η is the shape parameter that captures the variability inherent in the data.

Table 10 – MLEs, 95% CPs and MSEs under gamma frailty and $\alpha = 0.05$.

		IGP model (2.7)			IGP-Gamma frailty model (4.14)		
n	true values	MLE	95% CP	MSE	MLE	95% CP	MSE
20	$\theta = 2$	1.9962	0.8918	0.0025	2.0022	0.9474	0.0025
	$\eta = 15$	14.650	0.9060	3.1973	15.275	0.9530	3.3901
	$\alpha = 0.05$	–	–	–	0.0588	0.9996	0.0017
50	$\theta = 2$	1.9953	0.8884	0.0010	2.0006	0.9428	0.0010
	$\eta = 15$	14.582	0.8792	1.4056	15.1220	0.9506	1.3255
	$\alpha = 0.05$	–	–	–	0.0511	0.9640	0.0008
100	$\theta = 2$	1.9952	0.8888	0.0005	2.0003	0.9478	0.0005
	$\eta = 15$	14.532	0.8636	0.8016	15.049	0.9530	0.6222
	$\alpha = 0.05$	–	–	–	0.0490	0.9374	0.0005
200	$\theta = 2$	1.9948	0.8742	0.0003	1.9999	0.9478	0.0003
	$\eta = 15$	14.495	0.7822	0.5590	15.0100	0.9520	0.3234
	$\alpha = 0.05$	–	–	–	0.0490	0.9362	0.0002
500	$\theta = 2$	1.9948	0.8482	0.0001	2.0000	0.9498	0.0001
	$\eta = 15$	14.493	0.6128	0.3806	15.0160	0.9502	0.1300
	$\alpha = 0.05$	–	–	–	0.0497	0.9420	0.0001

Table 11 – MLEs, 95% CPs and MSEs under gamma frailty and $\alpha = 0.5$.

		IGP model (2.7)			IGP-Gamma frailty model (4.14)		
n	true values	MLE	95% CP	MSE	MLE	95% CP	MSE
20	$\theta = 2$	1.9449	0.5708	0.0120	1.9931	0.9282	0.0097
	$\eta = 15$	11.7230	0.3476	15.8270	15.5660	0.9494	7.5449
	$\alpha = 0.5$	–	–	–	0.4622	0.8688	0.0295
50	$\theta = 2$	1.9452	0.4774	0.0067	1.9956	0.9394	0.0040
	$\eta = 15$	11.3570	0.0974	15.1910	15.2830	0.9522	2.8256
	$\alpha = 0.5$	–	–	–	0.4793	0.9142	0.0117
100	$\theta = 2$	1.9423	0.3302	0.0052	1.9935	0.9392	0.0020
	$\eta = 15$	11.2990	0.0124	14.6430	15.2630	0.9512	1.4586
	$\alpha = 0.5$	–	–	–	0.4843	0.9268	0.0060
200	$\theta = 2$	1.9444	0.1888	0.0040	1.9960	0.9454	0.0010
	$\eta = 15$	11.1980	0.0000	14.9140	15.1600	0.9534	0.7024
	$\alpha = 0.5$	–	–	–	0.4869	0.9372	0.0030
500	$\theta = 2$	1.9443	0.0310	0.0035	1.9961	0.9430	0.0004
	$\eta = 15$	11.1590	0.0000	14.9370	15.1330	0.9488	0.2870
	$\alpha = 0.5$	–	–	–	0.4891	0.9306	0.0013

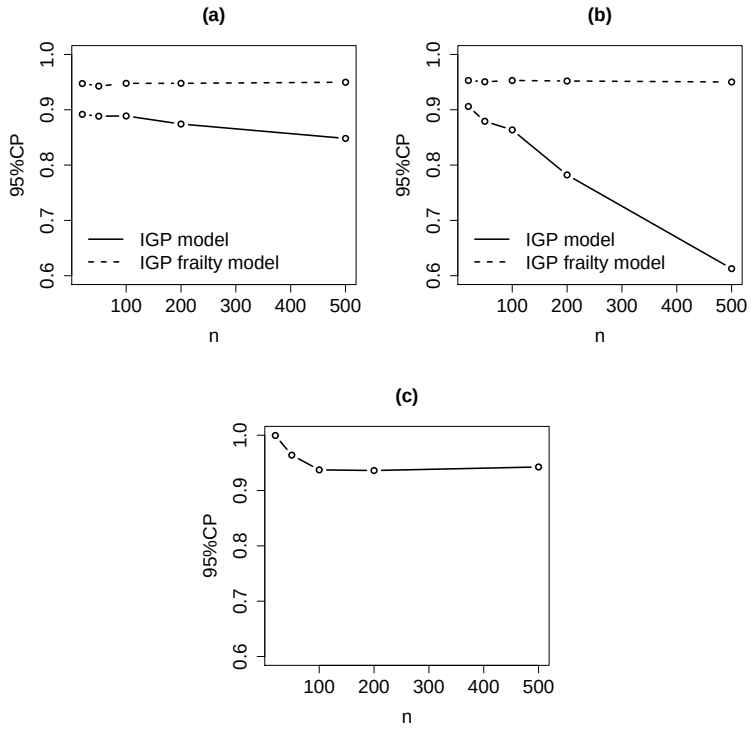

Figure 17 – 95% CPs under gamma frailty and $\alpha = 0.05$: (a) 95% CPs for θ, (b) 95% CPs for η, (c) 95% CPs for α.

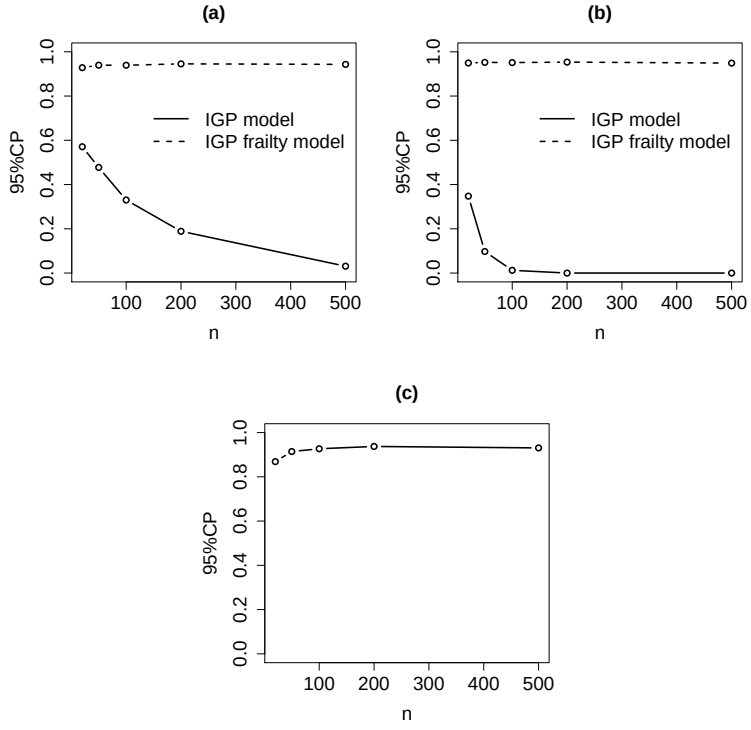

Figure 18 – 95% CPs under gamma frailty and $\alpha = 0.5$: (a) 95% CPs for θ, (b) 95% CPs for η, (c) 95% CPs for α.

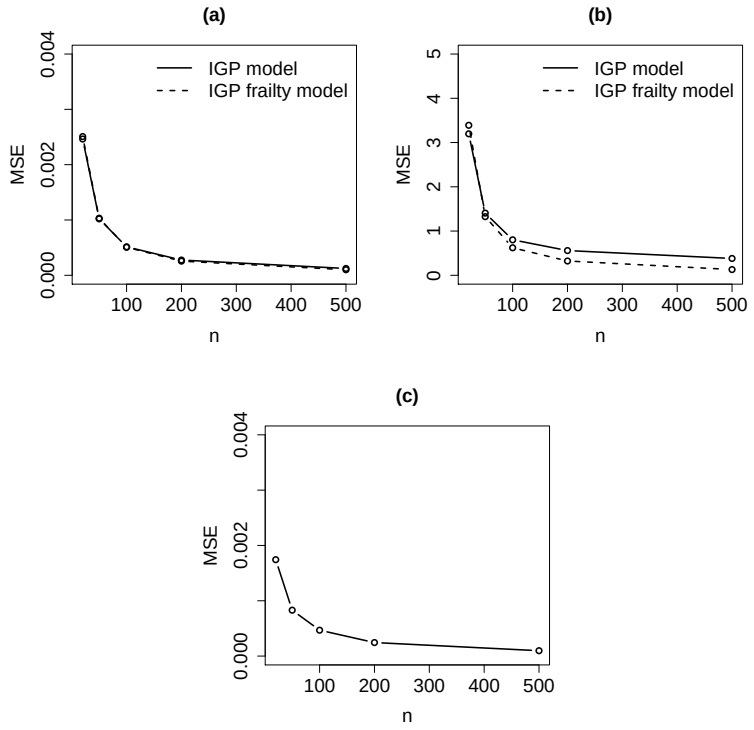

Figure 19 – MSEs under gamma frailty and $\alpha = 0.05$: (a) MSEs for θ, (b) MSEs for η, (c) MSEs for α.

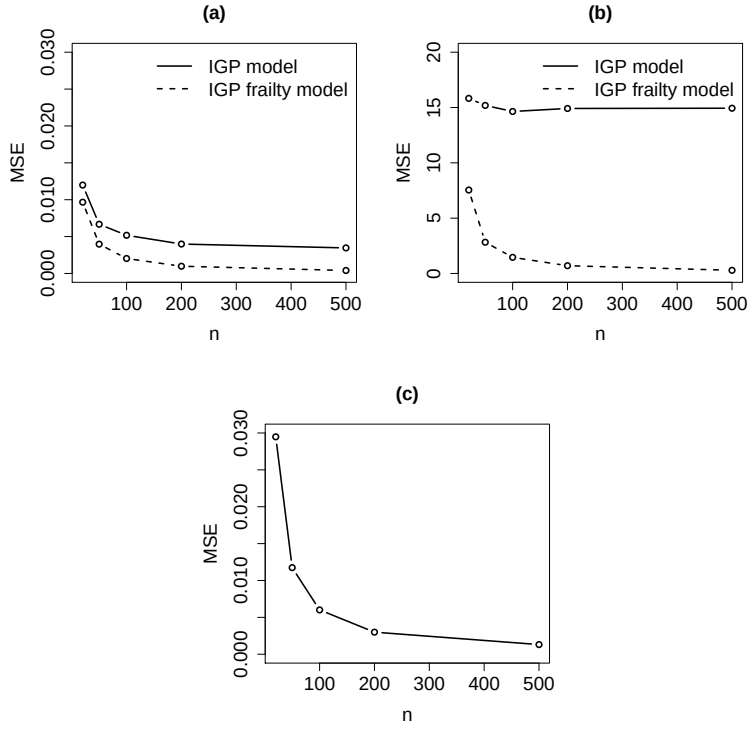

Figure 20 – MSEs under gamma frailty and $\alpha = 0.5$: (a) MSEs for θ, (b) MSEs for η, (c) MSEs for α.

4.3.2 IG distribution for frailty

Tables 12 and 13 show MLEs, 95% CPs and MSEs under $\alpha = 0.05$ and $\alpha = 0.5$, respectively. Likewise the results under gamma frailty, the MLEs in IGP model with frailty are closer to the corresponding true values as n grows. For IGP model, the MLEs of η are further from its true value as n and α increase and the MLEs of θ remain close to its true value under different scenarios.

Figures 21 and 22 show the 95% CPs considering $\alpha = 0.05$ and $\alpha = 0.5$, respectively, and Figures 23 and 24 show the MSEs of the MLEs considering $\alpha = 0.05$ and $\alpha = 0.5$, respectively. Likewise the results under gamma frailty, the MSEs decrease as n increases. Nevertheless, the 95% CPs are further from the nominal value as n increases whether the presence of frailty is ignored.

Regarding the low 95% CP values for θ and η in IGP model (2.7) under gamma and IG frailty distributions, we observe that for large sample sizes, the SEs of the MLEs are tiny then the 95% CIs are tight, which means that even a small bias leads to a 95% CI that does not embrace the corresponding true values.

Table 12 – MLEs, 95% CPs and MSEs under IG frailty and $\alpha = 0.05$.

		IGP model (2.7)			IGP-IG frailty model (4.20)		
n	true values	MLE	95% CP	MSE	MLE	95% CP	MSE
20	$\theta = 2$	1.9982	0.8990	0.0024	2.0041	0.9494	0.0025
	$\eta = 15$	14.6330	0.8966	3.2672	15.2440	0.9518	3.4128
	$\alpha = 0.05$	–	–	–	0.0622	1.0000	0.0024
50	$\theta = 2$	1.9955	0.8926	0.0010	2.0007	0.9458	0.0010
	$\eta = 15$	14.5800	0.8768	1.4284	15.1010	0.9502	1.3303
	$\alpha = 0.05$	–	–	–	0.0520	0.9702	0.0010
100	$\theta = 2$	1.9951	0.8824	0.0005	2.0002	0.9458	0.0005
	$\eta = 15$	14.5370	0.8546	0.8378	15.0450	0.9436	0.6579
	$\alpha = 0.05$	–	–	–	0.0502	0.9404	0.0005
200	$\theta = 2$	1.9954	0.8742	0.0003	2.0004	0.9444	0.0003
	$\eta = 15$	14.502	0.7814	0.5500	15.0030	0.9512	0.3174
	$\alpha = 0.05$	–	–	–	0.0494	0.9418	0.0003
500	$\theta = 2$	1.9949	0.8470	0.0001	2.0000	0.9468	0.0001
	$\eta = 15$	14.5050	0.6208	0.3710	15.0120	0.9490	0.1304
	$\alpha = 0.05$	–	–	–	0.0498	0.9474	0.0001

Table 13 – MLEs, 95% CPs and MSEs under IG frailty and $\alpha = 0.5$.

		IGP model (2.7)			IGP-IG frailty model (4.20)		
n	true values	MLE	95% CP	MSE	MLE	95% CP	MSE
20	$\theta = 2$	1.9517	0.5930	0.0100	1.9906	0.9170	0.0092
	$\eta = 15$	12.6520	0.4958	11.6590	15.5960	0.9454	7.3162
	$\alpha = 0.5$	–	–	–	0.4631	0.8576	0.0537
50	$\theta = 2$	1.9512	0.4974	0.0055	1.9910	0.9332	0.0038
	$\eta = 15$	12.3140	0.2652	9.6202	15.3730	0.9506	2.8987
	$\alpha = 0.5$	–	–	–	0.4683	0.8926	0.0205
100	$\theta = 2$	1.9517	0.3960	0.0039	1.9921	0.9360	0.0019
	$\eta = 15$	12.1790	0.0888	9.1002	15.2710	0.9532	1.3951
	$\alpha = 0.5$	–	–	–	0.4728	0.9064	0.0107
200	$\theta = 2$	1.9514	0.2312	0.0031	1.9919	0.9424	0.0010
	$\eta = 15$	12.1280	0.0062	8.8019	15.2270	0.9536	0.7025
	$\alpha = 0.5$	–	–	–	0.4714	0.9056	0.0056
500	$\theta = 2$	1.9511	0.0450	0.0027	1.9917	0.9236	0.0005
	$\eta = 15$	12.1060	0.0000	8.6116	15.2210	0.9318	0.3302
	$\alpha = 0.5$	–	–	–	0.4729	0.9008	0.0026

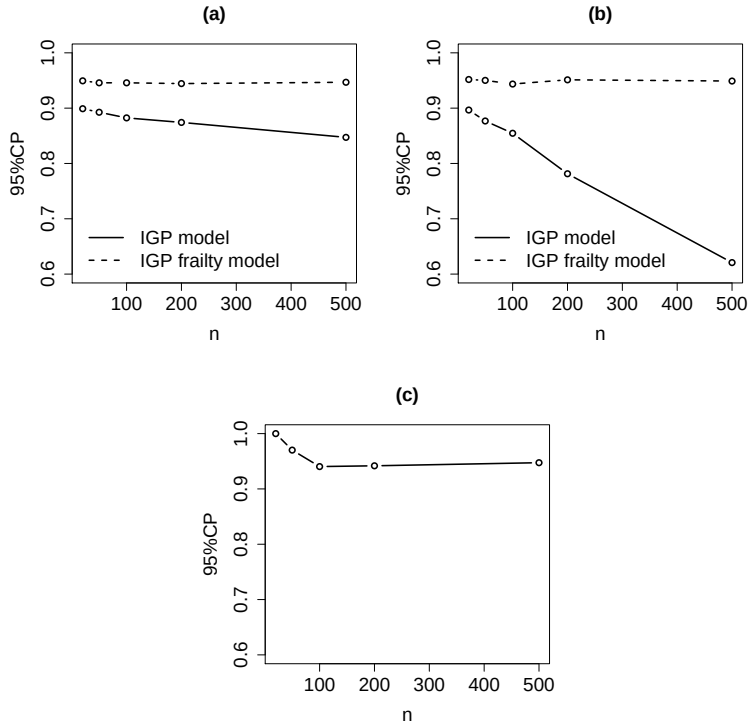

Figure 21 – 95% CPs under IG fraity and $\alpha = 0.05$: (a) 95% CPs for θ, (b) 95% CPs for η, (c) 95% CPs for α.

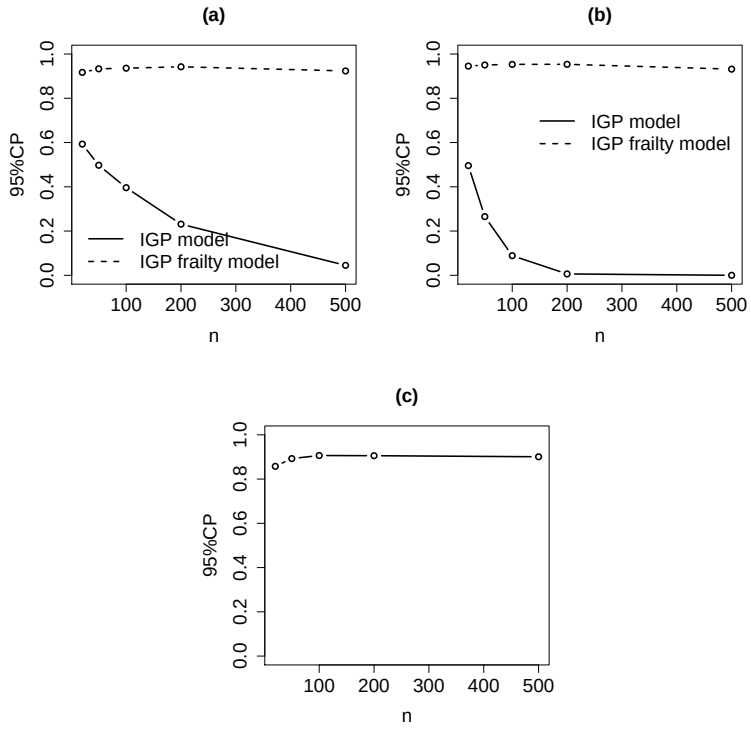

Figure 22 – 95% CPs under IG frailty and $\alpha = 0.5$: (a) 95% CPs for θ, (b) 95% CPs for η, (c) 95% CPs for α.

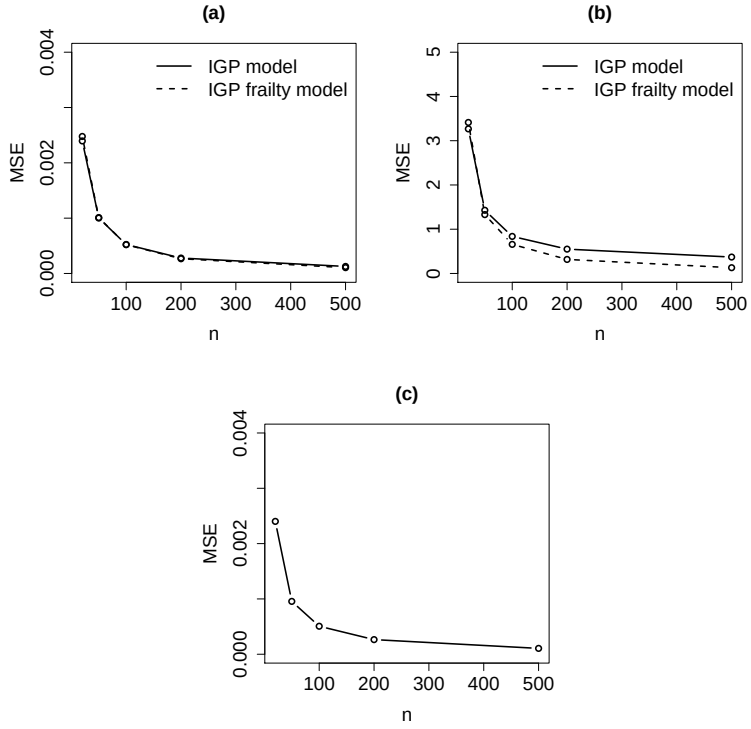

Figure 23 – MSEs under IG frailty and $\alpha = 0.05$: (a) MSEs for θ, (b) MSEs for η, (c) MSEs for α.

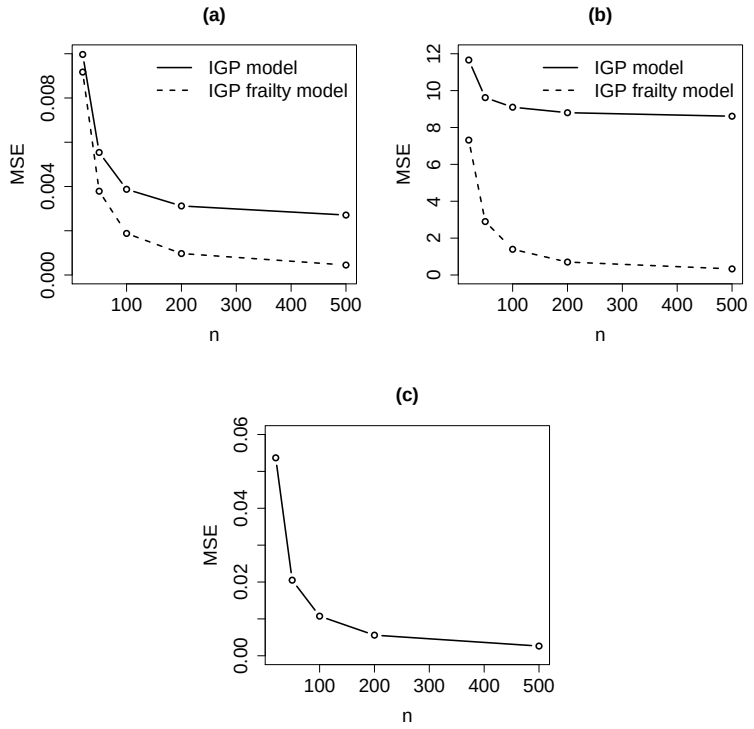

Figure 24 – MSEs under IG fraity and $\alpha = 0.5$: (a) MSEs for θ, (b) MSEs for η, (c) MSEs for α.

4.4 Application

In the application with the LASER and crack size data, we consider the following form for the mean function in IGP model: $g_{\boldsymbol{\theta}}(t) = \theta t$, $\theta > 0$. The parameter estimation was achieved by the Quasi-Newton optimization method through BFGS algorithm. The values used to initialize this algorithm were obtained as follows

- ✔ For IGP model, the starting values for θ and η are taken from Peng (2015), wherein the authors achieved the MLEs analytically,
- ✔ For IGP frailty model, the starting values for θ and η are identical to the MLEs in IGP model, and the starting value for α is equal to 1.

4.4.1 The LASER data (example 2.2.1)

Table 14 shows the MLEs, SEs and 95% CIs of the parameters under IGP model, IGP-Gamma frailty model and IGP-IG frailty model based on the LASER data. Due to the fact that α must assume only positive values, we constructed the 95% CIs of α under a one-to-one parameter transformation (KALBFLEISCH, 1985). We first obtained the confidence intervals for $\log(\alpha)$ and then transformed them back into confidence intervals for α. For illustrative purposes, the time unit is expressed in $1,000$ hours of operation, which means that the MLEs of θ must be divided by $1,000$ to be correctly interpreted.

Table 14 – MLEs, SEs and 95% CIs of the model parameters based on the LASER data.

Model	Parameter	MLE	SE	95% CI
IGP model (2.7)	θ	2.0372	0.0509	[1.9375; 2.1368]
	η	13.1300	1.3662	[10.4530; 15.8080]
IGP-Gamma	θ	2.0510	0.1004	[1.8542; 2.2478]
frailty model (4.14)	η	15.148	2.3398	[10.5620; 19.7340]
	α	0.2104	0.0974	[0.0849; 0.5214]
IGP-IG	θ	2.0563	0.1076	[1.8455; 2.2671]
frailty model (4.20)	η	15.1030	2.4479	[10.305; 19.9010]
	α	0.2478	0.1265	[0.0911; 0.6742]

From Table 14, we observe that the MLEs of the slope θ are similar in all models, whereas the MLEs of the shape parameter η are higher in both IGP frailty models than in IGP model because the variance α captures some of the variability inherent in the data. Furthermore, we noticed that the SEs of θ and η in both IGP frailty models are higher than in IGP model, which means that the SEs are considerably underestimated whether we ignore the unobserved heterogeneity. Indeed Chamberlain (1985) and Gail, Wieand and Piantadosi (1984) pointed out that the influence of the observed covariates is underestimated when the presence of omitted covariates is ignored.

To evaluate the goodness of fit for IGP model and IGP frailty model, Figure 25 displays the P-P plot and Q-Q plot along with the AD adherence test (MARSAGLIA; MARSAGLIA, 2004) of the observed degradation increments, in which we conclude that IGP-based models are suitable for these data because the dots in the charts are close to the diagonal line and the p-value in AD test is greater than 0.05.

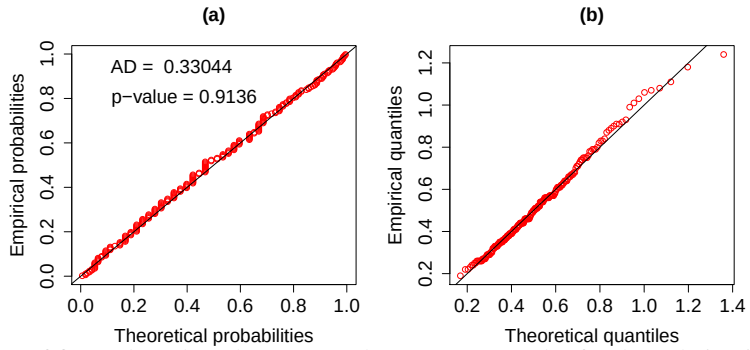

Figure 25 – Goodness of fit test based on the LASER data: (a) IG P-P plot for degradation increments and AD test, (b) IG Q-Q plot of the degradation increments.

In order to have a comparative approach between the models, Table 15 exhibits the model selection criteria AIC and BIC (for more details one may refer to section 2.6), from which we conclude that the IGP-IG frailty model best fitted this dataset given that the BIC and AIC values are the smallest.

Table 15 – AIC and BIC based on the LASER data.

Model	AIC	BIC
IGP model (2.7)	−146.07	−144.65
IGP-Gamma frailty model (4.14)	−174.57	−172.45
IGP-IG frailty model (4.20)	−175.81	−173.69

Additionally, the MLEs of the expected individual frailties ($\widehat{\mathrm{E}(z_i|\mathbf{Y})}$) are placed together with cumulative degradation values in Table 16, where the two most fragile components and the two less fragile components are highlighted in gray with their matching frailty estimates. We note that the highest means are directly related to the highest cumulative degradation values and vice versa. For illustrative purpose, Figure 26 shows the degradation paths from the LASER data along with the information from Table 16.

Table 16 – Cumulative degradation and MLEs of the expected individual frailties based on the LASER data.

		$\widehat{\mathrm{E}(z_i\|\mathbf{Y})}$	
unit	Cumulative Degradation	IGP-Gamma frailty model (4.14)	IGP-IG frailty model (4.20)
1	10.94	1.6902	1.7355
2	9.28	1.2311	1.2184
3	6.88	0.6805	0.6651
4	6.14	0.5589	0.5556
5	7.59	0.8659	0.8420
6	11.01	1.6993	1.7460
7	7.17	0.8343	0.8114
8	6.24	0.4995	0.5036
9	7.88	0.8950	0.8705
10	12.21	1.9484	2.0426
11	7.42	0.7611	0.7404
12	7.88	0.9892	0.9655
13	8.09	1.0230	0.9999
14	6.88	0.6973	0.6808
15	6.62	0.6339	0.6225

Finally, Table 17 shows the MLEs of the lifetime quantiles and their corresponding 95% CIs for threshold $\rho = 10\%$ according to example 2.2.1, from which we notice that the quantile MLEs in IGP frailty model are lower than in IGP model, and their 95% CIs in IGP frailty model are wider than in IGP model.

Figure 27 displays the charts of the lifetime CDF and PDF for the LASER components, from which we observe that the lifetime distributions for IGP model and IGP frailty model are unimodal and symmetrical and the IGP frailty model concentrates more probability mass around the median than the IGP model without frailty term.

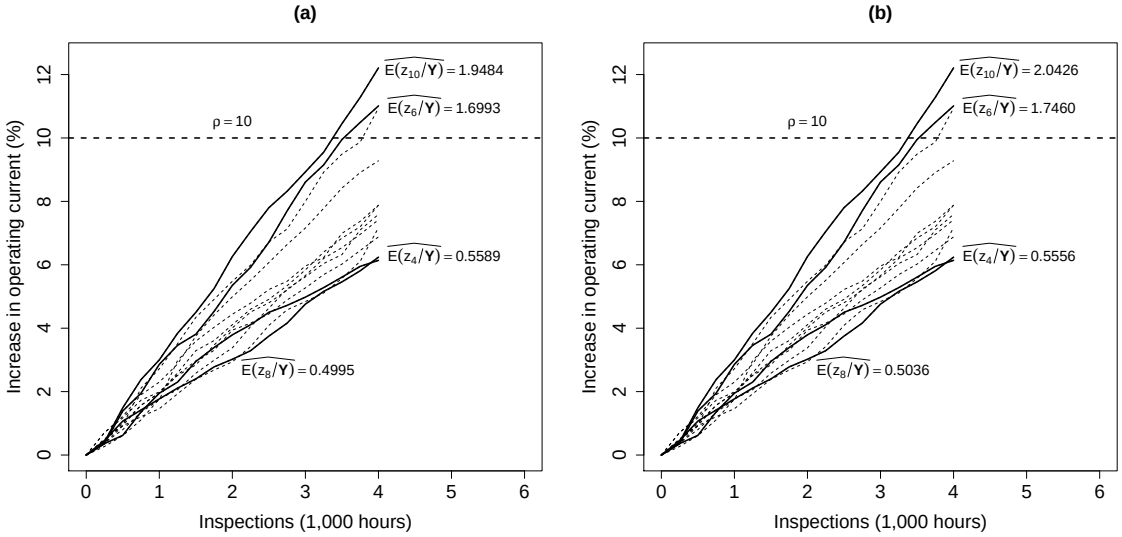

Figure 26 – Degradation paths from the LASER data and expected individual frailty MLEs under different models: (a) IGP-Gamma frailty model, (b) IGP-IG frailty model.

Table 17 – MLEs and 95% CIs of the lifetime quantiles based on the LASER data.

Model	quantile	MLE	95% CI
IGP model (2.7)	$t_{0.01}$	3.9341	[3.6806;4.1877]
	$t_{0.05}$	4.2250	[3.9788;4.4712]
	$t_{0.1}$	4.3801	[4.1367;4.6234]
	$t_{0.5}$	4.9274	[4.6881;5.1667]
	$t_{0.8}$	5.2870	[5.0450;5.5289]
IGP-Gamma frailty model (4.14)	$t_{0.01}$	3.8242	[3.2975;4.3509]
	$t_{0.05}$	4.1876	[3.6924;4.6827]
	$t_{0.1}$	4.3671	[3.8834;4.8508]
	$t_{0.5}$	4.9365	[4.4766;5.3963]
	$t_{0.8}$	5.2733	[4.8218;5.7248]
IGP-IG frailty model (4.20)	$t_{0.01}$	3.7917	[3.1956;4.3879]
	$t_{0.05}$	4.1748	[3.6377;4.7118]
	$t_{0.1}$	4.3587	[3.8420;4.8755]
	$t_{0.5}$	4.9266	[4.4461;5.4071]
	$t_{0.8}$	5.2595	[4.7879;5.7311]

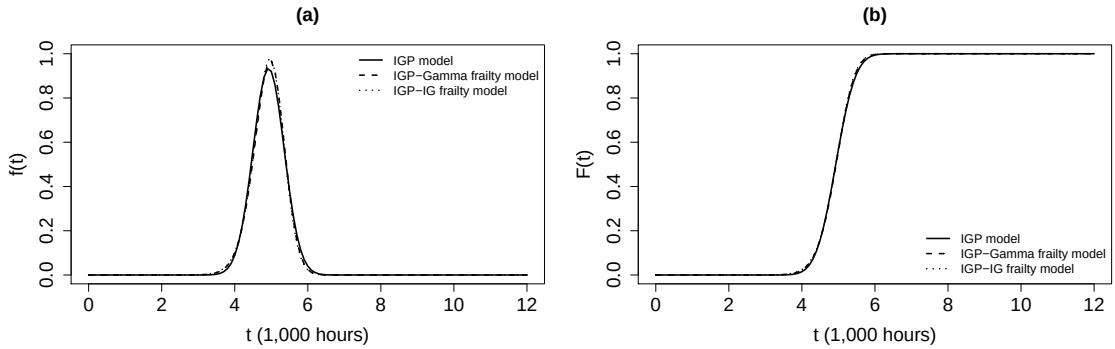

Figure 27 – Lifetime distribution based on the LASER data: (a) Lifetime PDF, (b) Lifetime CDF.

4.4.2 The crack size data (example 2.2.2)

In the application with crack size data, the following transformation was done: $D^*(t) = \log\left(\frac{D(t)}{0.9}\right)$ proposed by Lu and Meeker (1993) as a special case of Paris Law widely used to describe the growth of fatigue cracks in materials. This transformation satisfies $D(0) = 0$ in IGP model (2.7) and leaves the degradation paths close to linear behavior. Figure 28 shows the transformed degradation paths from the crack size data with the corresponding threshold ρ under the transformed data.

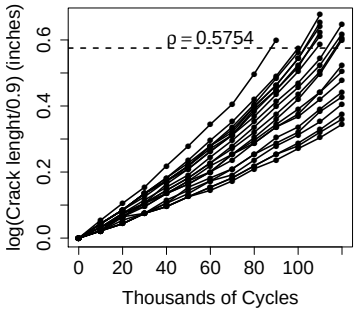

Figure 28 – Transformed degradation paths from the crack size data.

Table 18 shows the MLEs, SEs and 95% CIs of the parameters under different IGP models. Similarly to the application with LASER data, the 95% CIs of α are obtained under the exponential parameter transformation. For easy viewing, the unit scale of cycles is depicted in $1,000$ cycles, then the MLEs of θ need to be divided by $1,000$ in practice.

From Table 18, we observe that the MLE of α is lower in IGP-Gamma frailty model than in IGP-IG frailty model likewise its SE.

Figure 29 exhibits the P-P plot and Q-Q plot along with the AD adherence test of the observed degradation increments, from which we conclude that the IGP-based models are suitable for these data (p-value > 0.05).

Table 18 – MLEs, SEs and 95% CIs of the model parameters based on the crack size data.

Model	Parameter	MLE	SE	95% CI
IGP model (2.7)	θ	0.0047	0.0001	[0.0044; 0.0049]
	η	125.69	13.2510	[99.7160; 151.6600]
IGP-Gamma	θ	0.0049	0.0003	[0.0044; 0.0055]
frailty model (4.14)	η	145.5500	24.8930	[96.7630; 194.3400]
	α	0.4160	0.1454	[0.2097; 0.8252]
IGP-IG	θ	0.0050	0.0004	[0.0042; 0.0058]
frailty model (4.20)	η	138.7500	30.3990	[79.1680; 198.3300]
	α	0.7227	0.3702	[0.2648; 1.9721]

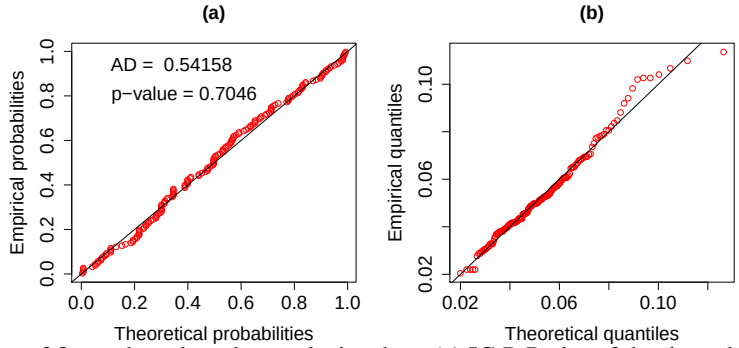

Figure 29 – Goodness of fit test based on the crack size data: (a) IG P-P plot of the degradation increments and AD test, (b) IG Q-Q plot of the degradation increments.

Additionally, Table 19 shows the model selection criteria AIC and BIC, from which we conclude that the IGP-Gamma frailty model best fitted this dataset given that the BIC and AIC values are the smallest.

Table 19 – AIC and BIC based on the crack size data.

Model	AIC	BIC
IGP model (2.7)	$-1,270.4$	$-1,268.4$
IGP-Gamma frailty model (4.14)	$-1,316.7$	$-1,313.5$
IGP-IG frailty model (4.20)	$-1,314.1$	$-1,310.9$

In order to analyze the individual frailties, Table 20 exhibits the MLEs of the expected individual frailties ($\widehat{\mathrm{E}(z_i|\mathbf{Y})}$) together with the corresponding cumulative degradation values. The two most fragile components and the two less fragile components are featured in gray. In general the highest means are directly related to the highest cumulative degradation values. Figure 30 displays the degradation paths from the crack size data with the four components highlighted in Table 20. It is worth mentioning that the frailty model takes into account the cumulative damage related to observation time, for example, the unit 1 does not have the highest degradation value but it was the first unit to reach the threshold value and did not remain until the end of the experiment.

Table 20 – Cumulative degradation and MLEs of the expected individual frailties based on the crack size data.

		$\widehat{\mathrm{E}(z_i\|\mathbf{Y})}$	
unit	Cumulative degradation	IGP-Gamma frailty model (4.14)	IGP-IG frailty model (4.20)
1	0.6001	1.7099	1.7426
2	0.5754	1.3346	1.2963
3	0.6763	1.5462	1.5333
4	0.6535	1.4607	1.4354
5	0.6419	1.4150	1.3838
6	0.6242	1.3460	1.3066
7	0.6122	1.2825	1.2367
8	0.5878	1.1921	1.1387
9	0.6477	1.2540	1.2044
10	0.6182	1.1344	1.0772
11	0.6061	1.0876	1.0283
12	0.6001	1.1138	1.0554
13	0.5241	0.8345	0.7728
14	0.4769	0.5585	0.5145
15	0.5041	0.6800	0.6257
16	0.4418	0.4864	0.4501
17	0.4274	0.4726	0.4379
18	0.4055	0.3813	0.3594
19	0.3754	0.2637	0.2623
20	0.3600	0.2159	0.2240
21	0.3444	0.1822	0.1974

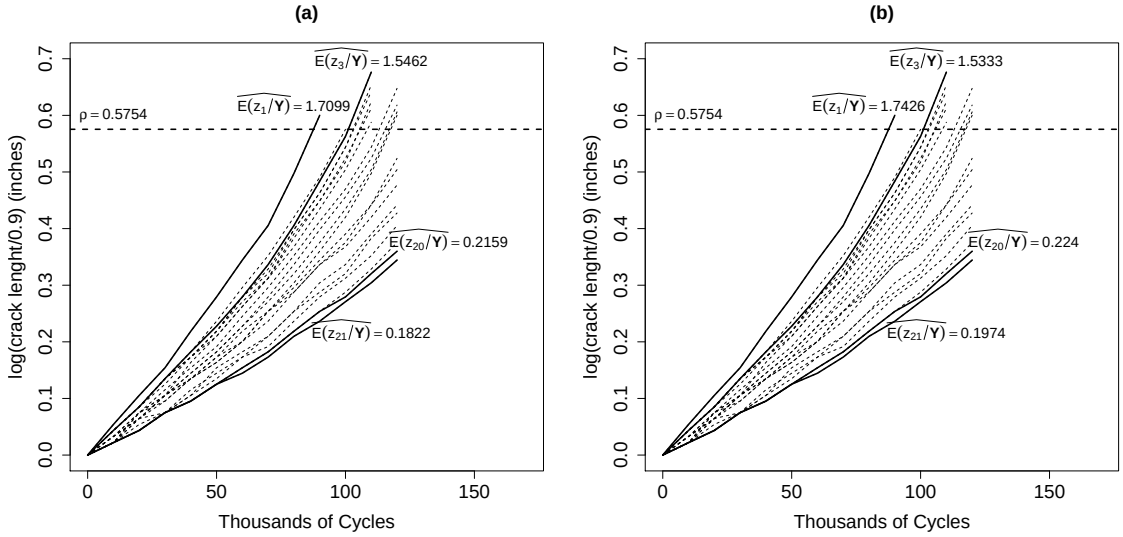

Figure 30 – (a) Degradation paths from the crack size data and expected individual frailty MLEs under different models: (a) IGP-Gamma frailty model, (b) IGP-IG frailty model.

Finally, Table 21 presents the MLEs of the lifetime quantiles with their corresponding 95% CIs considering the critical value $\rho = 1.6$ inches (see 2.2.3), or equivalently $\rho^* = 0.5754$ for transformed data and Figure 31 displays the charts of the lifetime CDF and PDF for the components.

Table 21 – MLEs and 95% CIs of the lifetime quantiles based on the crack size data.

Model	Quantile	MLE	95% CI
IGP model (2.7)	$t_{0.01}$	90.1820	[83.2820; 97.0810]
	$t_{0.05}$	99.9390	[93.3300; 106.5500]
	$t_{0.1}$	105.1500	[98.6510; 111.6400]
	$t_{0.5}$	123.5300	[117.1900; 129.8700]
	$t_{0.8}$	135.6100	[129.1500; 142.0700]
IGP-Gamma frailty model (4.14)	$t_{0.01}$	79.5580	[63.2580; 95.8580]
	$t_{0.05}$	93.1770	[78.2890; 108.0700]
	$t_{0.1}$	99.7460	[85.3810; 114.1100]
	$t_{0.5}$	119.7200	[106.4000; 133.0300]
	$t_{0.8}$	130.8500	[117.8500; 143.8500]
IGP-IG frailty model (4.20)	$t_{0.01}$	73.9050	[48.5510; 99.2590]
	$t_{0.05}$	90.6790	[69.9360; 111.4200]
	$t_{0.1}$	98.2260	[79.0710; 117.3800]
	$t_{0.5}$	119.0800	[102.4700; 135.7000]
	$t_{0.8}$	129.8900	[113.6100; 146.1600]

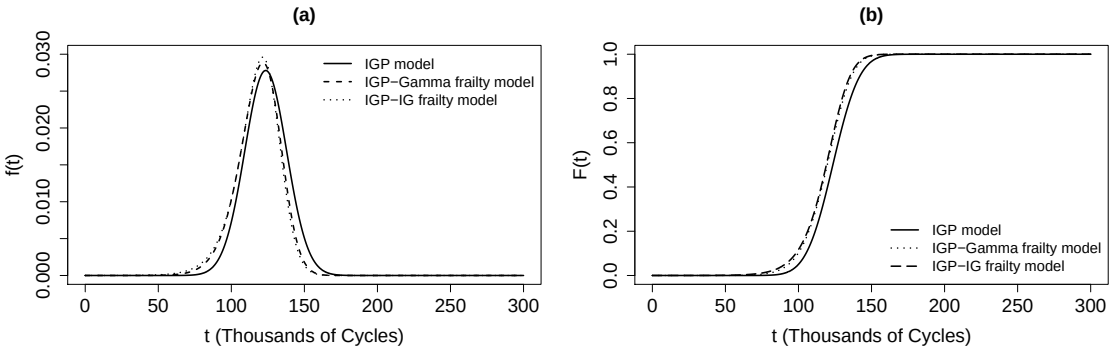

Figure 31 – Lifetime distribution based on the crack size data. (a) Lifetime PDF, (b) Lifetime CDF.

From Table 21 and Figure 31, we can observe that the PDF and CDF for IGP-Gamma frailty model and IGP-IG frailty model are similar to each other and differ from IGP model. Moreover, the presence of the frailty term slightly offsets the PDF to the left, which means that the time to failure is supposed to be lower in IGP frailty model than in IGP model.

4.5 Concluding remarks

We have proposed a frailty-based approach to estimation in the IGP model for degradation data. The motivation here is that the frailty model may be more appropriate to account for heterogeneity and of easy interpretation. In this study, we considered gamma and IG distribution for frailty. The methodology was implemented through the Quasi-Newton method and the BFGS algorithm in Ox software (DOORNIK, 2009) to obtain the MLEs of the model parameters. The algorithm reached convergence in the simulation study and in the application with real datasets. The simulation study showed that the asymptotic properties of the MLEs are compromised when we ignore the presence of frailty: the MSEs are small with large sample sizes but the CPs are not close to the nominal value, which is to say that the asymptotic intervals are not propitious to use. In the application with the LASER data and the crack size data, the IGP-IG and IGP-Gamma frailty models provided results similar to each other; the first one best fitted the LASER data and the second one best fitted the crack size data.

CHAPTER

5

MIXTURE INVERSE GAUSSIAN PROCESS IN DEGRADATION ANALYSIS AND BURN-IN POLICY

5.1 Introduction

In this chapter, we propose a decision rule for classifying a unit as normal or weak, and give an economic model for determining the optimal termination time and the other parameters of a burn-in test. We use a mixture IGP to fit the degradation paths. We describe the optimal burn-in procedure based on the proposed cost model. We analyze a real LASER dataset in the reliability literature and carry out an extensive Monte Carlo simulation study to illustrate the proposed methodology.

5.2 Mixture inverse Gaussian degradation process model

Commonly, electronic devices belong to heterogeneous population, consisting of two groups, the weak group and the normal one, wherein the weak group has a shorter mean lifetime than the normal one (ZHANG; YE; XIE, 2015). Mixture distributions have been commonly used to capture this sort heterogeneity, wherein the degradation paths are modeled through a mixture degradation process model.

Let $g_{\boldsymbol{\theta_1}}(t)$ and $g_{\boldsymbol{\theta_2}}(t)$ be the mean functions of the weak and normal groups of products, respectively. Then, the degradation path $D(t)$ in the mixture IGP is given by

$$D(t) \sim \begin{cases} \text{IG}(g_{\boldsymbol{\theta_1}}(t), \eta_1 g^2_{\boldsymbol{\theta_1}}(t)), \text{ for weak group,} \\ \text{IG}(g_{\boldsymbol{\theta_2}}(t), \eta_2 g^2_{\boldsymbol{\theta_2}}(t)), \text{ for normal group,} \end{cases} \tag{5.1}$$

where $g_{\boldsymbol{\theta_1}}(t)$ and $g_{\boldsymbol{\theta_2}}(t)$ are indexed by the parameter vectors $\boldsymbol{\theta_1}$ and $\boldsymbol{\theta_2}$, respectively, $g_{\boldsymbol{\theta_1}}(t) >$

$g_{\boldsymbol{\theta_2}}(t) > 0, \forall t \geq 0$, $\eta_1 > 0$ and $\eta_2 > 0$, then the mean function is greater in the weak group than in the normal group of products and the volatility parameters are different.

From (5.1), the degradation increment $Y = D(t+\Delta t) - D(t)$ in the time interval $\Delta t \equiv [t, t+\Delta t]$, has the following PDF:

$$f_Y(y) = p\sqrt{\frac{\eta_1}{2\pi y^3}}\Delta g_{\boldsymbol{\theta_1}}(t) e^{-\frac{\eta_1(y-\Delta g_{\boldsymbol{\theta_1}}(t))^2}{2y}} + (1-p)\sqrt{\frac{\eta_2}{2\pi y^3}}\Delta g_{\boldsymbol{\theta_2}}(t) e^{-\frac{\eta_2(y-\Delta g_{\boldsymbol{\theta_2}}(t))^2}{2y}}, \tag{5.2}$$

where $\Delta g_{\boldsymbol{\theta_1}}(t) = g_{\boldsymbol{\theta_1}}(t+\Delta t) - g_{\boldsymbol{\theta_1}}(t)$ is the time-function increment during the time interval Δt under weak units and $\Delta g_{\boldsymbol{\theta_2}}(t) = g_{\boldsymbol{\theta_2}}(t+\Delta t) - g_{\boldsymbol{\theta_2}}(t)$ is the time-function increment during the time interval Δt under normal units.

From (5.1), we can derive two particular cases:

✔ Case 1: When the degradation paths from both groups have the same volatility parameter, i.e., $\eta_1 = \eta_2 = \eta$, then we have

$$D(t) \sim \begin{cases} \text{IG}(g_{\boldsymbol{\theta_1}}(t), \eta g^2_{\boldsymbol{\theta_1}}(t)), & \text{for weak group,} \\ \text{IG}(g_{\boldsymbol{\theta_2}}(t), \eta g^2_{\boldsymbol{\theta_2}}(t)), & \text{for normal group;} \end{cases} \tag{5.3}$$

✔ Case 2: When the degradation paths from both groups have the same mean function, i.e., $g_{\boldsymbol{\theta_1}}(t) = g_{\boldsymbol{\theta_2}}(t) = g_{\boldsymbol{\theta}}(t)$, then we have

$$D(t) \sim \begin{cases} \text{IG}(g_{\boldsymbol{\theta}}(t), \eta_1 g^2_{\boldsymbol{\theta}}(t)), & \text{for weak group,} \\ \text{IG}(g_{\boldsymbol{\theta}}(t), \eta_2 g^2_{\boldsymbol{\theta}}(t)), & \text{for normal group.} \end{cases} \tag{5.4}$$

5.2.1 Lifetime distribution

The lifetime distribution information will be useful in developing a warranty policy for the units. The construction of the lifetime distribution is based on CDF lifetime in IGP model (2.12) in the following.

Let $D(t) \sim IG(g_{\boldsymbol{\theta_r}}(t), \eta g^2_{\boldsymbol{\theta_r}}(t))$, with $r = 1$ for the weak group and $r = 2$ for the normal group, one can obtain the lifetime CDF for the $r-$th group as

$$\begin{aligned} F_{T_r}(t) &= 1 - F_{IGP}(y = \rho | g_{\boldsymbol{\theta_r}}(t), \eta_r) \\ &= \Phi\left[-\sqrt{\frac{\eta_r}{\rho}}(\rho - g_{\boldsymbol{\theta_r}}(t))\right] - \exp(2\eta_r g_{\boldsymbol{\theta_r}}(t))\Phi\left[-\sqrt{\frac{\eta_r}{\rho}}(\rho + g_{\boldsymbol{\theta_r}}(t))\right]. \end{aligned} \tag{5.5}$$

Therefore, the lifetime PDF and the MTTF for the $r-$th group is readily obtained from (5.5).

5.2.2 Inference for unknown parameters

Consider a sample of n units with degradation collecting points $t_{i0} = 0, t_{i1}, \ldots, t_{in_i}$ and degradation values $D(t_{i1}), \ldots, D(t_{in_i})$. For each unit i and $1 \leq j \leq n_i$, define $Y_{ij} = D(t_{ij}) -$

$D(t_{i,j-1})$ to be the degradation increment in the time interval $[t_{i,j-1}, t_{ij}]$. From (5.2), the likelihood function is then given by

$$L(g_{\boldsymbol{\theta_1}}(t), g_{\boldsymbol{\theta_2}}(t), \eta_1, \eta_2, p) = \prod_{i=1}^{n} \left\{ p \prod_{j=1}^{n_i} \sqrt{\frac{\eta_1}{2\pi y_{ij}^3}} \Delta g_{\boldsymbol{\theta_1}}(t_{ij}) \exp\left[-\frac{\eta_1 (y_{ij} - \Delta g_{\boldsymbol{\theta_1}}(t_{ij}))^2}{2 y_{ij}} \right] \right.$$
$$\left. + (1-p) \prod_{j=1}^{n_i} \sqrt{\frac{\eta_2}{2\pi y_{ij}^3}} \Delta g_{\boldsymbol{\theta_1}}(t_{ij}) \exp\left[-\frac{\eta_2 (y_{ij} - \Delta g_{\boldsymbol{\theta_2}}(t_{ij}))^2}{2 y_{ij}} \right] \right\}, \tag{5.6}$$

where $\Delta g_{\boldsymbol{\theta_1}}(t_{ij}) = g_{\boldsymbol{\theta_1}}(t_{ij}) - g_{\boldsymbol{\theta_1}}(t_{i,j-1})$ is the time-function increment during the time interval $[t_{i,j-1}, t_{ij}]$ under weak units and $\Delta g_{\boldsymbol{\theta_2}}(t_{ij}) = g_{\boldsymbol{\theta_2}}(t_{ij}) - g_{\boldsymbol{\theta_2}}(t_{i,j-1})$ is the time-function increment during the time interval $[t_{i,j-1}, t_{ij}]$ under normal units.

Therefore, the log-likelihood function is given by

$$l(g_{\boldsymbol{\theta_1}}(t), g_{\boldsymbol{\theta_2}}(t), \eta_1, \eta_2, p) = \sum_{i=1}^{n} \log \left\{ p \prod_{j=1}^{n_i} \sqrt{\frac{\eta_1}{2\pi y_{ij}^3}} \Delta g_{\boldsymbol{\theta_1}}(t_{ij}) \exp\left[-\frac{\eta_1 (y_{ij} - \Delta g_{\boldsymbol{\theta_1}}(t_{ij}))^2}{2 y_{ij}} \right] \right.$$
$$\left. + (1-p) \prod_{j=1}^{n_i} \sqrt{\frac{\eta_2}{2\pi y_{ij}^3}} \Delta g_{\boldsymbol{\theta_2}}(t_{ij}) \exp\left[-\frac{\eta_2 (y_{ij} - \Delta g_{\boldsymbol{\theta_2}}(t_{ij}))^2}{2 y_{ij}} \right] \right\}. \tag{5.7}$$

The functions $g_{\boldsymbol{\theta_1}}(.)$ and $g_{\boldsymbol{\theta_2}}(.)$ have to be specified. The MLEs can be obtained by direct maximization of (5.7) with respect to the parameters. Intervals estimates and hypothesis tests can then be developed based on asymptotic properties of the MLEs.

5.3 Burn-in test and optimal burn-in time

A burn-in test is the process by which products are pre-tested prior to being placed in service. In general, this process forces certain failures to occur under supervised conditions so that the understanding of the product's load capacity can be established. For highly reliable products, we observe very few or no failures; then, we must propose a method to screen out the weak units from the normal ones based on degradation characteristics of such units. Our interest is determining the optimal burn-in time that classifies the components efficiently.

This procedure is essentially a hypothesis testing with the following assumptions

- ✔ H_0 (or null hypothesis): "the unit belongs to the normal group",
- ✔ H_a (or alternative hypothesis): "the unit belongs to the weak group".

The decision rule to screen out the weak units from the normal ones states when the null hypothesis must be rejected, as described below:

R: For fixed t_b, a unit is regarded as normal if and only if

$$D(t_b) \leq \xi(t_b), \tag{5.8}$$

where $\xi(t_b)$ denotes the unknown cutoff point at burn-in time t_b, which has to be determined.

The decision rule in (5.8) is liable to misclassification errors, and so we now introduce the misclassification probabilities associated with this decision rule.

Considering the general model (5.1), the probability of type I error (misclassifying a normal unit as weak), for each t_b, is given by

$$\alpha(t_b) = P(D(t_b) > \xi(t_b)|H_0) = 1 - F_{IG}(g_{\boldsymbol{\theta_2}}(t_b), \eta_2 g^2_{\boldsymbol{\theta_2}}(t_b)), \tag{5.9}$$

where $F_{IG}(.)$ is as defined in (2.6).

Similarly, the probability of type II error (misclassifying a weak unit as normal), for each t_b, is given by

$$\beta(t_b) = P(D(t_b) < \xi(t_b)|H_a) = F_{IG}(g_{\boldsymbol{\theta_1}}(t_b), \eta_1 g^2_{\boldsymbol{\theta_1}}(t_b)). \tag{5.10}$$

5.3.1 Optimal burn-in time and cutoff point

A concern in burn-in policy is to find a decision rule that maximizes the economic benefits (JENSEN, 1982). Based on this principle, we design an economic cost model, consisting of the following components:

- C_α: the cost of type I error,
- C_β: the cost of type II error,
- C_{op}: the cost of operating the burn-in procedure (from 0 up to t_b) for each unit,
- C_{mea}: the cost of collecting data for each unit,
- n: the total number of units subject to the burn-in test,
- p: the proportion of weak units.

C_α includes manufacturing costs and C_β includes warranty costs, while C_{op} includes labor costs and C_{mea} includes costs of setting up the measuring equipment.

The misclassification cost is the average of the costs C_α and C_β, weighted by their respective probabilities. Then, for each t_b, the misclassification cost is given by

$$MC(\xi(t_b)) = C_\alpha n(1-p)\alpha(t_b) + C_\beta np\beta(t_b). \tag{5.11}$$

The optimal cutoff point is the one that results in the minimal misclassification cost. In the following, we present the optimal cutoff point values for the different mixture IGPs presented earlier in section 5.2.

Theorem 5.3.1. For fixed t_b, the optimal cutoff point under model (5.1) is obtained through the equation

$$-\frac{\left(\xi(t_b)-g_{\boldsymbol{\theta_1}}(t_b)\right)^2\eta_1}{2\eta_1}+\frac{\left(\xi(t_b)-g_{\boldsymbol{\theta_2}}(t_b)\right)^2\eta_2}{2\eta_2}=\log(C), \tag{5.12}$$

which has two real roots given by

$$\begin{aligned}\widehat{\xi_1(t_b)} &= \frac{g_{\boldsymbol{\theta_1}}(t_b)\eta_1-g_{\boldsymbol{\theta_2}}(t_b)\eta_2-\log(C)+\frac{1}{2}\sqrt{\Delta}}{\eta_1-\eta_2},\\ \widehat{\xi_2(t_b)} &= \frac{g_{\boldsymbol{\theta_1}}(t_b)\eta_1-g_{\boldsymbol{\theta_2}}(t_b)\eta_2-\log(C)-\frac{1}{2}\sqrt{\Delta}}{\eta_1-\eta_2},\end{aligned}$$

where $C=\frac{C_\alpha(1-p)\sqrt{\eta_2}g_{\boldsymbol{\theta_2}}(t_b)}{C_\beta p\sqrt{\eta_1}g_{\boldsymbol{\theta_1}}(t_b)}$ and $\Delta=-4(\eta_1-\eta_2)(g^2_{\boldsymbol{\theta_1}}(t_b)\eta_1-g^2_{\boldsymbol{\theta_2}}(t_b)\eta_2+4(-g_{\boldsymbol{\theta_1}}(t_b)\eta_1$ $+g_{\boldsymbol{\theta_2}}(t_b)\eta_2+\log(C))^2$.

Proof. The proof is presented in Appendix A. □

There are two real roots for equation (5.12), and we have to check the value of the second derivative of the misclassification cost with respect to $\xi(t_b)$, to determine the minimizer. The second derivative of (5.11) with respect to $\xi(t_b)$ is given by

$$\frac{\partial^2 MC(\xi(t_b))}{\partial^2\xi(t_b)}=\frac{n\left(C_\beta e^{-b_1}g_{\boldsymbol{\theta_1}}(t_b)p\sqrt{\frac{\eta_1}{\xi(t_b)}}a_1-C_\alpha e^{-b_2}g_{\boldsymbol{\theta_2}}(t_b)(-1+p)\sqrt{\frac{\eta_2}{\xi(t_b)}a_2}\right)}{2\xi^3(t_b)\sqrt{2\pi}}, \tag{5.13}$$

where $a_1=-3\xi(t_b)-\xi^2(t_b)\eta_1+g^2_{\boldsymbol{\theta_1}}(t_b)\eta_1$, $a_2=3\xi(t_b)+\xi^2(t_b)\eta_2-g^2_{\boldsymbol{\theta_2}}(t_b)\eta_2$, $b_1=\frac{\left(\xi(t_b)-g_{\boldsymbol{\theta_1}}(t_b)\right)^2\eta_1}{2\xi(t_b)}$ and $b_2=\frac{\left(\xi(t_b)-g_{\boldsymbol{\theta_2}}(t_b)\right)^2\eta_2}{2\xi(t_b)}$.

We must take the solution which results in function (5.13) being positive, yielding a global minimal value for the misclassification cost in (5.11).

Corollary 5.3.2. For fixed t_b, the optimal cutoff point under model (5.3) is given by

$$\widehat{\xi(t_b)}=\frac{\left(g_{\boldsymbol{\theta_1}}(t_b)-g_{\boldsymbol{\theta_2}}(t_b)\right)\left(g_{\boldsymbol{\theta_1}}(t_b)+g_{\boldsymbol{\theta_2}}(t_b)\right)\eta}{\left(2\left(g_{\boldsymbol{\theta_1}}(t_b)-g_{\boldsymbol{\theta_2}}(t_b)\right)\eta-2\log\left[\frac{C_\alpha(1-p)g_{\boldsymbol{\theta_2}}(t_b)}{C_\beta p g_{\boldsymbol{\theta_1}}(t_b)}\right]\right.}. \tag{5.14}$$

Proof. The proof is exhibited in Appendix A. □

Corollary 5.3.3. For fixed t_b, the optimal cutoff point under model (5.4) is obtained through the equation

$$-\frac{(\xi(t_b)-g_{\boldsymbol{\theta}}(t_b))^2\eta_1}{2\eta_1}+\frac{(\xi(t_b)-g_{\boldsymbol{\theta}}(t_b))^2\eta_2}{2\eta_2}=\log\left[\frac{C_\alpha(1-p)\sqrt{\eta_2}}{C_\beta p\sqrt{\eta_1}}\right], \tag{5.15}$$

which has two real roots:

$$\widehat{\xi_1(t_b)} = \frac{g_{\boldsymbol{\theta}}(t_b)\eta_1 - g_{\boldsymbol{\theta}}(t_b)\eta_2 - \log\left[\frac{C_\alpha(1-p)\sqrt{\eta_2}}{C_\beta p\sqrt{\eta_1}}\right] + \sqrt{\Delta}}{\eta_1-\eta_2},$$
$$\widehat{\xi_2(t_b)} = \frac{g_{\boldsymbol{\theta}}(t_b)\eta_1 - g_{\boldsymbol{\theta}}(t_b)\eta_2 - \log\left[\frac{C_\alpha(1-p)\sqrt{\eta_2}}{C_\beta p\sqrt{\eta_1}}\right] - \sqrt{\Delta}}{\eta_1-\eta_2},$$

where $\Delta = -4g^2_{\boldsymbol{\theta}}(t_b)(\eta_1-\eta_2)^2 + \left(2g_{\boldsymbol{\theta}}(t_b)(\eta_1-\eta_2) - 2\log\left[\frac{C_\alpha(1-p)\sqrt{\eta_2}}{C_\beta p\sqrt{\eta_1}}\right]\right)^2$.

Proof. The proof is shown in Appendix A. □

In addition to the misclassification cost, we also need to pay attention to the burn-in test cost that includes the costs of conducting the degradation test and measuring the data.

For each unit i, let $t = 0, t_1, \ldots, t_{n_i}$ be the check points of a burn-in test, then the total number of data collecting points at t_b is $b+1$ for $1 \leq b \leq n_i$. Then the total cost of misclassification, for each t_b, is given by

$$TC(\xi(t_b)) = MC(\xi(t_b)) + C_{op} \times n \times t_b + C_{mea} \times n \times (b+1), \tag{5.16}$$

where $MC(\xi(t_b))$ is as given in (5.11). Then, the optimal burn-in time t_b can be obtained by minimizing (5.16).

5.4 Application - The LASER data revisited (example 2.2.1)

In the application with LASER data, we first analyze Figure 32, which displays the degradation paths separated into two groups: three units having the highest cumulative degradation belong to the weak group, while twelve units having the lowest cumulative degradation belong to the normal group, and we conclude that the mixture IG degradation process can be expressed by two mean functions $g_{\boldsymbol{\theta_1}}(t) = \theta_1 t$ and $g_{\boldsymbol{\theta_2}}(t) = \theta_2 t$, for the weak group and the normal one, respectively, with $\theta_1 > \theta_2 > 0$.

Additionally, we bring forward the mixture Wiener and gamma process models in a brief description. The aim here is to compare the proposed mixture IGP model with these well known models in the literature. For the sake of simplicity, the mixture Wiener and gamma processes are depicted under the case 1 (5.3).

Definition 5.4.1. The mixture Wiener process (TSENG; TANG, 2001) for the degradation up to time t, $D(t)$, considering two subpopulations, is an extension of Wiener process (2.3) and given by

$$D(t) \sim \begin{cases} v_1 t + \sigma B(t), & \text{for weak group,} \\ v_2 t + \sigma B(t), & \text{for normal group,} \end{cases} \tag{5.17}$$

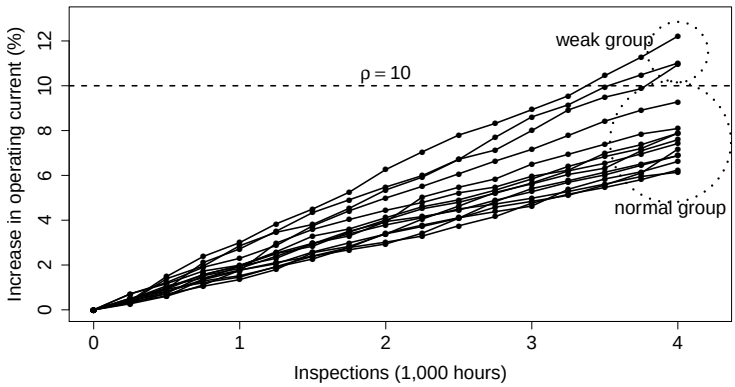

Figure 32 – Degradation paths from the LASER data separated into groups.

where v_1 and v_2 denote the drift parameters for weak and normal units, respectively, σ is the diffusion coefficient, and $B(t)$ is the standard Brownian motion.

Definition 5.4.2. The mixture gamma process (TSAI; TSENG; BALAKRISHNAN, 2011) for the degradation up to time t, $D(t)$, considering two subpopulations, is an extension of gamma process (2.4) and given by

$$D(t) \sim \begin{cases} \text{Gamma}\left(\varphi_{\boldsymbol{\psi_1}}(t), \upsilon\right) & \text{for weak group,} \\ \text{Gamma}\left(\varphi_{\boldsymbol{\psi_2}}(t), \upsilon\right), & \text{for normal group,} \end{cases} \tag{5.18}$$

where $\varphi_{\boldsymbol{\psi_1}}(t) > \varphi_{\boldsymbol{\psi_2}}(t), \forall t$ are the shape functions that take the forms $\varphi_{\boldsymbol{\psi_1}}(t) = \psi_1 t$ and $\varphi_{\boldsymbol{\psi_2}}(t) = \psi_2 t$ with $\psi_1 > \psi_2$ and $\upsilon > 0$ is the scale parameter.

Figure 33 shows the P-P plots along with the AD test (MARSAGLIA; MARSAGLIA, 2004) of the observed degradation increments under IG distribution, Normal distribution and gamma distribution, from which we notice that IG and gamma process models are more suitable for describing the LASER data than Wiener process (p-value < 0.05 for the normal group).

Table 22 shows the MLEs of the parameters and the corresponding log-likelihood and AIC values for the models in (5.1), (5.3), (5.4), (5.17) and (5.18). The MLEs for the models (5.1), (5.3) and (5.4) were obtained by the Quasi-Newton optimization method through BFGS algorithm, whereas the MLEs for the models (5.17) and (5.18) were taken from Tsai, Tseng and Balakrishnan (2011). Besides that, the starting values for the parameters in BFGS algorithm were identical to the MLEs from IGP model (2.7) taken from Table 14. It is worth mentioning that we did not face trouble in estimating the parameters of the Mixture IGP model due to the fact that the weak and normal groups are noticeable apart one from another.

For easy viewing, the time unit in all tables is expressed in $1,000$ hours of operation, then the MLEs of θ_1 and θ_2 in models (5.1) and (5.3), θ in model (5.4), v_1 and v_2 in model (5.17), ψ_1 and ψ_2 in model (5.18) must be divided by $1,000$ to be correctly interpreted. Similarly, the MLE of σ in model (5.17) must be divided by $\sqrt{1,000}$.

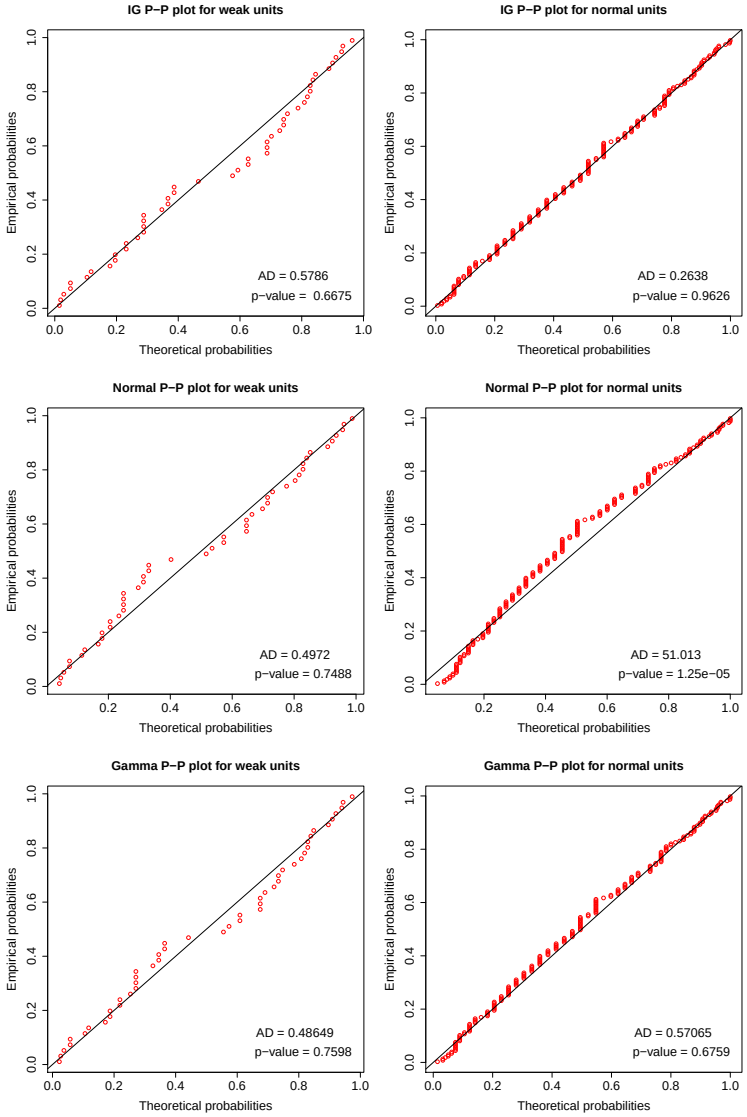

Figure 33 – P-P plots of the degradation increments under different distributions based on the LASER data.

From Table 22 we note that the model in (5.3) has the smallest AIC value, which corresponds to the mixture IGP with different mean functions and the same volatility parameter for both groups. Considering the model (5.3) as the best working model, we now investigate the optimal burn-in policy.

To construct the burn-in procedure described earlier in section 5.3, we set the cost parameters $C_\alpha = 65$, $C_\beta = 90$, $C_{op} = 0.0009$ and $C_{mea} = 0.0005$, as done in Tsai, Tseng and Balakrishnan (2011). Table 23 shows the estimated misclassification probabilities (5.9) and (5.10), the optimal cutoff point (5.14) and the total cost (5.16).

From Table 23, we observe that the smallest total cost is 54.7750 achieved at $t_b = 3{,}000$ h and the matching cutoff point is 6.7759. Therefore, the optimal burn-in policy consists in observing the components up to $3{,}000$ hours of operation, and all the units with $D(3{,}000) > 6.7759$ must be rejected and not delivered to market. For easy viewing, the corresponding cells are featured in gray.

Table 22 – MLEs of the model parameters, logL and AIC values based on the LASER data.

Model	Parameters	MLEs	logL	AIC
mixture IGP (5.1)	θ_1	2.7160	102.13	−194.26
	θ_2	1.7912		
	η_1	19.2410		
	η_2	16.0320		
	p	0.2660		
mixture IGP case 1 (5.3)	θ_1	2.6902	101.79	−195.59
	θ_2	1.8004		
	η	18.234		
	p	0.2661		
mixture IGP case 2 (5.4)	θ	2.0413	76.583	−145.17
	η_1	31.8490		
	η_2	11.7470		
	p	0.1610		
mixture Wiener process (5.17)	v_1	2.8087	73.6541	−139.31
	v_2	1.8252		
	σ	0.3454		
	p	0.2156		
mixture gamma process (5.18)	ψ_1	51.8910	97.1152	−186.23
	ψ_2	34.4520		
	υ	0.0521		
	p	0.2646		

Table 23 – MLEs of the misclassification probabilities, optimal cutoff point and total cost under mixture IGP model (5.3), based on the LASER data.

t_b	0.25	0.5	0.75	1	1.25	1.5	1.75	2
$\widehat{\xi(t_b)}$	0.60412	1.1639	1.7247	2.2858	2.8470	3.4082	3.9694	4.5307
$\widehat{\alpha(t_b)}$	0.1519	0.1204	0.0929	0.0718	0.0557	0.0435	0.0341	0.0268
$\widehat{\beta(t_b)}$	0.4054	0.2673	0.1911	0.1414	0.1067	0.0815	0.0629	0.0488
$\widehat{TC(t_b)}$	257.7500	188.9700	145.2900	115.7100	95.1340	80.7090	70.6470	63.7670
t_b	2.25	2.5	2.75	3	3.25	3.5	3.75	4
$\widehat{\xi(t_b)}$	5.0920	5.6533	6.2146	6.7759	7.3372	7.8985	8.4598	9.0211
$\widehat{\alpha(t_b)}$	0.0211	0.0167	0.0132	0.0105	0.0083	0.0066	0.0053	0.0042
$\widehat{\beta(t_b)}$	0.0381	0.0299	0.0235	0.0186	0.0147	0.0116	0.0092	0.0074
$\widehat{TC(t_b)}$	59.2490	56.5100	55.1230	54.7750	55.2270	56.3020	57.8620	59.8010

For the sake of analysis, one can refer to Table 38 in Appendix B then we observe that the LASER units 1, 2, 6 and 10 are classified as weak ones because $D(3,000) > 6.7759$ and the other LASER units are classified as normal ones. Therefore, we conclude that the optimal burn-in policy has screened out all the soft failures (units 1, 6 and 10). Additionally, this policy aims to predict failures in advance because the unit 2 is not a soft failure but it is supposed to belong to the weak group due to its high degradation values.

Finally, Table 24 shows the lifetime information for the weak and normal groups and Figure 34 displays the charts of the estimated lifetime CDF and PDF. From Table 24 we observe that the estimated lifetime percentiles and the MTTF in the weak group are apart from the ones in the normal group and almost all the weak components (95%) are expected fail up to $4,1794$ hours of operation. The same conclusions can be drawn from Figure 34 given that the PDF and CDF curves are different from each other. The lifetime information for weak and normal units let us check the differences between both groups and enables the industry to formulate a product guarantee policy for the delivered units.

Table 24 – MLEs and 95% CIs of the lifetime quantiles and MTTF based on the LASER data.

	weak group		normal group	
Quantity	MLE	95% CI	MLE	95% CI
$t_{0.05}$	3.2756	[3.2335; 3.3178]	4.8945	[4.8825; 4.9066]
$t_{0.5}$	3.7274	[3.5463; 3.9085]	5.5696	[5.5250; 5.6142]
$t_{0.8}$	3.9586	[3.8243; 4.0930]	5.9151	[5.8835; 5.9467]
$t_{0.95}$	4.1794	[4.1272; 4.2316]	6.2449	[6.2329; 6.2569]
MTTF	3.7275	[3.2625; 4.1924]	5.5696	[5.3142; 5.8251]

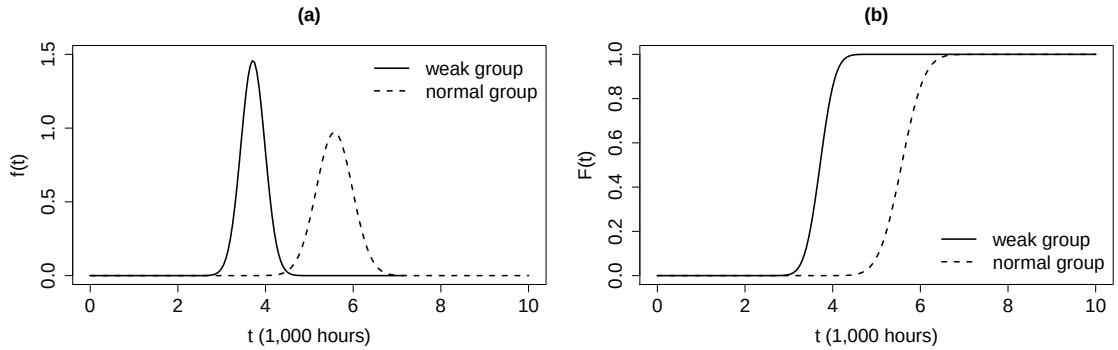

Figure 34 – Lifetime distribution for weak and normal groups based on the LASER data: (a) Lifetime PDF, (b) Lifetime CDF.

5.5 Simulation study

A simulation study was carried out. A total of $N = 1,000$ datasets with sample size $n = 200$ were generated. We generated the datasets through the mixture IGP model in (5.3). The true values of the parameters were set as the MLEs in Table 22. We made inference on parameters by considering the IGP model in (5.3), Wiener process model (5.17) and gamma process model (5.18). In other words, we generated data under the mixture IGP and estimated the parameters under the mixture Wiener and gamma processes, so that we can determine the effect of misspecifying a mixture IGP as a mixture Wiener or gamma processes.

Table 25 shows the MLEs of the parameters, from which we deduce that the MLEs based on the simulated data are close to the true parameter values in Table 22.

Table 25 – MLEs of the parameters based on the simulated data.

Model	Parameters	MLEs
mixture IGP case 1 (5.3)	θ_1	2.7019
	θ_2	1.7999
	η	18.238
	p	0.2665
mixture Wiener process (5.17)	ν_1	2.7035
	ν_2	1.8004
	σ	0.0106
	p	0.2656
mixture gamma process (5.18)	φ_1	52.7130
	φ_2	35.1570
	υ	0.0512
	p	0.2670

Let $\widehat{\alpha}_{IG}^{(k)}(t_b), \widehat{\beta}_{IG}^{(k)}(t_b), \widehat{\xi}_{IG}^{(k)}(t_b), \widehat{TC}_{IG}^{(k)}(t_b)$ denote the estimated misclassification probabilities, the cutoff point and the total cost of the k-th trial under model (5.3), respectively. The misclassification probabilities, the optimal cutoff point and the total cost under this model are then estimated empirically as

$$\overline{\alpha}_{IG}(t_b) = \frac{1}{N}\sum_{k=1}^{N}\widehat{\alpha}_{IG}^{(k)}(t_b), \overline{\beta}_{IG}(t_b) = \frac{1}{N}\sum_{k=1}^{N}\widehat{\beta}_{IG}^{(k)}(t_b), \overline{\xi}_{IG}(t_b) = \frac{1}{N}\sum_{k=1}^{N}\widehat{\xi}_{IG}^{(k)}(t_b)$$

$$\text{and } \overline{TC}_{IG}(t_b) = \frac{1}{N}\sum_{k=1}^{N}\widehat{TC}_{IG}^{(k)}(t_b).$$

Analogously, we estimated the misclassification probabilities, the optimal cutoff point and the total cost under model (5.17), and denoted them by

$$\overline{\alpha}_{W}(t_b), \overline{\beta}_{W}(t_b), \overline{\xi}_{W}(t_b) \text{ and } \overline{TC}_{W}(t_b),$$

and the misclassification probabilities, the optimal cutoff point and the total cost under model (5.18) are given by

$$\overline{\alpha}_G(t_b), \overline{\beta}_G(t_b), \overline{\xi}_G(t_b) \text{ and } \overline{TC}_G(t_b).$$

Tables 26, 27 and 28 show the estimated misclassification probabilities, optimal cutoff point and total cost under the models (5.3), (5.17) and (5.18), respectively.

Table 26 – Estimated misclassification probabilities, optimal cutoff point and total cost under mixture IGP model (5.3), based on the simulated data.

t_b	0.25	0.5	0.75	1	1.25	1.5	1.75	2
$\overline{\xi}_{IG}(t_b)$	0.6062	1.1667	1.7288	2.2912	2.8537	3.4163	3.9790	4.5416
$\overline{\alpha}_{IG}(t_b)$	0.1518	0.1192	0.0914	0.0702	0.0543	0.0421	0.0329	0.0257
$\overline{\beta}_{IG}(t_b)$	0.4034	0.2645	0.1881	0.1385	0.1041	0.0792	0.0608	0.0471
$\overline{TC}_{IG}(t_b)$	3384.9	2470.8	1892.4	1502.8	1233.5	1045.9	916.13	828.30

t_b	2.25	2.5	2.75	3	3.25	3.5	3.75	4
$\overline{\xi}_{IG}(t_b)$	5.1043	5.6670	6.2297	6.7924	7.3551	7.9178	8.4805	9.0432
$\overline{\alpha}_{IG}(t_b)$	0.0202	0.0159	0.0126	0.0099	0.0079	0.0063	0.0050	0.0040
$\overline{\beta}_{IG}(t_b)$	0.0366	0.0286	0.0224	0.0176	0.0139	0.0110	0.0087	0.0069
$\overline{TC}_{IG}(t_b)$	771.50	737.96	722.03	719.55	727.43	743.30	765.40	792.34

Table 27 – Estimated misclassification probabilities, optimal cutoff point and total cost under mixture Wiener process model (5.17), based on the simulated data.

t_b	0.25	0.5	0.75	1	1.25	1.5	1.75	2
$\overline{\xi}_{W}(t_b)$	0.6492	1.2122	1.7751	2.3381	2.9011	3.4641	4.0271	4.5900
$\overline{\alpha}_{W}(t_b)$	0.1184	0.0944	0.0718	0.0544	0.0413	0.0315	0.0241	0.0185
$\overline{\beta}_{W}(t_b)$	0.4372	0.2784	0.1925	0.1380	0.1011	0.0751	0.0563	0.0425
$\overline{TC}_{W}(t_b)$	3233.2	2302.5	1728.1	1351.0	1097.3	926.14	812.15	738.91

t_b	2.25	2.5	2.75	3	3.25	3.5	3.75	4
$\overline{\xi}_{W}(t_b)$	5.1530	5.7160	6.2790	7.4049	7.9679	8.5309	9.0939	10.713
$\overline{\alpha}_{W}(t_b)$	0.0143	0.0110	0.0085	0.0066	0.0051	0.0040	0.0031	0.0024
$\overline{\beta}_{W}(t_b)$	0.0323	0.247	0.0190	0.0146	0.0113	0.0087	0.0068	0.0053
$\overline{TC}_{W}(t_b)$	695.21	673.22	667.35	673.55	688.84	711.02	738.46	769.90

From Table 26, we observe that the optimal burn-in time based on the IGP model is $3,000$ hours of operation and the matching optimal cutoff point is 6.7924, with cells highlighted in gray. These results are similar to Table 23.

From Tables 27 and 28, we observe that the optimal burn-in time is $2,750$ hours for both Wiener and gamma process models and the cutoff point values are 6.2790 and 6.2077, respectively. For easy interpretation, the corresponding cells are featured in gray.

Thereby, to measure the effect of model misspecification, we analyze the relative bias (RB) of type I and II misclassification errors. For each burn-in time t_b, the RB of model

Table 28 – Estimated misclassification probabilities, optimal cutoff point and total cost under mixture gamma process model (5.18), based on the simulated data.

t_b	0.25	0.5	0.75	1	1.25	1.5	1.75	2
$\overline{\xi}_G(t_b)$	0.6244	1.1813	1.7393	2.2977	2.8562	3.4147	3.9733	4.5318
$\overline{\alpha}_G(t_b)$	0.1300	0.1027	0.0782	0.0595	0.0454	0.0348	0.0268	0.0207
$\overline{\beta}_G(t_b)$	0.4264	0.2739	0.1911	0.1382	0.1020	0.0763	0.0577	0.0439
$\overline{TC}_G(t_b)$	3295.2	2363.4.15	1784.3	1401.1	1141.1	963.76	844.21	766.02

t_b	2.25	2.5	2.75	3	3.25	3.5	3.75	4
$\overline{\xi}_G(t_b)$	5.0904	5.6491	6.2077	6.7663	7.3249	7.8836	8.4422	9.0008
$\overline{\alpha}_G(t_b)$	0.0160	0.0124	0.0097	0.0076	0.0059	0.0046	0.0036	0.0029
$\overline{\beta}_G(t_b)$	0.0336	0.0259	0.0200	0.0155	0.0120	0.0094	0.0073	0.0057
$\overline{TC}_G(t_b)$	718.00	692.28	683.24	686.74	699.77	720.06	745.90	776.02

misspecification of a mixture IG degradation model to be mistakenly treated as mixture Wiener process is given by

$$RB_{\alpha_W}(t_b) = \frac{\overline{\alpha}_W(t_b) - \overline{\alpha}_{IG}(t_b)}{\overline{\alpha}_{IG}(t_b)} \text{ and } RB_{\beta_W}(t_b) = \frac{\overline{\beta}_W(t_b) - \overline{\beta}_{IG}(t_b)}{\overline{\beta}_{IG}(t_b)}.$$

Similarly, the RB of model misspecification of a mixture IG degradation model to be mistakenly treated as mixture gamma process is given by

$$RB_{\alpha_G}(t_b) = \frac{\overline{\alpha}_G(t_b) - \overline{\alpha}_{IG}(t_b)}{\overline{\alpha}_{IG}(t_b)} \text{ and } RB_{\beta_G}(t_b) = \frac{\overline{\beta}_G(t_b) - \overline{\beta}_{IG}(t_b)}{\overline{\beta}_{IG}(t_b)}.$$

Tables 29 and 30 exhibit the RB values for Wiener and gamma process models $RB_{\alpha_W}(t_b)$ and $RB_{\alpha_G}(t_b)$, respectively.

Table 29 – Relative bias of type I and II errors for mixture Wiener process model (5.17), based on the simulated data.

t_b	0.25	0.5	0.75	1	1.25	1.5	1.75	2
$RB_{\alpha_W}(t_b)$	−0.2200	−0.2084	−0.2143	−0.2252	−0.2381	−0.2518	−0.2657	−0.2798
$RB_{\beta_W}(t_b)$	0.0838	0.0524	0.0231	−0.0037	−0.0286	−0.0521	−0.0745	−0.0959

t_b	2.25	2.5	2.75	3	3.25	3.5	3.75	4
$RB_{\alpha_W}(t_b)$	−0.2938	−0.3076	−0.3212	−0.3346	−0.3477	−0.3606	−0.3732	−0.3855
$RB_{\beta_W}(t_b)$	−0.1165	−0.1363	−0.1555	−0.1740	−0.1919	−0.2094	−0.2263	−0.2427

From Table 29, we note that the probability of type I error is underestimated for all burn-in times, while the probability of type II error is overestimated only for the first three burn-in times and underestimated for all other burn-in times. Moreover, the maximum values for RB_{α_W} and RB_{β_W} are -38.55% and $-24,27\%$, respectively, for burn-in time of $4,000$ hours of operation. These results are featured in gray.

Table 30 – Relative bias of type I and II errors for mixture gamma process model (5.18), based on the simulated data.

t_b	0.25	0.5	0.75	1	1.25	1.5	1.75	2
$RB_{\alpha_G}(t_b)$	−0.1441	−0.1380	−0.1437	−0.1526	−0.1628	−0.1737	−0.1847	−0.1959
$RB_{\beta_G}(t_b)$	0.0571	0.0356	0.0156	−0.0026	−0.0198	−0.0361	−0.0517	−0.0668
t_b	2.25	2.5	2.75	3	3.25	3.5	3.75	4
$RB_{\alpha_G}(t_b)$	−0.2070	−0.2180	−0.2290	−0.2399	−0.2506	−0.2611	−0.2720	−0.2820
$RB_{\beta_G}(t_b)$	−0.0814	−0.0957	−0.1095	−0.1231	−0.1363	−0.1492	−0.1619	−0.1743

Similarly, from Table 30, we note that the probability of type I error is underestimated for all burn-in times, while the probability of type II error is overestimated only for the first three burn-in times and underestimated for all the remaining burn-in times. Moreover, the maximum values for RB_{α_G} and RB_{β_G} are -28.20% and $-17,43\%$, respectively, which correspond to burn-in time of $4,000$ hours of operation (featured in gray).

These results show that the model misspecification influences the misclassification probabilities considerably, which do impact the optimal burn-in cost significantly.

5.6 Concluding remarks

In the case of highly reliable products wherein we have very few or no failures, it is quite difficult to determine the optimal burn-in time before such products being fielded to costumers. In this case, the optimal burn-in time can be obtained using degradation values. In this chapter, we have proposed a mixture IGP model for the analysis of degradation data and we have presented a decision rule to separate the weak units from the normal ones. We have then determined the optimal burn-in time and cutoff point based on a cost model. The methodology was implemented through the Quasi-Newton method and the BFGS algorithm in Ox software (DOORNIK, 2009) for obtaining the MLEs of the model parameters, which achieved convergence in the application with LASER data and in the simulation study. In the application with the LASER data, the proposed mixture IGP is shown to fit better than mixture Wiener and gamma processes. In the simulated study, we have shown that model misspecification influences the misclassification probabilities estimates considerably and consequently impacts the optimal burn-in costs.

CHAPTER

6

OPTIMAL BURN-IN POLICY BASED ON A SET OF CUTOFF POINTS

6.1 Introduction

In the chapter 5 it was considered an optimal burn-in policy that includes the optimal burn-in time and a single cutoff point that screen out the weak units from the normal ones in a production row. In this chapter, the optimal burn-in policy consists of the optimal burn-in time and a set of cutoff points rather than a single one. The main motivation is that this methodology exhibits several scenarios for the burn-in time and the cutoff points, in which we are able to choose the burn-in time and the number of cutoff points that lead to the minimum cost.

The mixture IGP model is used to capture the heterogeneity in the degradation paths according to the chapter 5 and under the case 1 (5.3). We state a decision rule for classifying an item as normal or weak based on burn-in time and a set of cutoff points. Then, an economic cost model is used to determine the optimal burn-in time and the optimal cutoff points, whose estimation is based on analytical method or an approximate method involving copula theory. Finally, an example on LASERs is analyzed to illustrate the proposed procedure.

6.1.1 Inference for unknown parameters

In this approach, the likelihood function is similar to equation (5.6) with some modification: for each unit i, its contribution in the likelihood function consists of all degradation values up to time t_b or the number n_i of degradation values (if $n_i < t_b$). Therefore the likelihood

function for n units being observed up to time t_b is given by

$$L(g_{\boldsymbol{\theta_1}}(t), g_{\boldsymbol{\theta_2}}(t), \eta, p) = \prod_{i=1}^{n} \left\{ p \prod_{j=1}^{b^*} \sqrt{\frac{\eta}{2\pi y_{ij}^3}} \Delta g_{\boldsymbol{\theta_1}}(t_{ij}) \exp\left[-\frac{\eta (y_{ij} - \Delta g_{\boldsymbol{\theta_1}}(t_{ij}))^2}{2y_{ij}} \right] \right.$$
$$\left. + (1-p) \prod_{j=1}^{b^*} \sqrt{\frac{\eta}{2\pi y_{ij}^3}} \Delta g_{\boldsymbol{\theta_1}}(t_{ij}) \exp\left[-\frac{\eta (y_{ij} - \Delta g_{\boldsymbol{\theta_2}}(t_{ij}))^2}{2y_{ij}} \right] \right\},$$

where $b^* = \min\{b, n_i\}$, $\Delta g_{\boldsymbol{\theta_1}}(t_{ij})$ and $\Delta g_{\boldsymbol{\theta_2}}(t_{ij})$ are as given in section 5.2.2.

In practical situations, this modification in the likelihood is reasonable, since the MLEs are conditioned to the stopping time. Additionally, the term b^* is useful in experiments where the units have different numbers of degradation values due to soft failures such as, for example, in the locomotive wheels data (example 2.2.2) and the fatigue crack size data (example 2.2.3). Consequently, the log-likelihood function is given by

$$l(g_{\boldsymbol{\theta_1}}(t), g_{\boldsymbol{\theta_2}}(t), \eta, p) = \sum_{i=1}^{n} \log \left\{ p \prod_{j=1}^{b^*} \sqrt{\frac{\eta}{2\pi y_{ij}^3}} \Delta g_{\boldsymbol{\theta_1}}(t_{ij}) \exp\left[-\frac{\eta (y_{ij} - \Delta g_{\boldsymbol{\theta_1}}(t_{ij}))^2}{2y_{ij}} \right] \right.$$
$$\left. + (1-p) \prod_{j=1}^{b^*} \sqrt{\frac{\eta}{2\pi y_{ij}^3}} \Delta g_{\boldsymbol{\theta_2}}(t_{ij}) \exp\left[-\frac{\eta (y_{ij} - \Delta g_{\boldsymbol{\theta_2}}(t_{ij}))^2}{2y_{ij}} \right] \right\}. \tag{6.1}$$

The MLEs can be obtained by direct maximization of (6.1) with respect to the parameters. Interval estimates can then be computed by resorting to the asymptotic properties of the MLEs.

6.1.2 Lifetime distribution

The construction of the lifetime distribution for the weak and normal groups is as given in section 5.2.1 considering the special case (5.3).

6.2 Optimal burn-in policy based on a set of cutoff points

The decision rule is based on the burn-in time t_b and a set of s cutoff points $\xi_1, \ldots, \xi_s$, with $1 \leq s \leq b$ as stated below:
R: For fixed t_b and s, a unit is regarded as normal if and only if

$$D(t_{b-s+j}) \leq \xi_j, \forall j = 1, \ldots, s \text{ with } 1 \leq s \leq b, \tag{6.2}$$

which means that we are making use of various cutoff points rather than a single cutoff point as shown in the decision rule (5.8) from chapter 5.

The misclassification probabilities associated with the decision rule (6.2) rely on null and alternative hypotheses stated earlier in section 5.3.

Considering model (5.3), the probability of type I error (misclassifying a normal unit as weak), for each t_b and s, is given below

$$\begin{aligned}\alpha(\xi_1,\ldots,\xi_s|t_b,s) &= P(D(t_{b-s+j}) > \xi_j, \text{ for some } j=1,\ldots,s|H_0)\\ &= 1-P\left(D(t_{b-s+1}) \le \xi_1,\ldots,D(t_b) \le \xi_s|H_0\right). \end{aligned} \tag{6.3}$$

Similarly, the probability of type II error (misclassifying a weak unit as normal), for each t_b and s, is given by

$$\begin{aligned}\beta(\xi_1,\ldots,\xi_s|t_b,s) &= P(D(t_{b-s+j}) \le \xi_j, \forall j=1,\ldots,s|H_a)\\ &= P\left(D(t_{b-s+1}) \le \xi_1,\ldots,D(t_b) \le \xi_s|H_a\right). \end{aligned} \tag{6.4}$$

The misclassification probabilities can be determined either by analytical methods or by approximate methods, depending on the number of cutoff points s.

6.2.1 Analytical methods for determining misclassification probabilities

For $s=1$, we have one cutoff point, in which case the probabilities in (6.3) and (6.4) are reduced to (5.9) and (5.10), respectively.

For $s=2$, we have two cutoff points, in which case the misclassification probabilities are obtained analytically through the CDF of bivariate IG distribution. In this context, we use the Theorem 6.2.1 below due to Al-Hussaini and ABD-El-Hakim (1981).

Theorem 6.2.1. Let X_1 and X_2 be two random variables with IG distribution: $X_1 \sim IG(\mu_{X_1},\lambda_{X_1})$ and $X_2 \sim IG(\mu_{X_2},\lambda_{X_2})$. Then, the joint CDF $F_{X_1,X_2}(x_1,x_2)$ is given by

$$\begin{aligned}F_{X_1,X_2}(x_1,x_2) &= [\Phi(a_1)+\exp(2\lambda_{X_1}\mu_{X_1})\Phi(-b_1)][\Phi(a_2)+\exp(2\lambda_{X_2}\mu_{X_2})\Phi(-b_2)]\\ &\quad +16\sqrt{\frac{\lambda_{X_1}\lambda_{X_2}}{\mu_{X_1}\mu_{X_2}}}\rho\exp\left(4\left(\frac{\lambda_{X_1}}{\mu_{X_1}}+\frac{\lambda_{X_2}}{\mu_{X_2}}\right)\right)\Phi(-\sqrt{2}b_1)\Phi(-\sqrt{2}b_2),\end{aligned}$$

where $a_j = \frac{\sqrt{\lambda_{X_j}}(x_j-\mu_{X_j})}{\mu_{X_j}\sqrt{x_j}}$, $b_j = \sqrt{\frac{4\lambda_{X_j}}{\mu_{X_j}}+a_j^2}$ and $\rho_{X_1,X_2} = \text{Corr}(X_1,X_2)$.

Proof. One may refer to Al-Hussaini and ABD-El-Hakim (1981). □

The formula for $\rho_{X_1,X_2} = \text{Corr}(X_1,X_2)$ can be obtained from Wasan (1969), who shows that the covariance formula between any two variables coming from an IGP is given by

$$\text{COV}(X(s),X(t)) = \text{VAR}(X(s)),$$

where $0<s<t$.

6.2.2 Approximate methods using copulas for misclassification probabilities

When $s > 2$, the misclassification probabilities may be obtained approximately, by the use of multivariate copulas with dimension equal to s described below.

A copula is a multivariate distribution whose marginals are all uniform over $(0,1)$. For a s-dimensional random vector U on the unit cube, a copula C is given by

$$C(u_1,\ldots,u_s) = P(U_1 \leq u_1,\ldots,U_s \leq u_s).$$

Let F be a s-dimensional distribution function with marginals $F_1,\ldots,F_s$. From Sklar (1959), there exists a s-dimensional copula C such that for all x in the domain of F, we have

$$F(x_1,\ldots,x_s) = C\{F_1(x_1),\ldots,F_s(x_s)\}.$$

In our work we have used elliptical copulas, which enable a flexible unstructured correlation matrix. A detailed discussion about elliptical distributions can be found in Fang, Kotz and Ng (1990). Let F be the multivariate CDF of an elliptical distribution. Let F_i be the CDF of the i-th marginal and F_i^{-1} be its inverse function (quantile function), for $i = 1,\ldots,s$. Then, the elliptical copula determined by F is

$$C(u_1,\ldots,u_s) = F\left(F_1^{-1}(u_1),\ldots,F_s^{-1}(u_s)\right). \tag{6.5}$$

By differentiating (6.5), we get the density of an elliptical copula to be

$$c(u_1,\ldots,u_s) = \frac{f\left(F_1^{-1}(u_1),\ldots,F_s^{-1}(u_s)\right)}{\prod_{i=1}^{s} f_i\left(F_i^{-1}(u_i)\right)},$$

where f is the joint PDF of the elliptical distribution, and $f_1,\ldots,f_s$ are the marginal density functions.

We resort to copula package (YAN, 2007) in R software (R Core Team, 2016). Actual elliptical copula classes implemented in copula package are Normal and t-copulas specified by multivariate normal and t distributions, respectively. Both these copulas have a dispersion matrix, inherited from the elliptical distribution, and t-copula has one extra parameter, namely, the degrees of freedom. Since copulas are invariant to monotonic transformations of the marginals, the correlation matrix determines the dependence structure. Commonly used correlation matrix structures are autorregressive of order 1, exchangeable, Toeplitz and unstructured. This method then computes the cumulative multivariate probabilities, and subsequently provides approximate misclassification probabilities from (6.3) and (6.4) for fixed t_b and s.

6.2.3 Optimal burn-in time and cutoff points

The misclassification cost is the average of the costs C_α and C_β, weighted by their respective probabilities. Then, for each t_b and s, the misclassification cost is a function of the

cutoff points $\xi_1, \ldots, \xi_s$ in the form

$$MC(\xi_1, \ldots, \xi_s | t_b, s) = C_\alpha n(1-p)\alpha(\xi_1, \ldots, \xi_s | t_b, s) + C_\beta np\beta(\xi_1, \ldots, \xi_s | t_b, s), \tag{6.6}$$

where $\alpha(\xi_1, \ldots, \xi_s | t_b, s)$ and $\beta(\xi_1, \ldots, \xi_s | t_b, s)$ are as given in (6.3) and (6.4), respectively.

Therefore, the total misclassification cost is the sum of the misclassification cost in (6.6) and additional costs for an entire sample and is of the form

$$TC(\xi_1, \ldots, \xi_s | t_b, s) = MC(\xi_1, \ldots, \xi_s | t_b, s) + C_{op} \times n \times t_b + C_{mea} \times n \times (b+1). \tag{6.7}$$

The optimal cutoff points are the ones that result in minimal misclassification cost in (6.6) for t_b and s, that is,

$$\widehat{\xi_1}, \ldots, \widehat{\xi_s} = \arg \min_{\xi_1, \ldots, \xi_s} MC(\xi_1, \ldots, \xi_s | t_b, s),$$

When $s = 1$, the optimal cutoff point is obtained analytically through equation (5.14); and when $s > 1$ the optimal cutoff points need to be determined numerically by iterative methods.

The optimal t_b and s are values that result in minimal total misclassification cost in (6.7):

$$\widehat{t_b}, \widehat{s} = \arg \min_{t_b, s} TC(\xi_1, \ldots, \xi_s | t_b, s).$$

In practical applications, the functions $g_{\boldsymbol{\theta_1}}(.)$ and $g_{\boldsymbol{\theta_2}}(.)$, the volatility parameter η and the proportion p are all unknown. For this reason, one may obtain the MLEs of the parameters described earlier in section 6.1.1 and make use of these values in (6.3), (6.4), (6.6) and (6.7).

6.3 Application

6.3.1 The LASER data (example 2.2.1)

For the application with LASER data, one may refer to chapter 5. Table 22 shows the MLEs of the parameters from mixture IGP under case 1: when the degradation paths from two groups have different mean functions and the same volatility parameter, referred to as model (5.3), from which we note that the weak group exhibit higher estimated angular coefficient than the normal group ($\widehat{\theta_1} > \widehat{\theta_2}$) and the estimated proportion of weak units in the sample is $26,61\%$.

For illustrative purposes, the time unit in all tables is expressed in $1,000$ hours, then the angular coefficients θ_1 and θ_2 must be divided by $1,000$ in practice.

6.3.2 Generated dataset

In practical situations, we have a large batch of units to be analyzed. To apply the proposed methodology, a dataset of size $n = 200$ with the same characteristics of the LASER

dataset was generated using the MLEs given in Table 22. The goal is to classify the units as normal or weak based on a burn-in test of $4,000$ hours of operation.

Table 41 in Appendix B displays the generated data indicating the weak and normal units and Figure 35 shows the simulated degradation paths indicating the critical value related to failure.

From Table 41, we observe that there are 58 (29%) weak units and 142 (71%) normal units. Due to the randomness in generating the data, the proportion of weak units in the artificial dataset is not exactly the same as the estimated proportion of weak units in the original LASER dataset. From Figure 35 we observe that the degradation paths hold linear pattern and are very similar to the original ones in LASER data.

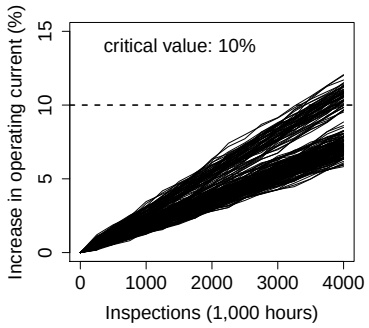

Figure 35 – Simulated degradation paths of 200 LASERs.

Table 31 shows the MLEs for different t_b values from minimum 500 h and the true parameter values appear in parentheses. In general, the MLEs become closer to the corresponding true values as the burn-in time increases.

Table 31 – MLEs of the parameters in (5.3) according to burn-in times t_b, based on simulated data.

t_b	$\theta_1(2.6902)$	$\theta_2(1.8004)$	$\eta(18.2340)$	$p(0.2661)$
0.50	2.7317	1.7946	18.4390	0.2795
0.75	2.6346	1.7769	18.4340	0.3045
1.00	2.6991	1.7947	18.8340	0.2912
1.25	2.7041	1.7877	18.3590	0.2704
1.50	2.7106	1.7818	18.9600	0.2668
1.75	2.7057	1.7811	18.7440	0.2731
2.00	2.6893	1.7885	18.4040	0.2835
2.25	2.6787	1.7850	18.3140	0.2954
2.50	2.6826	1.7935	18.6010	0.2877
2.75	2.6909	1.7950	18.4630	0.2893
3.00	2.6858	1.7923	18.5290	0.2889
3.25	2.6777	1.7899	18.6690	0.2896
3.50	2.6770	1.7882	18.7420	0.2901
3.75	2.6753	1.7920	18.6990	0.2899
4.00	2.6779	1.7924	18.6780	0.2900

To construct the burn-in procedure described earlier in section 6.2.3, we set the same cost parameters as given in section 5.4 and the results are split into two situations: $1 \leq s \leq 2$ and $s > 2$.

✔ When $1 \leq s \leq 2$

Table 32 shows the estimated total costs and the probabilities of misclassification under different t_b values from minimum 500 h and s values from 1 up to 2. The optimal burn-in time and number of cutoff points are $2,750$ h and $s = 2$, respectively, leading to the minimal total cost of 599.4861. The optimal cutoff points are 6.0180 and 6.5004, i.e, the optimal burn-in policy consists in observing the components up to $2,750$ hours of operation, and all the units with $D(2,500) > 6.0180$ or $D(2,750) > 6.5004$ must be rejected and not delivered to market. For easy viewing, the cells corresponding to these results are featured in gray.

For the sake of analysis, one can refer to Table 38 in Appendix B. For example, the weak components 5 and 61 are rejected by the optimal burn-in policy

- For unit 5, $D(2,500) = 6.62 > 6.0180$,
- For unit 61, $D(2,500) = 6.96 > 6.0180$.

However, the weak components 1 and 100 are not rejected by this policy

- For unit 1, $D(2,500) = 5.69 < 6.0180$ and $D(2,750) = 6.33 < 6.5004$),
- For unit 100, $D(2,500) = 5.79 < 6.0180$ and $D(2,750) = 6.39 < 6.5004$).

Under this policy, three weak components are not rejected and delivered to market, leading to the observed probability of type II error of 5.17% which is higher than the estimated one (0.81%). Concerning the normal components, all of them are accepted and delivered to market.

✔ When $s > 2$

The Normal and t-student from 1 to 5 degrees of freedom copulas were used to obtain the misclassification probabilities for the number of cutoff points higher than 2 $(s > 2)$.

The criterion assumed to choose the best copula consists in finding out the copula whose estimated misclassification probabilities for $s = 2$ was the closest to the corresponding values obtained by the analytical method. Thereby, we noted the t-copula with 1 degree of freedom (t_1) and the results are shown below.

Table 33 shows the estimated total costs considering copula theory, from which we notice that the optimal burn-in time and number of cutoff points are $3,000$ h and $s = 12$, respectively, leading to the minimal total cost of 686.6687 featured in gray.

Tables 34 and 35 show the estimated probability of type I and II errors, respectively, from which we conclude that the misclassification probabilities tend to decrease as burn-in

Table 32 – Estimated total cost and probabilities of type I and II errors for different values of t_b and s.

	$TC(\widehat{\xi}_1,\ldots,\widehat{\xi}_s\|t_b,s)$		$\alpha(\widehat{\xi}_1,\ldots,\widehat{\xi}_s\|t_b,s)$		$\beta(\widehat{\xi}_1,\ldots,\widehat{\xi}_s\|t_b,s)$		$\widehat{\xi}_1,\ldots,\widehat{\xi}_s$	
t_b	$s=1$	$s=2$	$s=1$	$s=2$	$s=1$	$s=2$	$s=1$	$s=2$
0.50	2388.8818	2389.9284	0.1208	0.1203	0.2320	0.2332	1.1586	(1.1607;1.1608)
0.75	2085.3670	2139.5356	0.1104	0.1109	0.1736	0.1827	1.6694	(1.6731;1.6732)
1.00	1481.0536	1552.3542	0.0731	0.0818	0.1197	0.1179	2.2677	(2.2519;2.2520)
1.25	1183.8672	1205.4909	0.0521	0.0683	0.0954	0.0683	2.8416	(2.4899;2.8627)
1.50	929.1636	864.4140	0.0360	0.0414	0.0657	0.0415	3.4036	(3.0558;3.4728)
1.75	835.7277	737.7367	0.0289	0.0297	0.0501	0.0287	3.9567	(3.6281;4.0638)
2.00	823.5396	710.2523	0.0263	0.0250	0.0427	0.0228	4.5041	(4.1950;4.6410)
2.25	784.4533	664.5760	0.0220	0.0188	0.0332	0.0162	5.0405	(4.7578;5.2121)
2.50	744.2518	632.0652	0.0168	0.0130	0.0265	0.0118	5.6194	(5.3566;5.8207)
2.75	723.4917	599.4861	0.0131	0.0066	0.0203	0.0081	6.1910	(6.0180;6.5004)
3.00	720.1626	616.3793	0.0104	0.0048	0.0160	0.0059	6.7403	(6.5888;7.0725)
3.25	728.8519	641.7614	0.0083	0.0036	0.0127	0.0043	7.2827	(7.1517;7.6362)
3.50	741.7310	670.8933	0.0064	0.0026	0.0098	0.0030	7.8364	(7.7268;8.2125)
3.75	768.5201	707.4199	0.0053	0.0020	0.0082	0.0024	8.3992	(8.3094;8.7969)
4.00	793.8918	744.0632	0.0042	0.0015	0.0064	0.0017	8.9635	(8.8952;9.3840)

time increases. The cells corresponding to the optimal burn-in time and cutoff points are featured in gray.

Table 33 – Estimated total cost for different values of t_b and s under t_1 copula.

t_b	$s=3$	$s=4$	$s=5$	$s=6$	$s=7$	$s=8$	$s=9$
0.75	1991.6201	–	–	–	–	–	–
1.00	1416.1506	1390.1332	–	–	–	–	–
1.25	1179.9117	1126.1684	1105.0808	–	–	–	–
1.50	906.6678	882.4789	871.5606	894.8505	–	–	–
1.75	859.5467	801.9121	841.4275	794.1043	806.0926	–	–
2.00	925.6880	808.7921	832.7379	777.5438	907.7153	816.8192	–
2.25	790.1508	880.6685	861.1221	755.9416	753.5009	766.0018	755.8983
2.50	793.5968	831.0500	726.8199	726.2244	721.3627	785.5936	714.4065
2.75	774.8139	718.6646	775.0801	706.3131	719.2641	741.3324	694.3394
3.00	759.3138	717.5317	711.4677	722.9218	707.5732	704.6590	703.5339
3.25	731.6504	795.1480	792.6829	724.6223	738.7455	719.2114	726.5759
3.50	765.5756	780.0877	808.4916	739.9365	835.5413	786.9763	759.8619
3.75	774.9722	800.7395	821.6631	834.2503	882.3471	855.0226	808.4283
4.00	789.5514	811.7325	790.2724	843.6182	849.9019	870.4556	788.7533

t_b	$s=10$	$s=11$	$s=12$	$s=13$	$s=14$	$s=15$	$s=16$
2.50	716.8341	–	–	–	–	–	–
2.75	712.3644	700.3879	–	–	–	–	–
3.00	705.5082	774.3641	686.6687	–	–	–	–
3.25	707.9439	740.3831	720.9134	727.9581	–	–	–
3.50	731.3081	732.3586	782.0207	732.2095	746.2420	–	–
3.75	838.4097	828.8112	796.8803	755.4353	755.4589	752.7242	–
4.00	787.3475	878.9960	803.7143	830.5440	795.4435	785.3977	777.7445

The optimal cutoff points related to the minimal total cost are shown in Table 36, therefore

Table 34 – Estimated probability of type I error for different values of t_b and s under t_1 copula.

t_b	$s=3$	$s=4$	$s=5$	$s=6$	$s=7$	$s=8$	$s=9$
0.75	0.1152	–	–	–	–	–	–
1.00	0.0704	0.0688	–	–	–	–	–
1.25	0.0458	0.0508	0.0513	–	–	–	–
1.50	0.0316	0.0328	0.0302	0.0358	–	–	–
1.75	0.0281	0.0273	0.0296	0.0244	0.0263	–	–
2.00	0.0318	0.0231	0.0271	0.0231	0.0302	0.0370	–
2.25	0.0202	0.0268	0.0211	0.0193	0.0206	0.0242	0.0192
2.50	0.0179	0.0224	0.0153	0.0169	0.0169	0.0172	0.0169
2.75	0.0131	0.0111	0.0154	0.0126	0.0122	0.0143	0.0104
3.00	0.0123	0.0114	0.0101	0.0101	0.0099	0.0089	0.0094
3.25	0.0083	0.0118	0.0122	0.0082	0.0088	0.0082	0.0076
3.50	0.0079	0.0105	0.0080	0.0051	0.0084	0.0086	0.0068
3.75	0.0056	0.0065	0.0061	0.0095	0.0076	0.0059	0.0061
4.00	0.0041	0.0059	0.0048	0.0064	0.0072	0.0050	0.0043

t_b	$s=10$	$s=11$	$s=12$	$s=13$	$s=14$	$s=15$	$s=16$
2.50	0.0156	–	–	–	–	–	–
2.75	0.0128	0.0130	–	–	–	–	–
3.00	0.0102	0.0104	0.0087	–	–	–	–
3.25	0.0070	0.0082	0.0074	0.0047	–	–	–
3.50	0.0063	0.0058	0.0096	0.0059	0.0077	–	–
3.75	0.0102	0.0061	0.0062	0.0045	0.0052	0.0048	–
4.00	0.0046	0.0051	0.0057	0.0035	0.0044	0.0039	0.0034

the optimal burn-in policy consists in observing the components up to 3,000 hours, and all the units must satisfy $D(250) \leq \widehat{\xi}_1, \ldots, D(3,000) \leq \widehat{\xi_{12}}$ to be delivered to market.

From exploratory analysis of Table 38 in Appendix B, the weak units 51 and 92 are rejected by the optimal burn-in policy:

- For unit 51, $D(2,250) = 5.80 > \widehat{\xi}_9 = 5.6336$,
- For unit 92, $D(2,000) = 5.56 > \widehat{\xi}_8 = 5.3350$.

However, the weak unit 1 is not rejected by the optimal burn-in policy. Under this policy, only one weak components is delivered to market, leading to the observed probability of type II error of 1.72% which is close to the estimated one (1.27%). In regard of the normal components, all of them are delivered to market. We also note that the probability of type II error under this policy is lower than in the policy with two cutoff points.

Finally, we can access the components lifetime distribution based on the estimates from Table 31 and a fixed threshold $\rho = 10\%$ (see example 2.2.1). Table 37 exhibits the lifetime information for the weak and normal groups under burn-in times 2,750 h (obtained through analytical method) and 3,000 h (obtained through approximate method). From Table 37 we observe that the estimated lifetime percentiles and MTTF in the weak group are apart from the

Table 35 – Estimated probability of type II error for different values of t_b and s under t_1 copula.

t_b	$s=3$	$s=4$	$s=5$	$s=6$	$s=7$	$s=8$	$s=9$
0.75	0.1494	–	–	–	–	–	–
1.00	0.1127	0.1108	–	–	–	–	–
1.25	0.1088	0.0868	0.0818	–	–	–	–
1.50	0.0714	0.0633	0.0660	0.0594	–	–	–
1.75	0.0584	0.0471	0.0513	0.0511	0.0497	–	–
2.00	0.0539	0.0464	0.0448	0.0395	0.0538	0.0228	–
2.25	0.0371	0.0448	0.4999	0.0327	0.0301	0.0267	0.0330
2.50	0.0347	0.0352	0.0269	0.0233	0.0222	0.0340	0.0212
2.75	0.0307	0.0243	0.0271	0.0183	0.0215	0.0222	0.0196
3.00	0.0211	0.0154	0.0154	0.0178	0.0154	0.0157	0.0146
3.25	0.0154	0.0203	0.0194	0.0132	0.0145	0.0112	0.0138
3.50	0.0135	0.0122	0.0200	0.0122	0.0249	0.0158	0.0143
3.75	0.0108	0.0126	0.0185	0.0155	0.0263	0.0250	0.0143
4.00	0.0060	0.0085	0.0616	0.0138	0.0124	0.0194	0.0055

t_b	$s=10$	$s=11$	$s=12$	$s=13$	$s=14$	$s=15$	$s=16$
2.50	0.0240	–	–	–	–	–	–
2.75	0.0192	0.0161	–	–	–	–	–
3.00	0.0139	0.0275	0.0127	–	–	–	–
3.25	0.0111	0.0150	0.0129	0.0192	–	–	–
3.50	0.0080	0.0096	0.0124	0.0090	0.0090	–	–
3.75	0.0141	0.0191	0.0130	0.0073	0.0061	0.0063	–
4.00	0.0050	0.0220	0.0069	0.0150	0.0063	0.0057	0.0048

Table 36 – Optimal cutoff points for $t_b = 3{,}000$ h and $s = 12$ under t_1 copula.

$\widehat{\xi_1}$	$\widehat{\xi_2}$	$\widehat{\xi_3}$	$\widehat{\xi_4}$	$\widehat{\xi_5}$	$\widehat{\xi_6}$
1.2083	1.7824	2.7676	3.3106	3.8165	4.9439

$\widehat{\xi_7}$	$\widehat{\xi_8}$	$\widehat{\xi_9}$	$\widehat{\xi_{10}}$	$\widehat{\xi_{11}}$	$\widehat{\xi_{12}}$
5.1440	5.3350	5.6336	6.1722	6.5208	6.8040

ones in the normal group and almost all the weak units are supposed to have failed up to $4,175$ h. The results are similar for different burn-in times. Figure 36 displays the charts for estimated CDF and PDF for burn-in time $3,000$ h, from which we conclude that the PDF and CDF curves are different from each other. We can note that the lifetime information for the simulated data are similar to the ones from the original LASER data (see Table 24 and Figure 34).

Table 37 – MLEs and 95% CIs of the lifetime quantiles and MTTF under different t_b values, considering simulated data.

		weak group		normal group	
t_b	Quantity	MLE	95% CI	MLE	95% CI
2.75	$t_{0.05}$	3.2774	[3.2638;3.2910]	4.9133	[4.9092;4.9174]
	$t_{0.5}$	3.7263	[3.6679;3.7847]	5.5862	[5.5711;5.6014]
	$t_{0.8}$	3.9560	[3.9127;3.9994]	5.9306	[5.9199;5.9414]
	$t_{0.95}$	4.1753	[4.1585;4.1922]	6.2594	[6.2553;6.2635]
	MTTF	3.7263	[3.5774;3.8753]	5.5863	[5.4995;5.6731]
3.00	$t_{0.05}$	3.2844	[3.2715;3.2973]	4.9218	[4.9179;4.9257]
	$t_{0.5}$	3.7333	[3.6779;3.7888]	5.5945	[5.5801;5.6089]
	$t_{0.8}$	3.9631	[3.9220;4.0042]	5.9388	[5.9286;5.9491]
	$t_{0.95}$	4.1824	[4.1665;4.1984]	6.2675	[6.2636;6.2714]
	MTTF	3.7334	[3.5917;3.8750]	5.5946	[5.5119;5.6773]

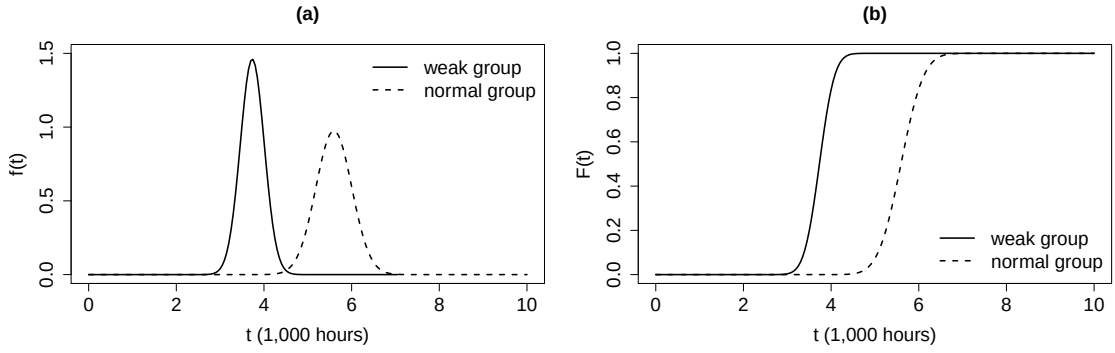

Figure 36 – Lifetime distribution for weak and normal groups considering simulated data: (a) Lifetime PDF, (b) Lifetime CDF.

6.4 Concluding remarks

In this chapter, motivated by a LASER data, we have proposed a mixture IGP model to analyze the degradation of highly reliable products. It is quite difficult to determine the optimal burn-in time within a rather short period of life testing, but this problem can be solved successfully if there exists a QC whose degradation over time can be related to the product's reliability. Firstly, we developed a burn-in methodology whose main objective is to find out the optimal burn-in policy to screen out the weak units from the normal ones in a production row. We have considered a set of cutoff points and two methods for the computation of the misclassification probabilities; more specifically, an analytical method for the case when we have at most 2 cutoff points and an approximate method based on copulas for the case when we have more than 2 cutoff points. Besides we build up an economic cost model in which the optimal burn-in policy is directly related to the minimum cost. Finally, we illustrated the methodology through a simulated LASER dataset with size 200 and the same characteristics as the LASER data from the reliability literature. The Quasi-Newton method through BFGS algorithm in R software (R Core Team, 2016) was used to obtain the MLEs of the model parameters, and also to determine the optimal cutoff points when $s > 1$. For $s > 2$, we resorted to copula package along with the BFGS algorithm to obtain the optimal cutoff points. These methods reached convergence in the situations mentioned. The optimal burn-in time and cutoff points were found for both cases analytical $(s \leq 2)$ and approximate $(s > 2)$. The approximate method based on copulas presented better results for this dataset.

CHAPTER

7

DISCUSSION, CONCLUSIONS AND FUTURE RESEARCH

Degradation analysis is a useful technique for accessing reliability information from highly reliable components, which take a long time to fail even when they are placed to operate under accelerated conditions. In this thesis we have proposed different methodologies for degradation data based on IG distribution. The random deteriorate rate model based on IG distribution aims to explain the heterogeneity commonly observed in degradation problems and the incorporation of a frailty parameter in IG process model brings additional information that may be useful in practice. Besides these two approaches, the mixture IG process captures the variability in the degradation paths when they come from a mixture of deterioration processes.

The IG random deterioration rate model with measurement errors presented interesting asymptotic properties with respect to its maximum likelihood estimators and the application with real datasets presented similar results to the random deterioration rate model with gamma distribution addressed in the literature. The IGP frailty model was regarded as an extension of the traditional IG process and presented meritorious results in the simulated study. In the application with real datasets, the IGP-Gamma and IGP-IG frailty models presented similar results and we could estimate the individual frailties even as the component's lifetime distribution through the proposed methodology. Both IG random rate and IGP frailty models aim to capture the temporal variability inherent in the degradation data, even as the variability among the paths and within the same path.

The mixture IG process presented satisfactory results in burn-in tests and the simulation study showed that the model misspecification affects the misclassification probabilities, and consequently, the computation of the costs and the achievement of an optimal burn-in policy. The optimal burn-in policy based on a set of cutoff points is a more flexible method which improves the way the weak components are separated from the normal ones in a production row. In the application with the LASER data, we obtained the optimal burn-in policy consisting

of the optimal stopping time and cutoff points even as the other parameters of the burn-in test. Furthermore, we could assess the component's lifetime distribution, which is a very interesting information particularly in developing warranty strategies regarding the units labeled as normal and sent to market.

The entire inferential procedure in this thesis was based on maximum likelihood estimation combined with other methods such as, for example, Laplace transform for solving analytical integrals, Gaussian quadrature for estimating the non analytical integrals and copula theory for obtaining multivariate IG probabilities.

The present study leaves some open topics to be addressed in the future. Regarding the assumptions resorted to the degradation process, we can drop the statement that the degradation paths start from the origin, then the paths may have an unknown starting point which can be fixed or random. Moreover, we can deal with problems where the degradation paths exhibit decreasing behavior and functional forms other than linear.

In the subject of IG process with frailty, we may purpose to introduce the accelerated IG process with frailty for modeling degradation data, in which some accelerating covariates will be included in the intensity function of the IG process. Besides that, we may consider the generalized gamma as a flexible class of frailty distributions in which gamma, IG and lognormal distributions are particular cases.

In the field of burn-in policies, we may look upon the proposal of Xiang, Coit and Feng (2013), in which the components are split into n subpopulations from various stochastic processes. Additionally, we may develop a simulation study to verify the feasibility of copula theory for the estimation of the misclassification probabilities when the decision rule consists of more than two cutoff points.

Furthermore, it will be of interest to explore the EM algorithm (Expectation-Maximization algorithm), which is widely used for maximum likelihood estimation in random effects and frailty models. In many problems, calculating the conditional expectation required in the E-step of this algorithm may be unfeasible, then the E-step can be fulfilled through the stochastic EM algorithm (NIELSEN, 2000).

Finally, the Bayesian inference is an alternative approach for estimating the quantities of interest. The Bayesian methods are widely used in several areas notably in the last decades due to the recent advances in computational Markov chain Monte Carlo (MCMC) methods.

BIBLIOGRAPHY

AALEN, O. O. Modelling heterogeneity in survival analysis by the compound poisson distribution. **The Annals of Applied Probability**, Institute of Mathematical Statistics, v. 2, n. 4, p. 951–972, 1992. Cited on page 58.

ABRAMOWITZ, M.; STEGUN, I. A. Laplace transforms. In: ____. **Handbook of Mathematical Functions. Ninth printing**. New York: Dover, 1972. cap. 29, p. 1019–1030. Cited on page 35.

AL-HUSSAINI, E. K.; ABD-EL-HAKIM, N. S. Bivariate inverse gaussian distribution. **Annals of the Institute of Statistical Mathematics**, v. 33, n. 1, p. 57–66, 1981. Cited on page 99.

BROWN, R. A brief account of microscopical observations made in the months of june, july and august 1827, on the particles contained in the pollen of plants; and on the general existence of active molecules in organic and inorganic bodies. **Philosophical Magazine Series 2**, v. 4, n. 21, p. 161–173, 1828. Cited on page 28.

BRYCHKOV, Y. A. **Handbook of special functions: derivatives, integrals, series and other formulas**. [S.l.]: CRC Press, 2008. Cited on page 119.

CARRASCO, J. M.; FERRARI, S. L.; ARELLANO-VALLE, R. B. Errors-in-variables beta regression models. **Journal of Applied Statistics**, v. 41, n. 7, p. 1530–1547, 2014. Cited on page 41.

CHAMBERLAIN, G. Heterogeneity, omitted variable bias, and duration dependence. In: HECKMAN, J. J.; SINGER, B. S. (Ed.). **Longitudinal Analysis of Labor Market Data**. [S.l.]: Cambridge University Press, 1985. p. 3–38. Cited on page 72.

CHEN, Z.; ZHENG, S. Lifetime distribution based degradation analysis. **IEEE Transactions on Reliability**, v. 54, n. 1, p. 3–10, 2005. Cited on page 20.

CHHIKARA, R. S.; FOLKS, J. L. **The Inverse Gaussian Distribution: Theory, Methodology, and Applications**. New York: Marcel Dekker, 1989. Cited 2 times on pages 28 and 32.

CHINNAM, R. B. On-line reliability estimation of individual components, using degradation signals. **IEEE Transactions on Reliability**, v. 48, n. 4, p. 403–412, 1999. Cited on page 20.

CLAYTON, D. G. A model for association in bivariate life tables and its application in epidemiological studies of familial tendency in chronic disease incidence. **Biometrika**, v. 65, n. 1, p. 141–151, 1978. Cited 2 times on pages 34 and 58.

COX, D. R. Regression models and life-tables. **Journal of the Royal Statistical Society. Series B (Methodological)**, v. 34, n. 2, p. 187–220, 1972. Cited on page 34.

CRK, V. Reliability assessment from degradation data. In: **Reliability and Maintainability Symposium, 2000. Proceedings. Annual**. [S.l.: s.n.], 2000. p. 155–161. Cited on page 20.

CROWDER, M.; LAWLESS, J. On a scheme for predictive maintenance. **European Journal of Operational Research**, v. 176, n. 3, p. 1713 – 1722, 2007. Cited on page 53.

CROWTHER, M. J.; ANDERSSON, T. M.-L.; LAMBERT, P. C.; ABRAMS, K. R.; HUMPHREYS, K. Joint modelling of longitudinal and survival data: incorporating delayed entry and an assessment of model misspecification. **Statistics in Medicine**, v. 35, n. 7, p. 1193–1209, 2016. Cited on page 41.

DESMOND, A. Stochastic models of failure in random environments. **Canadian Journal of Statistics**, Wiley-Blackwell, v. 13, n. 3, p. 171–183, 1985. Cited on page 32.

DOKSUM, K. A. Degradation rate models for failure time and survival data (stma v33 3067). **CWI Quarterly**, v. 4, p. 195–203, 1991. Cited on page 21.

DOORNIK, J. A. **An Object-Oriented Matrix Programming Language Ox 6.** [S.l.]: Timberlake Consultants Ltd, 2009. Cited 4 times on pages 31, 51, 79, and 95.

EGHBALI, G.; ELSAYED, E. A. **Reliability estimate using degradation data**. [S.l.], 2001. Cited on page 20.

ELBERS, C.; RIDDER, G. True and spurious duration dependence: The identifiability of the proportional hazard model. **The Review of Economic Studies**, Oxford University Press, Review of Economic Studies, Ltd., v. 49, n. 3, p. 403–409, 1982. Cited 2 times on pages 35 and 58.

EPRI. **Steam generator integrity assessment guidelines: revision 2**. [S.l.], 2006. Cited on page 20.

ESARY, J.; MARSHALL, A. W. Shock models and wear processes. **The Annals of Probability**, Institute of Mathematical Statistics, v. 1, n. 4, p. 627–649, 1973. Cited on page 21.

FANG, K.; KOTZ, S.; NG, K. W. **Symmetric multivariate and related distributions**. [S.l.]: London ; New York : Chapman and Hall, 1990. Cited on page 100.

FENYVESI, L.; LU, H.; JACK, T. Prediction of corrosion defect growth on operating pipelines. In: AMERICAN SOCIETY OF MECHANICAL ENGINEERS. **2004 International Pipeline Conference**. [S.l.], 2004. p. 225–230. Cited on page 20.

FREITAS, M. A.; COLOSIMO, E. A.; SANTOS, T. R. d.; PIRES, M. C. Reliability assessment using degradation models: bayesian and classical approaches. **Pesquisa Operacional**, scielo, v. 30, p. 194 – 219, 2010. Cited on page 20.

FREITAS, M. A.; TOLEDO, M. L. G. de; COLOSIMO, E. A.; PIRES, M. C. Using degradation data to assess reliability: a case study on train wheel degradation. **Quality and Reliability Engineering International**, v. 25, n. 5, p. 607–629, 2009. Cited on page 26.

GAIL, M. H.; WIEAND, S.; PIANTADOSI, S. Biased estimates of treatment effect in randomized experiments with nonlinear regressions and omitted covariates. **Biometrika**, v. 71, n. 3, p. 431–444, 1984. Cited on page 72.

GELMAN, A.; CARLIN, J. B.; STERN, H. S.; RUBIN, D. B. Bayesian data analysis. In: ____. Third. Boca Raton, FL, USA: Chapman & Hall/CRC, 2014. cap. 1, p. 3–28. Cited on page 58.

GORJIAN, N.; MA, L.; MITTINTY, M.; YARLAGADDA, P.; SUN, Y. A review on degradation models in reliability analysis. In: **Engineering Asset Lifecycle Management: Proceedings of the 4th World Congress on Engineering Asset Management, 28-30 September 2009**. London: Springer, 2010. p. 369–384. Cited on page 20.

HOUGAARD, P. Survival models for heterogeneous populations derived from stable distributions. **Biometrika**, v. 73, n. 2, p. 387–396, 1986. Cited 2 times on pages 22 and 58.

____. Frailty models for survival data. **Lifetime Data Analysis**, v. 1, n. 3, p. 255–273, 1995. Cited on page 35.

HUDAK, S. J.; SAXENA, A.; BUCCI, R.; MALCOLM, R. **Development of standard methods of testing and analyzing fatigue crack growth rate data**. [S.l.], 1978. Cited on page 26.

HUYSE, L.; ROODSELAAR, V. Effects of inline inspection sizing uncertainties on the accuracy of the largest features and corrosion rate statistics. In: **In 2010 8th International Pipeline Conference (IPC2010)**. Calgary,Alberta,Canada: [s.n.], 2010. Cited on page 20.

JENSEN, F. Case studies in system burn-in. **Reliability Engineering**, v. 3, n. 1, p. 13–22, 1982. Cited 2 times on pages 22 and 84.

KALBFLEISCH, J. G. Probability and statistical inference: Volume 2: Statistical inference. In: ____. Second. New York, N.Y., USA: Springer-Verlag New York, 1985. cap. 13, p. 194–220. Cited on page 71.

KASS, R. E.; STEFFEY, D. Approximate bayesian inference in conditionally independent hierarchical models (parametric empirical bayes models). **Journal of the American Statistical Association**, v. 84, n. 407, p. 717–726, 1989. Cited on page 38.

KUO, W. Reliability enhancement through optimal burn-in. **IEEE Transactions on Reliability**, R-33, n. 2, p. 145–156, 1984. Cited on page 22.

LAWLESS, J.; CROWDER, M. Covariates and random effects in a gamma process model with application to degradation and failure. **Lifetime Data Analysis**, v. 10, n. 3, p. 213–227, 2004. Cited on page 21.

LEEMIS, L. M.; BENEKE, M. Burn-in models and methods: A review. **IIE Transactions**, v. 22, n. 2, p. 172–180, 1990. Cited on page 22.

LEHMANN, A. Failure time models based on degradation processes. In: ____. **Advances in Degradation Modeling: Applications to Reliability, Survival Analysis, and Finance**. Boston, MA: Birkhäuser Boston, 2010. p. 209–233. Cited on page 19.

LESAFFRE, E.; SPIESSENS, B. On the effect of the number of quadrature points in a logistic random effects model: an example. **Journal of the Royal Statistical Society: Series C (Applied Statistics)**, v. 50, n. 3, p. 325–335, 2001. Cited on page 41.

LIN, J.; ASPLUND, M. Comparison study of heavy haul locomotive wheels' running surfaces wearing. **Eksploatacja i Niezawodność**, v. 16, n. 2, p. 276–287, 2014. Cited on page 22.

LIN, J.; PULIDO, J.; ASPLUND, M. Analysis for locomotive wheels' degradation. In: **2014 Reliability and Maintainability Symposium**. [S.l.: s.n.], 2014. p. 1–7. Cited on page 22.

LIU, L.; YU, Z. A likelihood reformulation method in non-normal random effects models. **Statistics in Medicine**, v. 27, n. 16, p. 3105–3124, 2008. Cited on page 41.

LIU, Z.; MA, X.; YANG, J.; ZHAO, Y. Reliability modeling for systems with multiple degradation processes using inverse gaussian process and copulas. **Mathematical Problems in Engineering**, Hindawi Publishing Corporation, v. 1, p. 1–10, 2014. Cited on page 21.

LU, C. J.; MEEKER, W. Q. Using degradation measures to estimate a time-to-failure distribution. **Technometrics**, v. 35, n. 2, p. 161–174, 1993. Cited 4 times on pages 20, 26, 38, and 75.

MARSAGLIA, G.; MARSAGLIA, J. Evaluating the anderson-darling distribution. **Journal of Statistical Software**, v. 9, n. 2, p. 1–5, 2004. Cited 2 times on pages 72 and 87.

MCGILCHRIST, C. A.; AISBETT, C. W. Regression with frailty in survival analysis. **Biometrics**, v. 47, n. 2, p. 461–466, 1991. Cited on page 58.

MEEKER, W. Q.; ESCOBAR, L. A. Statistical methods for reliability data: Degradation data, models, and data analysis. In: ____. New York, N.Y., USA: John Wiley & Sons, 1998. cap. 13. Cited 3 times on pages 26, 47, and 48.

MEEKER, W. Q.; ESCOBAR, L. A.; LU, C. J. Accelerated degradation tests: Modeling and analysis. **Technometrics**, v. 40, n. 2, p. 89–99, 1998. Cited 2 times on pages 20 and 38.

NELSON, K. P.; LIPSITZ, S. R.; FITZMAURICE, G. M.; IBRAHIM, J.; PARZEN, M.; STRAWDERMAN, R. Use of the probability integral transformation to fit nonlinear mixed-effects models with nonnormal random effects. **Journal of Computational and Graphical Statistics**, v. 15, n. 1, p. 39–57, 2006. Cited on page 41.

NIELSEN, G. G.; GILL, R. D.; ANDERSEN, P. K.; SØRENSEN, T. I. A. A counting process approach to maximum likelihood estimation in frailty models. **Scandinavian Journal of Statistics**, v. 19, n. 1, p. 25–43, 1992. Cited on page 58.

NIELSEN, S. F. The stochastic em algorithm: estimation and asymptotic results. **Bernoulli**, Bernoulli Society for Mathematical Statistics and Probability, v. 6, n. 3, p. 457–489, 06 2000. Available at: <http://projecteuclid.org/euclid.bj/1081616701>. Cited on page 110.

NOORTWIJK, J. van. A survey of the application of gamma processes in maintenance. **Reliability Engineering & System Safety**, v. 94, n. 1, p. 2–21, 2009. Cited 4 times on pages 21, 27, 28, and 29.

OAKES, D. Bivariate survival models induced by frailties. **Journal of the American Statistical Association**, v. 84, n. 406, p. 487–493, 1989. Cited on page 22.

OLIVEIRA, V. R. B. de; COLOSIMO, E. A. Comparison of methods to estimate the time-to-failure distribution in degradation tests. **Quality and Reliability Engineering International**, John Wiley & Sons, Ltd., v. 20, n. 4, p. 363–373, 2004. Cited on page 20.

PANDEY, M.; LU, D. Estimation of parameters of degradation growth rate distribution from noisy measurement data. **Structural Safety**, v. 43, p. 60 – 69, 2013. Cited 3 times on pages 20, 37, and 46.

PANDEY, M. D.; NOORTWIJK, J. M. van. Gamma process model for time-dependent structural reliability analysis. In: **Bridge Maintenance, Safety, Management and Cost, Proceedings of the Second International Conference on Bridge Maintenance, Safety and Management (IABMAS), Kyoto, Japan**. [S.l.: s.n.], 2004. p. 18–22. Cited on page 33.

PARK, C.; PADGETT, W. J. Accelerated degradation models for failure based on geometric brownian motion and gamma processes. **Lifetime Data Analysis**, v. 11, n. 4, p. 511–527, 2005. Cited on page 21.

PENG, C. Y. Inverse gaussian processes with random effects and explanatory variables for degradation data. **Technometrics**, v. 57, n. 1, p. 100–111, 2015. Cited 3 times on pages 21, 33, and 71.

PENG, C. Y.; TSENG, S. T. Mis-specification analysis of linear degradation models. **IEEE Transactions on Reliability**, v. 58, n. 3, p. 444–455, 2009. Cited 3 times on pages 20, 42, and 53.

PIESSENS, R.; DONCKER-KAPENGA, E. de; ÜBERHUBER, C. W.; KAHANER, D. K. **Quadpack: a subroutine package for automatic integration**. [S.l.]: Springer Science & Business Media, 2012. v. 1. Cited on page 51.

PINHEIRO, J. C.; BATES, D. M. Approximations to the log-likelihood function in the nonlinear mixed-effects model. **Journal of Computational and Graphical Statistics**, American Statistical Association, Taylor & Francis, Ltd., Institute of Mathematical Statistics, Interface Foundation of America, v. 4, n. 1, p. 12–35, 1995. Cited on page 41.

QIN, H.; ZHANG, S.; ZHOU, W. Inverse gaussian process-based corrosion growth modeling and its application in the reliability analysis for energy pipelines. **Frontiers of Structural and Civil Engineering**, v. 7, n. 3, p. 276–287, 2013. Cited on page 21.

R Core Team. **R: A Language and Environment for Statistical Computing**. Vienna, Austria, 2016. Available at: <https://www.R-project.org/>. Cited 3 times on pages 31, 100, and 108.

RESEARCH, I. W. **Mathematica**. 11.0. ed. Champaign, Illinios, 2016. Cited on page 35.

SAKAMOTO, Y.; ISHIGURO, M.; KITAGAWA, G. **Akaike information criterion statistics**. 1. ed. [S.l.]: Springer Netherlands, 1986. v. 1. Cited on page 36.

SCHWARZ, G. Estimating the dimension of a model. **The Annals of Statistics**, Institute of Mathematical Statistics, v. 6, n. 2, p. 461–464, 1978. Cited on page 36.

SESHADRI, V. **The inverse Gaussian distribution: statistical theory and applications**. [S.l.]: Springer Science & Business Media, 2012. v. 137. Cited on page 30.

SKLAR, M. **Fonctions de répartition à n dimensions et leurs marges**. [S.l.]: Université Paris 8, 1959. Cited on page 100.

TANG, L. C.; CHANG, D. S. Reliability prediction using nondestructive accelerated-degradation data: case study on power supplies. **IEEE Transactions on Reliability**, v. 44, n. 4, p. 562–566, 1995. Cited on page 32.

TSAI, C. C.; TSENG, S. T.; BALAKRISHNAN, N. Optimal burn-in policy for highly reliable products using gamma degradation process. **IEEE Transactions on Reliability**, v. 60, n. 1, p. 234–245, 2011. Cited 3 times on pages 23, 87, and 88.

TSENG, S.-T.; PENG, C. Y. Optimal burn-in policy by using an integrated wiener process. **IIE Transactions**, v. 36, n. 12, p. 1161–1170, 2004. Cited on page 23.

TSENG, S. T.; TANG, J. Optimal burn-in time for highly reliable products. **International Journal of Industrial Engineering-Theory Applications and Practice**, Publishing Horizons, v. 8, n. 4, p. 329–338, 2001. Cited on page 86.

TSENG, S.-T.; TANG, J.; KU, I.-H. Determination of burn-in parameters and residual life for highly reliable products. **Naval Research Logistics**, Wiley Subscription Services, Inc., A Wiley Company, v. 50, n. 1, p. 1–14, 2003. Cited on page 22.

UNKEL, S.; FARRINGTON, C. P. A new measure of time-varying association for shared frailty models with bivariate current status data. **Biostatistics**, v. 13, n. 4, p. 665–679, 2012. Cited on page 22.

VAUPEL, J. W.; MANTON, K. G.; STALLARD, E. The impact of heterogeneity in individual frailty on the dynamics of mortality. **Demography**, v. 16, n. 3, p. 439–454, 1979. Cited 2 times on pages 21 and 35.

VILLASEÑOR, J. A.; GONZALEZ-ESTRADA, E. Tests of fit for inverse gaussian distributions. **Statistics & Probability Letters**, v. 105, p. 189 – 194, 2015. Cited on page 47.

WANG, P.; COIT, D. W. Reliability and degradation modeling with random or uncertain failure threshold. In: **2007 Annual Reliability and Maintainability Symposium**. [S.l.: s.n.], 2007. p. 392–397. Cited on page 19.

WANG, X. A pseudo-likelihood estimation method for nonhomogeneous gamma process model with random effects. **Statistica Sinica**, v. 18, n. 3, p. 1153–1163, 2008. Cited on page 21.

____. Wiener processes with random effects for degradation data. **Journal of Multivariate Analysis**, v. 101, n. 2, p. 340–351, 2010. Cited on page 21.

WANG, X.; XU, D. An inverse gaussian process model for degradation data. **Technometrics**, v. 52, n. 2, p. 188–197, 2010. Cited on page 21.

WASAN, M. T. On an inverse gaussian process. **Scandinavian Actuarial Journal**, v. 1968, n. 1-2, p. 69–96, 1968. Cited on page 21.

____. **First passage time distribution of Brownian motion with positive drift (inverse Gaussian distribution)**. [S.l.]: Kingston, Ont. : Dept. of Mathematics, Queen's University, 1969. Cited on page 99.

WIENER, N. Differential-space. **Journal of Mathematics and Physics**, v. 2, n. 1-4, p. 131–174, 1923. Cited on page 28.

WIENKE, A. **Frailty models in survival analysis**. [S.l.]: CRC Press, 2010. Cited on page 35.

WU, S.; XIE, M. Classifying weak, and strong components using roc analysis with application to burn-in. **IEEE Transactions on Reliability**, v. 56, n. 3, p. 552–561, 2007. Cited on page 23.

XIANG, Y.; COIT, D. W.; FENG, Q. n subpopulations experiencing stochastic degradation: reliability modeling, burn-in, and preventive replacement optimization. **IIE Transactions**, v. 45, n. 4, p. 391–408, 2013. Cited 2 times on pages 23 and 110.

XIAO, N.-C.; HUANG, H.-Z.; WANG, Z.; LIU, Y.; ZHANG, X.-L. Unified uncertainty analysis by the mean value first order saddlepoint approximation. **Structural and Multidisciplinary Optimization**, v. 46, n. 6, p. 803–812, 2012. Cited on page 37.

YAN, J. Enjoy the joy of copulas: With a package copula. **Journal of Statistical Software**, v. 21, n. 1, p. 1–21, 2007. Cited on page 100.

YE, Z. S.; CHEN, N. The inverse gaussian process as a degradation model. **Technometrics**, v. 56, n. 3, p. 302–311, 2014. Cited 2 times on pages 21 and 53.

YUAN, X. **Stochastic modeling of deterioration in nuclear power plant components**. Tese (Doctor of Philosophy in Civil Engineering) — University of Waterloo, Waterloo, 2007. Cited on page 19.

ZHANG, M.; YE, Z.; XIE, M. Optimal burn-in policy for highly reliable products using inverse gaussian degradation process. In: ____. **Engineering Asset Management - Systems, Professional Practices and Certification: Proceedings of the 8th World Congress on Engineering Asset Management (WCEAM 2013) & the 3rd International Conference on Utility Management & Safety (ICUMAS)**. Cham: Springer International Publishing, 2015. p. 1003–1011. Cited 2 times on pages 23 and 81.

ZUO, M. J.; JIANG, R.; YAM, R. C. M. Approaches for reliability modeling of continuous-state devices. **IEEE Transactions on Reliability**, v. 48, n. 1, p. 9–18, 1999. Cited on page 20.

APPENDIX

A

PROOFS OF THE THEOREMS, PROPOSITIONS AND COROLLARIES

A.1 Proof of proposition 4.2.1

Let $w_i = \frac{1}{z_i}$ then $w_i \sim$ Inverse Gamma $\left(\frac{1}{\alpha}, \frac{1}{\alpha}\right)$ with PDF: $f(w_i) = \frac{\exp\left(-\frac{1}{w_i \alpha}\right)}{w_i^{\frac{1}{\alpha}+1} \alpha^{\frac{1}{\alpha}} \Gamma\left[\frac{1}{\alpha}\right]}$.

Applying this transformation, the unconditional reliability function charges the same functional form as (2.19), then (4.4) becomes

$$R(y|\Delta g_{\boldsymbol{\theta}}(t), \eta, \boldsymbol{\alpha}) = \begin{cases} 0, \text{ if } R_{IGP}(y|\Delta g_{\boldsymbol{\theta}}(t), \eta) = 0, \\ \mathscr{L}[f(w_i)](H_{IGP}(y|\Delta g_{\boldsymbol{\theta}}(t), \eta)), \text{ if } 0 < R_{IGP}(y|\Delta g_{\boldsymbol{\theta}}(t), \eta) < 1, \\ 1, \text{ if } R_{IGP}(y|\Delta g_{\boldsymbol{\theta}}(t), \eta) = 1. \end{cases}$$

whose solution of the Laplace transform leads to (4.15).

A.2 Proof of proposition 4.2.2

Considering $R(y|\Delta g_{\boldsymbol{\theta}}(t), \eta, \boldsymbol{\alpha})$ in (4.21) and the relation (4.5), we have

$$f(y|\Delta g_{\boldsymbol{\theta}}(t), \eta, \boldsymbol{\alpha}) = \begin{cases} 0, \text{ if } f_{IGP}(y|\Delta g_{\boldsymbol{\theta}}(t), \eta) = 0, \\ -\frac{2\alpha^{-\frac{1}{2\alpha}}}{\Gamma\left(\frac{1}{\alpha}\right)} \left[\frac{\partial (H_{IGP}(y|\Delta g_{\boldsymbol{\theta}}(t), \eta))^{\frac{1}{2\alpha}}}{\partial y} A + (H_{IGP}(y|\Delta g_{\boldsymbol{\theta}}(t), \eta))^{\frac{1}{2\alpha}} \frac{\partial A}{\partial y} \right], \\ \text{if } f_{IGP}(y|\Delta g_{\boldsymbol{\theta}}(t), \eta) > 0, \end{cases}$$

where A is as given in proposition 4.2.1.

Using the derivative of the modified Bessel function of the second kind with respect to the argument (BRYCHKOV, 2008):

$$\frac{\partial \text{BesselK}[x,w]}{\partial w} = -\frac{1}{2}\left(\text{BesselK}[x-1,w] + \text{BesselK}[x+1,w]\right), \forall x \in \mathbb{R} \text{ and } w \neq 0,$$

and taking into account that,

$$\frac{\partial H_{IGP}(y|\Delta g_{\boldsymbol{\theta}}(t),\eta)}{\partial y} = h_{IGP}(y|\Delta g_{\boldsymbol{\theta}}(t),\eta),$$

one may obtain (4.16).

A.3 Proof of proposition 4.2.3

From (4.8),

$$f_T(t) = \frac{2\alpha^{-\frac{1}{2\alpha}}}{\Gamma\left(\frac{1}{\alpha}\right)}\left[\frac{\partial H_{IGP}(y|\Delta g_{\boldsymbol{\theta}}(t),\eta)}{\partial t} + \frac{\partial A}{\partial t}\right].$$

Taking into account that

$$\frac{\partial H_{IGP}(y|\Delta g_{\boldsymbol{\theta}}(t),\eta)}{\partial t} = -\frac{\partial \log R_{IGP}(y|\Delta g_{\boldsymbol{\theta}}(t),\eta)}{\partial t} = -\frac{1}{R_{IGP}(y|\Delta g_{\boldsymbol{\theta}}(t),\eta)} f_{T_{IGP}}(t),$$

and the derivative of the Bessel function in the previous proof, one may obtain (4.17).

A.4 Proof of proposition 4.2.4

Analogous to the proof of 4.2.1, let $w_i = \frac{1}{z_i}$, then the second term in (4.11) can be rewritten as

$$L_{2i} = w_i^{n_i} \times \mathscr{L}[f(w_i)]\left(\sum_{j=1}^{n_i} H_{IGP}(y_{ij}|\Delta g_{\boldsymbol{\theta}}(t_{ij}),\eta))\right),$$

whose solution is (4.18).

A.5 Proof of proposition 4.2.5

Considering $z_i \sim$ Gamma $\left(\frac{1}{\alpha},\alpha\right)$, the formula (4.13) becomes

$$\begin{aligned} f(z_i|\mathbf{Y}) &\propto z_i^{\frac{1}{\alpha}-n_i-1} \exp\left[-\sum_{j=1}^{n_i} H_{IGP}(y_{ij}|\Delta g_{\boldsymbol{\theta}}(t_{ij}),\eta)\frac{1}{z_i}\right] \exp\left(-\frac{z_i}{\alpha}\right) \\ &\propto z_i^{\frac{1}{\alpha}-n_i-1} \exp\left[-\frac{1}{2}\left(\frac{2\sum_{j=1}^{n_i} H_{IGP}(y_{ij}|\Delta g_{\boldsymbol{\theta}}(t_{ij}),\eta)}{z_i} + \frac{2z_i}{\alpha}\right)\right], \end{aligned}$$

which corresponds to the PDF of the Generalized IG distribution in (4.19). The mean and variance are obtained from this distribution.

A.6 Proof of proposition 4.2.6

The unconditional reliability function (4.4) has not exactly the same form as (2.19), but it is possible to express it through a different Laplace transform:

$$R(y|\Delta g_{\boldsymbol{\theta}}(t),\eta,\boldsymbol{\alpha}) = \begin{cases} 0, \text{ if } R_{IGP}(y|\Delta g_{\boldsymbol{\theta}}(t),\eta) = 0, \\ (2\pi\alpha)^{-\frac{1}{2}} \exp\left(\frac{1}{\alpha}\right) \mathscr{L}[g(z_i)](\frac{1}{2\alpha}), \text{ if } 0 < R_{IGP}(y|\Delta g_{\boldsymbol{\theta}}(t),\eta) < 1, \\ 1, \text{ if } R_{IGP}(y|\Delta g_{\boldsymbol{\theta}}(t),\eta) = 1. \end{cases} \tag{A.1}$$

where $g(z_i) = z_i^{-\frac{3}{2}} \exp\left[-\frac{1}{z}\left(H_{IGP}(y|\Delta g_{\boldsymbol{\theta}}(t),\eta) + \frac{1}{2\alpha}\right)\right]$. The solution leads to (4.21).

A.7 Proof of proposition 4.2.9

The second term in (4.11) can be rewritten as

$$L_{2i} = (\alpha 2\pi)^{-\frac{1}{2}} \exp\left(\frac{1}{\alpha}\right) \times \mathscr{L}[g(z_i)]\left(\frac{1}{2\alpha}\right),$$

where $g(z_i) = z_i^{-n_i-\frac{3}{2}} \exp\left[-\frac{1}{z}\left(\sum_{i=1}^{n_i} H_{IGP}(y_{ij}|\Delta g_{\boldsymbol{\theta}}(t_{ij}),\eta) + \frac{1}{2\alpha}\right)\right]$.

The solution through Laplace transform leads to (4.24).

A.8 Proof of proposition 4.2.10

Considering $z_i \sim IG\left(1,\frac{1}{\alpha}\right)$, the formula (4.13) becomes

$$\begin{aligned} f(z_i|\mathbf{Y}) &\propto \left(\frac{1}{z_i}\right)^{n_i} \exp\left[-\sum_{j=1}^{n_i} H_{IGP}(y_{ij}|\Delta g_{\boldsymbol{\theta}}(t_{ij}),\eta)\frac{1}{z_i}\right] \left(\frac{1}{z_i^3}\right)^{\frac{1}{2}} \exp\left[-\frac{z_i}{2\alpha} - \frac{1}{2z_i\alpha}\right] \\ &\propto z_i^{-\frac{3}{2}-n_i} \exp\left[-\frac{1}{2}\left(\frac{2\sum_{j=1}^{n_i} H_{IGP}(y_{ij}|\Delta g_{\boldsymbol{\theta}}(t_{ij}),\eta) + \frac{1}{\alpha}}{z_i} + \frac{z_i}{\alpha}\right)\right], \end{aligned}$$

which corresponds to the PDF of the Generalized IG distribution in (4.25). The mean and variance are obtained from this distribution.

A.9 Proof of theorem 5.3.1

Taking the first derivative of (5.11) with respect to $\xi(t_b)$, we get

$$\frac{\partial MC(\xi(t_b))}{\partial \xi(t_b)} = \frac{n\left(C_\beta e^{-\frac{\left(\xi(t_b)-g_{\boldsymbol{\theta_1}}(t_b)\right)^2\eta_1}{2\xi(t_b)}} g_{\boldsymbol{\theta_1}}(t_b) p\sqrt{\frac{\eta_1}{\xi(t_b)}} + C_\alpha e^{-\frac{\left(\xi(t_b)-g_{\boldsymbol{\theta_2}}(t_b)\right)^2\eta_2}{2\xi(t_b)}} g_{\boldsymbol{\theta_2}}(t_b)(-1+p)\sqrt{\frac{\eta_2}{\xi(t_b)}}\right)}{\xi(t_b)\sqrt{2\pi}}. \tag{A.2}$$

Equating (A.2) to zero, i.e.,

$$\frac{\partial MC(\xi(t_b))}{\partial \xi(t_b)} = 0,$$

we obtain (5.12). The two roots are obtained through Bhaskara formula.

A.9.1 Proof of corollary 5.3.2

Assuming $\eta_1 = \eta_2 = \eta$ in (5.12), we have a linear equation with respect to $\xi(t_b)$.

A.9.2 Proof of corollary 5.3.3

Assuming $g_{\boldsymbol{\theta_1}}(t_b) = g_{\boldsymbol{\theta_2}}(t_b) = g_{\boldsymbol{\theta}}(t_b)$ in (5.12), we obtain (5.15) and the optimal cutoff point is found analogously to theorem 5.3.1.

APPENDIX

B

DATASETS

Table 38 – LASER data (example 2.2.1)

	inspection times (in 1,000 hours)																
unit	0	0.25	0.50	0.75	1.00	1.25	1.50	1.75	2	2.25	2.50	2.75	3	3.25	3.50	3.75	4
1	0	0.47	0.93	2.11	2.72	3.51	4.34	4.91	5.48	5.99	6.72	7.13	8.00	8.92	9.49	9.87	10.94
2	0	0.71	1.22	1.90	2.30	2.87	3.75	4.42	4.99	5.51	6.07	6.64	7.16	7.78	8.42	8.91	9.28
3	0	0.71	1.17	1.73	1.99	2.53	2.97	3.30	3.94	4.16	4.45	4.89	5.27	5.69	6.02	6.45	6.88
4	0	0.36	0.62	1.36	1.95	2.30	2.95	3.39	3.79	4.11	4.50	4.72	4.98	5.28	5.61	5.95	6.14
5	0	0.27	0.61	1.11	1.77	2.06	2.58	2.99	3.38	4.05	4.63	5.24	5.62	6.04	6.32	7.10	7.59
6	0	0.36	1.39	1.95	2.86	3.46	3.81	4.53	5.35	5.92	6.71	7.70	8.61	9.15	9.95	10.49	11.01
7	0	0.36	0.92	1.21	1.46	1.93	2.39	2.68	2.94	3.42	4.09	4.58	4.84	5.11	5.57	6.11	7.17
8	0	0.46	1.07	1.42	1.77	2.11	2.40	2.78	3.02	3.29	3.75	4.16	4.76	5.16	5.46	5.81	6.24
9	0	0.51	0.93	1.57	1.96	2.59	3.29	3.61	4.11	4.60	4.91	5.34	5.84	6.40	6.84	7.20	7.88
10	0	0.41	1.49	2.38	3.00	3.84	4.50	5.25	6.26	7.05	7.80	8.32	8.93	9.55	10.45	11.28	12.21
11	0	0.44	1.00	1.57	1.96	2.51	2.84	3.47	4.01	4.51	4.80	5.20	5.66	6.20	6.54	6.96	7.42
12	0	0.39	0.80	1.35	1.74	2.98	3.59	4.03	4.44	4.79	5.22	5.48	5.96	6.23	6.99	7.37	7.88
13	0	0.30	0.74	1.52	1.85	2.39	2.95	3.51	3.92	5.03	5.47	5.84	6.50	6.94	7.39	7.85	8.09
14	0	0.44	0.70	1.05	1.35	1.80	2.55	2.83	3.39	3.72	4.09	4.83	5.41	5.76	6.14	6.51	6.88
15	0	0.51	0.83	1.29	1.52	1.91	2.27	2.78	3.42	3.78	4.11	4.38	4.63	5.38	5.84	6.16	6.62

Table 39 – Locomotive wheels data (example 2.2.2)

	inspection distances (in 1,000 kilometers)												
unit	0	50	100	150	200	250	300	350	400	450	500	550	600
1	0	2.7000	4.0659	5.6609	7.2631	8.6850	10.4017	12.0305	13.4421	14.9470	16.6277	18.1337	19.6648
2	0	2.8998	4.9251	6.6984	8.6252	10.4220	12.4066	14.3119	16.1846	17.9799	19.8565	21.8192	23.7242
3	0	3.7028	6.4751	9.2832	11.8857	14.6862	17.3731	20.2155	22.8683	25.6566	28.364	31.0904	33.8826
4	0	4.6583	8.3716	12.2653	15.9242	19.5283	23.2358	27.0731	30.6517	34.3705	38.2276	41.8718	45.4724
5	0	6.6897	12.2041	17.9402	23.5024	29.1228	34.8227	40.4531	46.0059	51.6525	57.3747	62.9516	68.5743
6	0	4.8609	8.6231	12.5503	16.3594	20.2660	24.0793	27.9391	31.7847	35.6754	39.5580	43.3766	47.2591
7	0	2.8000	5.5000	10.6000	12.9000	16.4000	19.6000	25.1000	28.4000	32.5000	37.6000	42.3000	46.5000
8	0	3.0743	5.2000	7.3039	9.5605	11.4660	13.6586	15.6574	17.7745	19.9214	22.0137	24.1333	26.2075
9	0	6.3538	11.4653	16.7972	22.0818	27.3303	32.5504	37.9657	43.0866	48.4552	53.683	59.0720	64.3083
10	0	4.2360	7.5336	10.7680	14.1162	17.4094	20.7214	23.8505	27.1674	30.4357	33.793	37.0533	40.4565
11	0	11.5675	22.2514	32.8311	43.5843	54.1357	64.7981	75.3103	85.9533				
12	0	14.7473	28.4222	42.2152	55.8604	69.5656	83.2889						
13	0	6.5000	15.7000	18.4000	22.2000	26.5000	29.6000	33.6000	38.5000	43.2000	47.1000	51.8000	55.1000
14	0	7.9946	14.9741	22.0686	28.9677	35.9954	42.9094	49.9912	56.9346	64.0608	70.9726	77.9534	

Table 40 – Crack size data (example 2.2.3)

	Number of cycles (in 1,000 cycles)												
unit	0	10	20	30	40	50	60	70	80	90	100	110	120
1	0.90	0.95	1.00	1.05	1.12	1.19	1.27	1.35	1.48	1.64			
2	0.90	0.94	0.98	1.03	1.08	1.14	1.21	1.28	1.37	1.47	1.60		
3	0.90	0.94	0.98	1.03	1.08	1.13	1.19	1.26	1.35	1.46	1.58	1.77	
4	0.90	0.94	0.98	1.03	1.07	1.12	1.19	1.25	1.34	1.43	1.55	1.73	
5	0.90	0.94	0.98	1.03	1.07	1.12	1.19	1.24	1.34	1.43	1.55	1.71	
6	0.90	0.94	0.98	1.03	1.07	1.12	1.18	1.23	1.33	1.41	1.51	1.68	
7	0.90	0.94	0.98	1.02	1.07	1.11	1.17	1.23	1.32	1.41	1.52	1.66	
8	0.90	0.93	0.97	1.00	1.06	1.11	1.17	1.23	1.30	1.39	1.49	1.62	
9	0.90	0.92	0.97	1.01	1.05	1.09	1.15	1.21	1.28	1.36	1.44	1.55	1.72
10	0.90	0.92	0.96	1.00	1.04	1.08	1.13	1.19	1.26	1.34	1.42	1.52	1.67
11	0.90	0.93	0.96	1.00	1.04	1.08	1.13	1.18	1.24	1.31	1.39	1.49	1.65
12	0.90	0.93	0.97	1.00	1.03	1.07	1.10	1.16	1.22	1.29	1.37	1.48	1.64
13	0.90	0.92	0.97	0.99	1.03	1.06	1.10	1.14	1.20	1.26	1.31	1.40	1.52
14	0.90	0.93	0.96	1.00	1.03	1.07	1.12	1.16	1.20	1.26	1.30	1.37	1.45
15	0.90	0.92	0.96	0.99	1.03	1.06	1.10	1.16	1.21	1.27	1.33	1.40	1.49
16	0.90	0.92	0.95	0.97	1.00	1.03	1.07	1.11	1.16	1.22	1.26	1.33	1.40
17	0.90	0.93	0.96	0.97	1.00	1.05	1.08	1.11	1.16	1.20	1.24	1.32	1.38
18	0.90	0.92	0.94	0.97	1.01	1.04	1.07	1.09	1.14	1.19	1.23	1.28	1.35
19	0.90	0.92	0.94	0.97	0.99	1.02	1.05	1.08	1.12	1.16	1.20	1.25	1.31
20	0.90	0.92	0.94	0.97	0.99	1.02	1.05	1.08	1.12	1.16	1.19	1.24	1.29
21	0.90	0.92	0.94	0.97	0.99	1.02	1.04	1.07	1.11	1.14	1.18	1.22	1.27

Table 41 – LASER generated data.

	inspection times (in 1,000 hours)																	
unit	0	0.25	0.50	0.75	1	1.25	1.50	1.75	2	2.25	2.50	2.75	3	3.25	3.50	3.75	4	group
1	0	0.64	1.32	1.86	2.24	2.68	3.28	3.92	4.50	5.06	5.69	6.33	6.75	7.69	8.34	8.86	9.68	weak
2	0	0.36	1.00	1.34	1.68	2.27	2.92	3.13	3.66	4.00	4.75	5.00	5.22	5.78	6.05	6.32	6.72	normal
3	0	0.46	1.36	1.88	2.45	2.80	3.11	3.67	4.03	4.44	4.90	5.71	5.98	6.37	6.76	7.33	7.68	normal
4	0	0.58	1.11	1.49	1.81	2.31	2.82	3.16	3.72	4.07	4.52	4.75	5.06	5.39	5.80	6.31	6.72	normal
5	0	1.13	1.59	2.10	2.62	3.30	3.93	4.64	5.23	5.95	6.62	7.46	7.92	8.30	8.96	9.77	10.57	weak
6	0	0.54	0.78	1.19	1.93	2.43	2.94	3.62	4.23	4.87	5.53	6.08	6.35	6.93	7.15	7.64	8.23	normal
7	0	0.32	0.85	1.09	1.38	1.92	2.32	2.83	3.13	3.94	4.51	5.30	5.68	6.17	6.91	7.26	7.61	normal
8	0	0.35	0.74	1.16	1.51	1.86	2.08	2.54	2.90	3.43	3.71	3.96	4.27	4.47	4.98	5.59	5.94	normal
9	0	0.25	0.74	1.20	1.68	2.06	2.45	3.13	3.73	4.28	4.52	4.75	5.27	5.48	5.97	6.31	6.93	normal
10	0	0.67	1.20	1.91	2.55	2.89	3.24	3.83	4.30	4.91	5.10	5.40	5.72	6.33	6.91	7.22	7.90	normal
11	0	0.75	1.29	1.57	1.89	2.14	2.73	3.00	3.74	4.23	4.86	5.23	5.81	6.22	6.76	7.36	7.67	normal
12	0	0.51	1.22	1.46	1.90	2.29	2.57	2.93	3.43	3.98	4.41	4.98	5.40	5.89	6.29	7.07	7.63	normal
13	0	0.31	0.67	1.10	1.53	1.81	2.55	2.99	3.47	3.93	4.51	4.84	5.32	5.64	5.82	6.32	6.68	normal
14	0	0.62	1.26	1.94	2.59	3.29	3.83	4.49	4.90	5.47	6.24	7.11	7.60	8.09	8.70	9.45	10.31	weak
15	0	0.50	1.57	1.99	2.52	3.25	3.57	3.91	4.14	4.93	5.40	5.97	6.25	6.93	7.37	8.19	8.85	normal
16	0	0.93	1.65	2.28	3.09	3.69	4.46	4.93	5.46	6.01	6.52	7.00	7.53	8.51	9.05	9.72	10.33	weak
17	0	0.28	0.55	1.12	1.49	2.11	2.44	2.83	3.36	3.89	4.42	5.11	5.50	5.81	6.45	7.06	7.52	normal
18	0	0.56	0.95	1.54	2.02	2.30	2.75	3.00	3.49	3.95	4.47	4.93	5.35	5.62	6.00	6.58	7.28	normal
19	0	0.72	1.18	1.76	2.40	2.67	3.12	3.36	3.79	4.27	4.53	5.07	5.51	5.99	6.37	6.70	7.24	normal
20	0	0.18	0.54	0.81	1.44	2.01	2.36	2.85	3.11	3.55	4.40	5.17	5.49	5.89	6.51	7.11	7.52	normal
21	0	0.67	1.28	1.71	2.07	2.49	2.91	3.26	3.55	4.02	4.43	4.86	5.52	5.87	6.24	6.55	7.02	normal
22	0	0.58	0.99	1.89	2.25	3.13	3.77	4.18	5.02	5.98	6.65	7.20	8.01	8.54	8.89	9.41	10.34	weak
23	0	0.63	1.51	2.13	2.80	3.81	4.82	5.41	6.22	7.41	7.99	8.58	9.12	9.80	10.40	10.91	11.42	weak
24	0	0.86	1.64	2.51	3.00	3.85	4.44	4.92	5.66	6.42	7.25	8.10	8.67	9.16	9.86	10.42	10.97	weak
25	0	0.44	1.09	1.54	2.10	2.46	2.74	3.00	3.50	3.97	4.41	4.78	5.51	6.04	6.60	7.14	7.66	normal
26	0	0.46	1.02	1.60	2.39	2.83	3.32	4.10	4.92	5.82	6.24	7.41	8.21	8.57	9.45	10.08	10.54	weak
27	0	0.41	0.63	1.01	1.38	1.62	1.93	2.36	2.94	3.20	3.69	4.05	4.45	4.86	5.48	5.73	6.19	normal
28	0	0.29	0.68	1.02	1.35	1.71	2.20	2.60	2.87	3.31	3.73	4.15	4.83	5.45	5.78	6.13	6.43	normal
29	0	0.63	1.22	1.81	2.43	3.08	3.78	4.73	5.43	6.33	7.22	7.97	8.59	9.04	9.56	10.26	10.81	weak
30	0	0.32	0.91	1.30	1.67	2.12	2.77	3.14	3.50	3.97	4.63	4.94	5.45	6.05	6.36	6.91	7.16	normal
31	0	0.68	0.92	1.44	1.72	1.95	2.26	2.87	3.26	3.85	4.39	4.70	5.03	5.30	5.73	6.14	6.74	normal
32	0	0.31	0.78	1.24	1.79	2.15	2.49	2.79	3.22	3.84	4.19	4.66	5.05	5.32	5.65	5.98	6.37	normal
33	0	0.35	0.84	1.23	1.71	1.98	2.84	3.31	3.79	4.25	4.69	5.31	5.78	6.10	6.48	6.89	7.32	normal
34	0	0.45	1.11	1.39	1.96	2.41	2.83	3.38	3.94	4.25	4.68	5.18	5.94	6.28	6.87	7.69	8.27	normal
35	0	0.28	0.68	1.07	1.64	1.92	2.28	2.65	3.08	3.66	4.04	4.56	5.19	5.58	5.88	6.24	6.79	normal
36	0	1.00	1.75	2.37	3.05	3.74	4.35	5.06	5.66	6.12	6.89	7.68	8.23	9.18	10.52	11.27	11.70	weak
37	0	0.31	0.58	1.05	1.42	1.89	2.16	2.57	2.80	3.06	3.69	4.19	4.48	5.25	5.58	5.84	6.42	normal
38	0	0.51	0.90	1.43	1.92	2.24	2.80	3.33	3.57	3.77	4.50	4.88	5.15	5.82	6.20	6.53	6.99	normal
39	0	0.22	0.71	0.97	1.34	1.71	1.97	2.91	3.57	4.33	4.84	5.20	5.47	5.83	6.25	6.78	7.05	normal
40	0	0.27	0.57	0.93	1.35	1.55	2.21	2.52	3.15	3.90	4.42	4.95	5.70	6.26	6.55	6.86	7.30	normal

41	0	0.66	1.22	1.88	2.44	3.45	4.34	4.94	5.32	6.23	7.02	8.00	8.73	9.08	9.72	10.54	11.32	weak
42	0	0.35	0.60	1.00	1.56	2.18	2.77	3.06	3.38	3.66	3.92	4.32	4.74	5.01	5.60	6.61	7.05	normal
43	0	0.42	0.99	1.86	2.44	3.03	3.63	4.13	4.71	5.22	5.81	6.48	7.29	8.05	8.64	9.06	9.52	weak
44	0	0.25	0.75	0.99	1.43	1.61	2.08	2.36	3.03	3.57	4.03	4.48	5.24	5.77	6.16	6.76	7.19	normal
45	0	0.44	1.05	1.70	2.00	2.58	2.92	3.16	3.83	4.19	4.73	5.65	6.06	6.41	6.79	7.13	7.62	normal
46	0	0.24	0.76	1.64	2.03	2.42	2.65	3.02	3.27	3.61	4.06	4.43	4.97	5.56	5.94	6.35	6.64	normal
47	0	0.70	1.82	2.43	3.46	3.97	4.44	5.30	5.94	6.40	7.19	7.67	8.39	8.98	9.41	10.10	10.61	weak
48	0	0.72	1.13	1.35	1.81	2.16	2.61	3.02	3.44	3.94	4.63	4.99	5.48	5.86	6.07	6.60	6.96	normal
49	0	0.31	0.57	0.93	1.49	2.14	2.46	3.16	3.96	4.53	4.76	5.22	5.60	6.06	6.49	6.85	7.38	normal
50	0	0.54	1.09	1.39	1.62	2.06	2.61	3.07	3.38	3.95	4.41	4.80	5.32	5.91	6.67	7.09	7.63	normal
51	0	0.60	1.57	2.28	2.86	3.32	4.12	4.59	5.13	5.80	6.39	6.90	7.24	7.77	8.51	9.27	9.83	weak
52	0	0.34	0.84	1.20	1.81	2.03	2.47	2.93	3.27	3.74	4.08	4.56	4.99	5.62	6.01	6.31	6.86	normal
53	0	0.74	1.27	1.57	2.49	3.15	4.16	4.96	5.57	6.09	6.82	7.42	8.05	8.53	9.02	9.52	10.21	weak
54	0	0.84	1.61	2.12	2.56	3.06	3.39	4.05	4.56	5.36	6.07	6.60	7.41	7.94	8.53	9.24	9.84	weak
55	0	0.51	1.01	1.29	1.73	2.11	2.51	2.98	3.28	4.05	4.79	5.10	5.50	5.80	6.14	6.68	7.25	normal
56	0	0.40	0.70	1.95	2.28	2.64	3.02	3.88	4.58	4.89	5.49	5.79	6.18	6.53	6.90	7.54	8.04	normal
57	0	0.26	0.85	1.25	1.63	1.90	2.68	3.07	3.41	3.65	4.31	4.74	5.11	5.39	5.64	6.16	6.64	normal
58	0	0.45	1.36	2.22	3.05	3.71	4.42	5.29	6.35	7.19	7.72	8.69	9.15	9.93	10.59	11.32	12.06	weak
59	0	0.93	1.21	1.69	2.08	2.48	2.95	3.36	3.73	4.12	4.52	4.98	5.37	5.82	6.21	6.56	7.42	normal
60	0	0.26	0.70	1.12	1.38	1.70	1.97	2.49	3.12	3.45	4.00	4.36	4.69	5.06	5.57	6.13	6.33	normal
61	0	1.06	1.83	2.52	3.13	3.65	4.03	4.89	5.43	6.31	6.96	8.18	8.73	9.57	10.21	10.78	11.51	weak
62	0	0.48	0.86	1.53	2.11	2.67	3.01	3.34	3.78	4.20	4.61	4.98	5.32	5.62	6.02	6.47	7.01	normal
63	0	0.31	0.79	1.05	1.46	2.04	2.44	3.08	3.51	4.11	4.52	4.82	5.17	5.61	6.25	6.83	7.53	normal
64	0	0.49	0.80	1.11	2.05	2.91	3.33	3.71	4.21	4.86	5.42	6.01	6.45	6.82	7.07	7.48	7.81	normal
65	0	0.59	0.82	1.33	1.92	2.21	2.46	2.75	3.46	4.09	4.45	5.34	5.67	6.10	6.67	7.12	7.90	normal
66	0	0.44	0.67	1.13	1.57	1.75	2.12	2.41	2.82	3.46	4.01	4.48	4.86	5.37	5.89	6.57	6.99	normal
67	0	0.37	0.87	1.54	1.93	2.23	2.63	3.25	3.82	4.45	4.89	5.47	5.83	6.16	6.85	7.70	8.06	normal
68	0	0.40	0.82	1.46	1.93	2.34	2.69	2.95	3.52	3.78	4.08	4.35	4.67	4.87	5.39	5.72	6.34	normal
69	0	1.08	1.73	2.41	3.02	3.48	4.25	4.78	5.38	6.11	6.84	7.85	8.58	9.69	10.40	11.31	12.01	weak
70	0	0.44	1.12	1.70	2.29	2.80	3.44	4.00	4.60	5.64	6.53	7.38	8.35	8.98	9.95	10.62	11.04	weak
71	0	0.35	0.78	1.30	1.94	2.52	2.98	3.30	3.56	4.09	4.57	5.16	5.65	6.12	6.45	6.78	7.95	normal
72	0	0.17	0.98	1.26	1.49	1.95	2.55	2.95	3.39	3.77	4.16	4.60	5.29	5.83	6.39	6.73	7.18	normal
73	0	0.45	0.84	1.29	1.53	1.98	2.47	2.92	3.26	3.73	4.05	4.53	5.01	5.43	5.80	6.19	6.43	normal
74	0	0.28	0.87	1.15	1.85	2.66	3.02	3.34	3.71	4.45	5.05	5.63	6.11	6.35	6.85	7.27	7.78	normal
75	0	0.40	0.70	0.92	1.24	1.83	2.36	2.81	3.24	3.81	4.13	4.47	5.24	5.68	5.95	6.28	6.58	normal
76	0	0.42	1.24	1.76	2.23	2.67	3.04	4.10	4.62	5.18	5.89	6.57	7.21	7.71	8.42	9.26	9.97	weak
77	0	0.30	0.92	1.33	1.55	2.06	2.56	3.09	3.46	3.92	4.21	4.62	5.34	6.32	6.66	6.97	7.33	normal
78	0	1.00	1.77	2.26	2.77	3.16	3.64	4.39	5.07	5.52	6.00	6.59	7.21	7.96	8.56	8.94	9.62	weak
79	0	0.35	0.67	1.09	1.40	2.09	2.48	3.27	3.78	4.11	4.62	5.00	5.35	5.86	6.21	6.58	6.78	normal
80	0	0.35	1.17	1.89	2.29	2.66	3.40	3.76	4.32	5.00	5.36	5.78	6.12	6.60	6.88	7.37	8.06	normal
81	0	0.72	1.60	2.23	3.32	4.04	4.68	5.26	5.89	6.37	6.83	7.54	8.03	8.72	9.60	10.08	10.65	weak
82	0	0.39	0.72	1.15	1.56	2.04	2.37	2.81	3.07	3.42	3.87	4.44	4.83	5.31	5.74	5.99	6.45	normal
83	0	0.50	1.02	1.61	2.35	2.98	3.45	3.88	4.27	5.23	5.46	5.79	6.42	6.78	7.35	7.81	8.08	normal
84	0	0.65	1.25	2.02	3.07	3.68	4.45	5.42	5.97	6.44	7.11	8.00	8.78	9.39	9.91	10.47	11.20	weak

85	0	0.83	1.29	1.56	2.32	2.61	3.31	3.67	4.11	4.67	5.09	5.38	5.99	6.44	6.69	7.19	7.66	normal
86	0	0.53	0.88	1.52	2.05	2.73	3.64	4.76	6.12	6.62	7.37	7.98	8.44	9.13	9.86	10.24	11.31	weak
87	0	0.87	1.58	1.89	2.43	2.90	3.37	3.89	4.90	5.96	6.39	6.92	7.57	8.50	9.30	10.02	10.57	weak
88	0	0.27	0.56	1.14	1.79	2.17	2.45	2.71	2.93	3.15	3.53	4.00	4.29	4.97	5.55	5.84	6.34	normal
89	0	0.41	0.78	1.23	1.43	1.83	2.13	2.51	2.88	3.61	4.17	4.50	4.88	5.36	5.71	6.10	6.36	normal
90	0	0.47	0.95	1.51	2.04	2.41	2.77	3.15	3.62	4.02	4.35	4.54	4.84	5.30	5.86	6.49	7.10	normal
91	0	0.26	0.60	0.90	1.51	2.00	2.41	3.12	3.68	4.03	4.83	5.14	5.59	6.27	6.58	6.89	7.29	normal
92	0	0.39	0.98	1.78	2.39	3.22	3.96	4.68	5.56	6.18	7.14	7.54	8.24	8.68	9.59	10.24	10.84	weak
93	0	0.30	0.77	1.49	1.88	2.23	2.76	3.54	4.11	4.64	5.16	5.88	6.29	6.88	7.49	7.79	8.28	normal
94	0	0.36	0.88	1.20	1.81	2.27	2.69	3.13	3.80	4.35	4.61	5.15	5.37	5.69	6.24	6.79	7.16	normal
95	0	0.33	0.88	1.33	1.75	2.30	2.63	3.65	4.01	4.51	5.20	5.81	6.55	6.89	7.28	7.67	7.89	normal
96	0	0.71	1.05	1.58	2.01	2.25	2.55	3.28	3.69	3.91	4.43	4.97	5.62	5.94	6.37	6.82	7.23	normal
97	0	0.68	1.01	1.66	2.01	2.35	3.08	3.53	4.02	4.31	4.87	5.41	5.65	6.17	6.57	6.98	7.41	normal
98	0	0.58	0.97	1.50	2.60	3.18	4.10	4.67	5.41	5.95	6.54	7.24	7.88	8.51	9.25	9.75	10.27	weak
99	0	0.31	0.73	1.12	1.59	1.90	2.48	3.11	3.75	4.24	4.48	4.92	5.41	5.74	6.15	6.59	6.91	normal
100	0	0.46	1.11	1.50	2.06	2.81	3.20	3.87	4.47	5.04	5.79	6.39	7.53	8.17	8.68	9.17	10.06	weak
101	0	0.80	1.45	2.19	3.02	3.35	3.80	4.47	4.99	5.39	6.19	7.22	7.91	8.69	9.22	9.57	9.96	weak
102	0	0.39	1.22	1.57	2.09	2.58	2.98	3.25	3.64	4.07	4.49	5.03	5.53	6.05	6.32	6.63	7.07	normal
103	0	0.63	0.93	1.38	1.67	2.09	2.45	2.89	3.15	3.45	3.96	4.52	4.82	5.51	6.14	6.58	6.88	normal
104	0	0.41	0.99	1.50	2.23	2.47	2.84	3.72	4.38	4.73	5.19	5.61	6.11	6.44	7.26	8.04	8.49	normal
105	0	0.52	0.93	1.37	2.03	2.51	2.83	3.22	3.46	3.81	4.23	4.49	5.17	5.56	5.90	6.30	6.56	normal
106	0	0.27	0.90	1.38	1.77	2.11	2.38	3.20	3.55	3.77	4.11	4.84	5.19	5.55	5.92	6.66	7.10	normal
107	0	0.50	0.86	1.27	1.72	2.05	2.63	2.94	3.69	3.98	4.17	4.58	5.07	5.56	6.31	6.72	7.24	normal
108	0	0.41	0.73	1.41	1.72	2.09	2.71	3.29	3.69	4.28	4.83	5.13	5.71	6.17	6.47	7.15	7.62	normal
109	0	0.79	1.28	1.54	2.01	2.37	2.73	3.40	4.15	4.57	5.01	5.52	5.94	6.42	7.10	7.49	7.82	normal
110	0	0.40	1.08	1.54	2.12	2.66	3.02	3.67	4.12	4.48	4.74	5.04	5.42	5.77	6.55	7.08	7.42	normal
111	0	0.68	1.66	2.21	2.85	3.26	3.81	4.46	4.93	5.92	6.40	7.26	7.91	8.85	9.54	10.35	11.02	weak
112	0	0.40	0.81	1.20	1.71	2.31	2.91	3.31	3.74	4.33	4.71	5.09	5.57	5.97	6.25	6.66	6.88	normal
113	0	0.65	1.27	1.85	2.14	2.48	2.73	3.08	3.47	3.94	4.27	4.59	5.21	5.77	6.04	6.65	6.89	normal
114	0	0.36	0.74	1.23	1.67	2.23	2.72	3.15	3.65	4.03	4.50	4.86	5.13	5.66	6.03	6.71	7.16	normal
115	0	0.38	0.83	1.25	1.81	2.48	2.93	3.44	4.02	4.76	5.13	5.37	5.94	6.37	7.29	7.72	8.09	normal
116	0	0.33	0.99	1.31	1.75	2.11	2.68	3.19	4.08	4.45	4.78	5.02	5.50	5.75	6.15	6.47	6.91	normal
117	0	0.35	0.89	1.20	1.60	2.05	2.59	2.98	3.41	3.81	4.27	4.77	5.20	5.55	6.01	6.33	6.69	normal
118	0	0.47	0.96	1.30	1.62	2.35	2.63	3.35	3.99	4.39	4.66	5.30	6.01	6.40	6.79	7.07	7.90	normal
119	0	0.35	0.80	1.11	1.42	2.24	2.60	3.15	3.54	3.89	4.48	4.98	5.28	5.51	5.93	6.48	7.05	normal
120	0	0.54	0.92	1.26	1.89	2.68	3.46	3.95	4.48	5.07	5.40	5.73	6.08	6.50	7.00	7.55	7.76	normal
121	0	0.57	1.07	1.48	1.96	2.22	2.47	2.92	3.36	3.78	4.34	4.75	5.05	5.37	5.81	6.22	6.53	normal
122	0	0.54	1.33	1.89	2.57	3.32	4.22	4.74	5.50	6.17	6.80	7.38	8.22	8.88	9.20	9.81	10.68	weak
123	0	0.62	1.00	1.54	2.03	2.48	3.07	4.04	5.02	5.90	6.28	7.24	7.71	8.61	9.37	10.15	10.77	weak
124	0	0.33	0.86	1.93	2.19	2.50	3.03	3.23	3.56	3.73	4.12	4.39	4.65	5.01	5.38	5.94	6.67	normal
125	0	0.45	1.03	1.53	2.05	2.64	3.22	3.53	3.79	4.08	4.41	4.82	5.38	5.88	6.54	6.90	7.25	normal
126	0	0.62	1.49	2.10	3.15	3.66	4.15	4.55	5.38	6.15	6.92	8.01	8.45	9.31	10.00	10.67	11.26	weak
127	0	0.58	1.12	2.03	2.82	3.68	4.38	5.04	5.67	6.62	7.12	7.97	8.68	9.11	9.68	10.29	10.90	weak
128	0	0.44	0.73	1.28	1.60	1.97	2.27	2.54	2.81	3.05	3.74	4.15	4.70	5.19	5.89	6.55	7.11	normal

129	0	0.50	0.77	1.14	2.26	2.45	2.83	3.16	3.56	3.92	4.28	4.60	4.98	5.39	5.64	6.29	6.86	normal
130	0	0.55	1.20	1.58	1.97	2.56	2.87	3.18	3.87	4.10	4.84	5.16	5.72	6.24	6.98	7.32	7.81	normal
131	0	0.73	1.32	2.03	2.53	3.17	3.70	4.55	5.38	6.01	6.70	7.10	7.75	8.60	9.15	9.86	10.74	weak
132	0	0.69	1.07	1.80	2.75	3.45	4.05	4.82	5.38	5.92	6.46	6.99	7.60	8.64	9.74	10.21	10.76	weak
133	0	0.69	1.44	1.82	2.31	2.75	3.74	4.42	5.63	6.54	7.30	7.82	8.66	9.17	10.01	10.61	11.33	weak
134	0	0.33	0.70	1.02	1.39	1.83	2.38	2.76	3.36	3.68	4.35	4.65	4.98	5.23	5.65	6.31	6.59	normal
135	0	0.51	0.74	0.98	1.26	1.65	2.01	2.35	3.12	3.43	3.89	4.21	4.70	5.27	6.00	6.50	6.89	normal
136	0	0.40	0.88	1.18	1.48	1.88	2.30	2.54	2.91	3.50	3.92	4.36	4.60	4.97	5.36	5.57	6.08	normal
137	0	0.64	1.20	1.93	2.41	2.76	3.37	3.91	5.05	5.68	6.25	6.91	7.93	8.32	8.97	9.79	10.38	weak
138	0	1.04	1.41	1.80	2.22	2.50	2.85	3.26	3.93	4.36	4.79	5.20	5.76	6.13	6.65	6.95	7.41	normal
139	0	0.36	0.99	1.24	1.56	1.99	2.35	2.81	3.09	3.55	3.89	4.29	4.52	4.86	5.69	6.09	6.70	normal
140	0	0.81	1.39	2.16	3.06	3.85	4.61	5.12	5.43	6.02	6.59	7.38	7.88	8.55	9.61	10.24	10.92	weak
141	0	0.70	0.96	1.26	1.78	2.28	2.81	3.17	3.41	3.69	4.09	4.77	5.43	5.83	6.09	6.65	7.10	normal
142	0	0.49	0.74	1.21	1.70	1.95	2.46	2.86	3.32	3.82	4.23	4.58	4.82	5.30	5.76	6.11	6.32	normal
143	0	0.56	1.02	1.44	1.76	2.03	2.44	3.67	4.30	4.79	5.14	5.87	6.38	6.55	7.04	7.26	7.86	normal
144	0	0.42	0.87	1.43	2.13	2.38	2.64	2.92	3.19	3.48	4.10	4.39	4.85	5.30	5.72	6.40	7.15	normal
145	0	1.21	1.89	2.38	3.09	3.61	4.32	5.38	6.09	6.83	7.44	8.16	8.81	9.37	9.79	10.59	11.51	weak
146	0	0.51	1.29	1.73	2.44	2.76	3.19	3.50	3.93	4.44	4.95	5.28	5.72	6.42	6.83	7.23	7.58	normal
147	0	0.50	1.11	1.60	2.25	3.00	3.81	4.38	4.80	5.37	5.98	6.60	6.97	7.59	8.48	9.20	9.84	weak
148	0	0.63	1.19	1.86	2.31	2.62	3.10	3.43	3.86	4.17	4.77	5.45	5.82	6.17	6.36	6.76	7.29	normal
149	0	0.91	1.69	2.07	2.87	3.45	4.14	4.63	5.25	5.75	6.54	7.20	7.65	8.34	8.87	9.58	10.12	weak
150	0	0.63	1.22	1.92	2.62	3.22	3.90	4.58	5.32	6.76	7.27	7.71	8.33	9.15	9.84	10.35	10.81	weak
151	0	0.66	1.33	2.12	2.82	3.40	3.84	4.91	5.28	5.81	6.38	7.06	7.70	8.47	9.04	10.21	10.92	weak
152	0	0.92	1.30	1.88	2.97	3.41	4.24	4.88	5.53	6.31	7.07	7.85	8.65	9.68	10.20	10.72	11.26	weak
153	0	0.58	0.97	1.80	2.85	3.43	4.34	5.15	5.77	6.47	7.32	7.79	8.37	8.90	9.40	10.13	11.36	weak
154	0	0.80	1.18	1.60	1.91	2.61	3.06	3.33	3.59	4.02	4.40	4.86	5.37	5.77	6.30	6.79	7.28	normal
155	0	0.46	0.94	1.29	1.59	2.19	2.51	3.26	3.59	4.41	4.75	5.07	5.34	5.88	6.19	6.65	7.02	normal
156	0	0.24	0.90	1.10	1.51	1.98	2.32	3.04	3.93	4.60	5.38	6.02	6.42	6.78	7.29	8.20	8.61	normal
157	0	0.19	0.72	1.10	2.13	2.59	2.91	3.15	4.20	4.54	4.96	5.72	6.40	6.71	7.27	7.85	8.20	normal
158	0	0.64	1.15	1.79	2.53	3.69	4.21	4.89	5.48	5.95	6.46	7.08	7.60	8.08	8.88	9.51	10.27	weak
159	0	0.82	1.31	1.87	2.25	2.63	3.39	3.57	3.90	4.34	4.68	5.35	5.57	5.98	6.30	7.04	7.40	normal
160	0	0.76	1.37	2.09	2.65	3.44	3.91	4.29	5.21	5.68	6.10	6.56	7.03	7.60	8.16	8.82	9.64	weak
161	0	0.60	1.12	1.53	1.96	2.13	2.63	3.06	3.31	4.09	4.65	5.21	5.64	6.33	6.59	6.84	7.06	normal
162	0	0.55	1.59	2.37	2.98	3.73	4.38	5.22	6.33	6.69	7.31	7.97	8.39	8.99	9.64	10.46	11.08	weak
163	0	0.45	0.86	1.40	1.79	2.18	2.77	3.15	3.52	3.76	4.44	5.13	5.45	5.96	6.40	6.96	7.51	normal
164	0	0.62	0.99	1.46	1.91	2.43	2.90	3.34	3.67	4.00	4.52	4.98	5.30	5.93	6.23	6.68	7.28	normal
165	0	0.43	0.87	1.22	1.62	1.98	2.35	2.64	3.33	3.82	4.10	4.68	5.07	5.49	5.98	6.35	6.92	normal
166	0	0.54	0.94	1.82	2.55	3.33	3.81	4.55	5.15	5.99	6.40	6.77	7.66	8.47	9.04	10.05	10.63	weak
167	0	0.77	1.43	2.36	3.13	4.19	4.71	5.27	5.64	6.29	6.89	7.70	8.37	8.81	9.39	10.10	10.92	weak
168	0	0.45	0.77	1.06	1.45	1.78	2.33	2.81	3.27	3.69	4.30	4.85	5.82	6.37	6.61	6.97	7.22	normal
169	0	0.71	1.48	2.19	2.77	3.49	4.18	4.81	5.55	6.09	6.76	7.18	7.86	8.54	9.23	9.65	10.57	weak
170	0	0.45	0.77	0.98	1.42	2.00	2.43	2.86	3.13	3.43	3.71	4.03	4.27	4.70	5.20	5.71	6.41	normal
171	0	0.80	1.32	2.08	2.81	3.53	4.28	5.07	5.81	6.50	7.09	7.68	8.46	9.10	9.74	10.22	10.95	weak
172	0	0.45	0.92	1.61	2.02	2.47	2.87	3.31	3.74	4.13	4.94	5.17	5.79	6.25	6.84	7.33	7.63	normal

173	0	0.36	0.76	1.35	1.85	2.05	2.24	2.60	2.91	3.31	3.74	4.26	4.61	4.89	5.31	5.58	6.01	normal
174	0	0.35	0.66	1.08	1.45	1.79	2.12	2.47	3.02	3.41	3.97	4.34	4.67	5.13	5.45	6.04	6.89	normal
175	0	0.52	1.16	2.44	3.06	3.58	4.57	4.98	5.43	6.00	6.56	7.50	8.20	8.61	9.11	9.62	10.04	weak
176	0	0.58	1.10	1.55	2.33	3.07	3.73	4.69	5.23	5.82	6.98	7.49	8.12	8.56	9.08	9.61	10.32	weak
177	0	0.48	0.88	1.27	1.75	2.03	2.60	3.07	3.39	3.73	4.03	4.39	4.74	5.33	5.71	6.22	6.76	normal
178	0	0.36	0.59	0.93	1.38	1.69	2.08	2.55	2.99	3.17	3.71	3.98	4.25	4.58	4.99	5.66	5.93	normal
179	0	0.45	0.91	1.44	1.82	2.07	2.35	2.82	3.37	3.75	4.16	4.56	5.33	5.58	5.93	6.78	7.27	normal
180	0	0.22	0.99	1.31	2.07	2.61	2.87	3.34	4.08	4.30	4.53	5.35	5.88	6.13	6.71	7.00	7.60	normal
181	0	0.42	0.78	1.07	1.61	2.20	2.43	2.85	3.10	3.59	4.09	4.36	4.95	5.26	5.59	5.88	6.60	normal
182	0	0.29	0.58	1.01	1.31	1.64	2.00	2.61	3.04	3.40	3.71	4.15	4.50	5.01	5.40	5.61	5.83	normal
183	0	0.27	0.63	1.13	1.52	1.90	2.30	2.57	3.23	3.99	4.33	4.87	5.23	5.50	5.88	6.40	6.85	normal
184	0	0.42	0.66	1.19	2.12	2.43	3.00	3.38	3.95	4.48	4.96	5.18	5.35	5.69	5.95	6.10	6.38	normal
185	0	0.68	1.02	1.56	2.03	2.85	3.24	3.62	4.07	4.55	4.85	5.35	6.07	6.47	6.71	7.07	7.53	normal
186	0	0.69	1.44	1.76	2.32	2.70	3.10	3.57	4.00	4.54	5.00	5.22	5.48	5.86	6.50	6.78	7.13	normal
187	0	0.20	0.78	1.25	1.61	2.07	2.56	2.84	3.39	3.97	4.37	5.11	5.63	6.15	6.50	6.94	7.26	normal
188	0	0.45	0.64	1.23	1.51	1.71	2.19	2.64	3.11	3.71	4.13	4.38	4.85	5.29	5.62	6.05	6.62	normal
189	0	0.48	0.86	1.14	1.55	1.91	2.34	2.59	3.20	3.45	3.79	4.32	4.52	4.83	5.40	6.49	6.94	normal
190	0	0.57	1.18	1.60	2.02	2.48	2.90	3.48	3.81	4.13	4.61	4.97	5.50	5.80	6.51	7.02	7.30	normal
191	0	0.36	0.76	1.18	1.63	2.10	2.33	2.68	3.50	4.02	4.52	4.91	5.15	5.79	6.17	6.57	6.87	normal
192	0	0.42	0.87	1.22	1.55	2.26	2.94	3.25	3.69	4.08	4.42	5.10	5.53	6.04	6.51	6.83	7.34	normal
193	0	0.48	1.21	1.58	2.34	2.59	3.00	3.40	3.91	4.25	4.64	5.19	5.71	6.31	6.62	6.98	7.55	normal
194	0	0.42	1.14	1.94	2.68	3.19	3.78	4.31	4.94	5.46	5.84	6.58	7.66	8.22	9.45	10.16	10.85	weak
195	0	0.25	0.68	1.03	1.32	1.65	2.04	2.45	2.93	3.37	3.89	4.29	4.87	5.48	6.03	6.54	7.23	normal
196	0	0.42	1.15	1.60	1.89	2.22	3.09	3.53	3.78	4.16	4.59	4.99	5.44	6.02	6.40	6.65	7.02	normal
197	0	0.61	1.46	2.02	2.84	3.56	4.63	5.19	5.90	6.57	7.13	7.71	8.26	8.83	9.36	10.04	10.48	weak
198	0	0.31	0.80	1.00	1.76	2.37	2.72	3.03	3.71	4.40	4.79	5.12	5.64	6.33	6.71	7.64	7.85	normal
199	0	0.28	0.74	1.48	1.95	2.42	2.87	3.39	3.79	4.29	4.98	5.54	6.12	6.39	6.77	7.07	7.62	normal
200	0	0.33	0.71	0.98	1.42	2.09	2.44	2.81	3.33	3.69	4.18	5.46	5.90	6.49	6.88	7.29	7.59	normal